

Optical Monitoring and Operational Modal Analysis of Large Wind Turbines

Proefschrift

ter verkrijging van de grad van doctor

aan de Technische Universiteit Delft,

op gezag van de Rector Magnificus prof. ir. K.C.A.M. Luyben,

voorzitter van het College voor Promoties,

in het openbaar te verdedigen op donderdag, 13 juni 2013 om 10:00 uur

door

Muammer ÖZBEK

Master of Science in Civil Engineering

İstanbul Boğaziçi University

geboren te Kayseri, Turkije

Dit proefschrift is goedgekeurd door de promotor:

Prof. dr. ir. D.J. Rixen

Samenstelling promotiecommissie:

Rector Magnificus,	voorzitter
Prof. dr. ir. D.J. Rixen	Technische Universiteit Delft, promotor
Prof. dr. ir. A. de Boer	Technische Universiteit Twente
Dr. eng. A. Brandt	University of Southern Denmark
Prof. dr. G.J.W. van Bussel	Technische Universiteit Delft
Dr. ir. C. Devriendt	Vrije Universiteit Brussel
Prof.dr.ir. R.P.B.J. Dollevoet	Technische Universiteit Delft
Prof. dr.ir. L.J. Sluys	Technische Universiteit Delft, reservelid

ISBN 978-94-6191-767-6

The research presented in this thesis has been carried out at the Faculty of 3ME (Mechanical, Maritime and Materials Engineering), Delft University of Technology and partly funded by We@Sea Research Program, financed by the Dutch Ministry of Economical Affairs.

to my family

Summary

Identification of the dynamic properties and the corresponding structural response of wind turbines is essential for optimizing the energy produced, ensuring safe and reliable operation and increasing the life-time of the system. As the sizes of modern wind turbines increase, their dynamic behaviors get more complicated and it becomes more important to predict the response characteristics of new designs through simulations.

Modern computation and simulation tools provide designers with great opportunities to detect and solve most of the possible problems at very early stages and improve their designs. Indeed, several important system properties such as eigenfrequencies and mode shapes, which govern the dynamic response of the turbine, can be estimated very accurately by using structural analysis programs. However, some important dynamic parameters (e.g. damping) cannot be modeled precisely without supplementary information obtained from in-field tests and measurements.

Considering the fact that only the models validated by real response measurements are able to represent the complicated dynamic behavior of the structure, various tests have been applied on both parked and rotating turbines for several decades. However, some further improvements are still needed for testing and analyzing the dynamic characteristics of these specific structures in an accurate and efficient way. This thesis aims at making a contribution to this challenging field of experimental and operational modal analyses through several aspects;

- Two non-contact optical measurement systems (laser interferometry and photogrammetry) are proposed as alternative turbine monitoring systems. In Chapter 2 and 3, it is demonstrated that optical measurement systems enable the dynamic response of the turbine to be measured with a high precision and spatial resolution both at parked condition and in operation. The pros and cons of the methods and the acquired accuracies are discussed in detail.
- In Chapter 3, the vibration data recorded on a 2.5 MW -80 meter diameter- wind turbine by using 3 different measurement systems (laser interferometry, photogrammetry and conventional strain gauges) are analyzed by using modal

analysis algorithms based on NExT (Natural Excitation Technique) and LSCE (Least Square Complex Exponential) techniques. Several important turbine parameters (eigenfrequencies and damping ratios) are extracted and compared with the results presented in literature.

- In Chapter 4, the main challenges in testing and analyzing the in-operation vibration characteristics of wind turbines are discussed in detail. The factors affecting the accuracies of the estimated modal parameters and the applicability limits of some state of the art system identification tools are examined. In order to investigate specifically the performance of the identification algorithms, numeric response data generated by an analytical model and an aeroelastic simulation tool were used.
- In Chapter 5, an alternative method (based on NExT) is proposed for identification of the systems with high modal damping. The introduced technique aims at improving the capabilities of NExT in extracting the highly damped eigenmodes such as the aeroelastic modes of an operating wind turbine. It is demonstrated that the proposed approach enables the eigenfrequencies of the high damping modes to be estimated by using data series which are approximately 30 times shorter than those required for standard NExT algorithm. Results of the analyses show that eigenfrequencies of highly damped modes can be estimated with an average accuracy of 95%. The stability of the proposed method and the possible effects of measurement noise on the estimated modal parameters are also investigated in Chapter 5.

Samenvatting

Identificatie van de dynamische eigenschappen en het daarmee samenhangende gedrag van de structuur van windturbines, is essentieel voor de optimalisatie van de geproduceerde energie, voor het waarborgen van veilig en betrouwbaar gedrag en voor het verhogen van de levensduur van het systeem. Naarmate de afmetingen van moderne wind turbines toenemen, wordt hun dynamisch gedrag meer gecompliceerd en het wordt dan ook belangrijker om het dynamische gedrag van nieuwe ontwerpen nauwkeurig te voorspellen met behulp van simulaties.

Moderne reken- en simulatie gereedschappen bieden de ontwerpers veel mogelijkheden om al in een vroeg stadium mogelijke problemen te voorspellen en op te lossen en het ontwerp te verbeteren. Diverse belangrijke systeem eigenschappen zoals eigenfrequenties en trilvormen, die het dynamisch gedrag van de windturbine beschrijven, kunnen zeer nauwkeurig worden geschat met behulp van programmatuur voor de analyse van structurele eigenschappen. Maar sommige belangrijke dynamische parameters (bijvoorbeeld demping) kunnen niet nauwkeurig worden gemodelleerd zonder aanvullende informatie verkregen met behulp van veldexperimenten.

Het feitelijke en vaak gecompliceerde gedrag van de structuur kan pas goed voorspeld worden door systeem modellen welke zijn gevalideerd aan de hand van veld experimenten. Daarom zijn in recente decennia experimenten uitgevoerd, zowel aan stilstaande als aan roterende windturbines. Om de dynamische eigenschappen van deze specifieke structuren zowel accuraat als efficiënt te bepalen zijn echter verdere verbeteringen nodig in tests en in analyses. Dit proefschrift tracht een bijdrage te leveren op dit uitdagende gebied van experimentele en operationele modale analyse, als volgt:

- Twee contactloze optische meetsystemen (laser interferometrie en fotogrammetrie) worden voorgesteld als alternatieve systemen voor het bewaken van het dynamische gedrag van wind turbines. In hoofdstuk 2 en 3 wordt aangetoond dat men met behulp van optische meetsystemen het dynamische gedrag van de wind turbine kan meten met grote nauwkeurigheid en met hoge ruimtelijke resolutie, zowel met stilstaande rotor als

met draaiende rotor. De voor- en nadelen van beide methoden en de daarmee verkregen nauwkeurigheden worden in detail beschreven.

- In hoofdstuk 3 wordt beschreven hoe drie verschillende meetsystemen (laser interferometrie, fotogrammetrie, en conventionele rekstrookjes) worden toegepast in veldexperimenten met een 2,5 MW windturbine van 80 meter diameter. De metingen worden geanalyseerd met behulp van modale analyse algoritmen gebaseerd op de *Natural Excitation Technique* (NExT) en de *Least Square Complex Exponential* (LSCE) techniek. Uit de analyse worden diverse belangrijke windturbine parameters verkregen (eigenfrequenties en dempingsverhoudingen) en hun waarden worden vergeleken met resultaten beschreven in de literatuur.

- In hoofdstuk 4 wordt in detail aandacht besteed aan het meten en het analyseren van de dynamische eigenschappen van operationele windturbines. Nagegaan wordt hoe bepaalde factoren de nauwkeurigheid van de schattingen van de modale parameters beïnvloeden, en wat de mogelijke grenzen zijn aan de toepasbaarheid van enkele moderne systeemidentificatie gereedschappen. Om met name de prestaties van de identificatie algoritmen te onderzoeken werden systeem responsies gegenereerd zowel door een analytisch model als door een aero-elastische code.

- In hoofdstuk 5 wordt, uitgaande van NExT, een alternatieve methode voorgesteld om systemen met sterke modale demping te identificeren. De voorgestelde methode heeft als doel de bruikbaarheid van NExT voor de bepaling van de sterk gedempte trilvormen te vergroten zodat ook de aero-elastische trilvormen van een windturbine met draaiende rotor kunnen worden bepaald. Aangetoond wordt dat de voorgestelde aanpak het mogelijk maakt de eigenfrequenties van de sterk gedempte trilvormen af te schatten met behulp van data reeksen welke ongeveer dertig maal korter zijn dan voor het standaard NExT algoritme nodig zou zijn. De verkregen resultaten laten zien dat de eigenfrequenties van sterk gedempte trilvormen kunnen worden geschat met een gemiddelde nauwkeurigheid van 95 %. Ook werd de stabiliteit van de voorgestelde methode onderzocht, evenals de mogelijke invloed van meetruis op de geschatte modale parameters.

Table of Contents

Summary.....	i
Samevatting.....	iii
Introduction	1
Feasibility of Monitoring Large Wind Turbines Using Photogrammetry	19
Operational Modal Analysis of a 2.5 MW Wind Turbine Using Optical Measurement Techniques and Strain Gauges	47
Challenges in Testing and Monitoring the In-Operation Vibration Characteristics of Wind Turbines	81
An Alternative NExT (Natural Excitation Technique) Based Eigenfrequency Estimator for Analyzing Highly Damped Systems	115
Conclusions and Future Research Topics	159
Acknowledgements.....	165
Curriculum vitae	168

CHAPTER 1

Introduction

Research Objectives and Outline of the Thesis

Growing energy demands require wind turbine manufacturers to design more efficient and higher capacity wind turbines which inevitably results in larger and larger new models to be put into service. However, an important consequence of this increase in size and flexibility of the structure is the complicated dynamic interaction between different parts of the turbine. Motion of the blades interacts with aerodynamic forces, electro-magnetic forces in the generator and the structural dynamics of several turbine components (drive train, nacelle and tower). Understanding these dynamic interactions and the corresponding structural response is essential for optimizing the energy produced, ensuring safe and reliable operation and increasing the life-time of the system. This requires improving the design methodologies and in-operation control strategies. Therefore, more attention is paid to developing theoretical models for estimating the behavior of new wind turbines.

Contemporary aeroelastic simulation tools coupled with structural dynamics models enable designers to detect understand and solve most of the possible problems at very early stages and optimize their designs [1-9]. Indeed, several important system properties such as eigenfrequencies and mode shapes, which govern the dynamic response of the turbine, can be estimated very accurately by using structural analysis programs. However, there are still some parameters (e.g. damping) which cannot be modeled precisely.

Damping, together with the above mentioned system characteristics, plays a crucial role in predicting maximum dynamic loads and fatigue stresses acting on the structure. The overall damping has a very complex mechanism which requires considering several physical factors simultaneously. Thus, it is very difficult to be modeled without supplementary information obtained from in-field tests and measurements. Some of its components like material damping can nowadays be reasonably well taken into

account. However, modeling the damping occurring in bearings, joints and gearing or the damping due to ground (soil) - structure interaction is still not possible. Similarly, identifying the aeroelastic component of damping which is due to the combined effect of structural deformations and aerodynamic forces is a very challenging task and always needs experimental verification. Therefore, considering the fact that only the models validated by real response measurements are able to represent the complicated interactions among different parts of the structure, various tests have been applied on both parked and rotating turbines for several decades [10-22].

However, testing and analyzing the dynamic characteristics of these specific structures in an accurate and efficient way still require;

- Development of new measurement techniques and sensor technologies which enable 3D deformations of turbine components to be measured at several locations simultaneously with a high precision and spatial resolution.
- Evaluating the efficiencies of currently used system identification algorithms in analyzing the vibration data recorded on a MW scale large wind turbine.
- Modifying and optimizing these analysis techniques to overcome possible problems that may be encountered due to the complicated nature of turbine structure and wind loading.

The main objectives of the research presented in this thesis are indeed directly related to the issues which are expressed above in a general framework. These objectives can be described in more detail as follows;

1. Investigating the feasibility of monitoring wind turbine dynamics by using non-contact optical measurement systems (photogrammetry and laser interferometry) and evaluating the acquired accuracy.

It is state of the art to use accelerometers and/or strain gauges placed inside the blade or tower for dynamic measurements performed on wind turbines [8-16, 23-26]. However, these measurement systems are sensitive to lightning and electromagnetic fields. Besides, some extra installations inside the blades such as placement of cables for power supply and data transfer are required for these applications. The signals from rotating sensors on the blades are transferred to

stationary computer via slip rings or by radio/wireless transmission. For large commercial turbines the required installations and preparations (sensor calibration) may be very expensive and time consuming [27,28].

The complicated nature of wind loads also makes the efficient use of these sensors on these specific structures very difficult. The deflections under the action of wind loading can be considered as the sum of a static component due to average wind speed and a dynamic component due to turbulence [29]. Accelerometers cannot provide very accurate information about the static component. Therefore, several researchers suggest that in wind response measurements, accelerometers should be used together with other systems such as GPS (Global Positioning System) which are able to detect the static deformations accurately [30-32]. Although GPS-accelerometer combination is widely used to monitor the response of several structures such as high-rise buildings and bridges, it cannot easily be applied to wind turbines because of the technical difficulties in placing GPS sensors in the blade.

The dynamic response characteristics of the structure can be thoroughly understood only if the deformations of the turbine components are measured at several locations simultaneously. The measurement accuracy and the spatial resolution are the two important factors which determine whether the recorded data can be used for some specific applications such as condition monitoring and damage detection or not.

Due to the technical limitations in sensor installations, the conventional systems mentioned above can only be applied at certain locations on the turbine. Unfortunately, the last 10-15 meters of the blades (close to tip) are not accessible and therefore cannot be instrumented. In practice, sensors are usually placed at the root regions of the blades. However, some motions such as bending of the rotor axis, small tilt and yaw motion of the nacelle and teeter cannot be detected by strain gauges placed at these locations. Besides, the response measured at the root region only may not provide useful information about the location and extent of a possible damage close to the tip of the blade. The reliability of the extracted information is directly related to the number of measurement points.

Fiber-optic strain gauges are proposed to be a promising alternative to accelerometers and conventional strain gauges since optical sensors are not prone to electro-magnetic fields or lightning. However, it is reported that some feasibility tests are still needed to ensure the effective and cost efficient use of this measurement system. The factors affecting the performance of fiber-optic sensors such as sensitivity to humidity and temperature variations and the corresponding error compensation methods should also be investigated further [33,34]. Similarly, additional long term durability tests are required to determine whether the bonding between optic-fiber and composite blade material deteriorates over time due to repetitive loading and severe environmental factors or not.

Fiber-optic strain gauges are expected to provide a high spatial resolution but installation costs significantly increase depending on the number of sensors. Besides, high capacity decoders are needed to be able to acquire data from many sensors simultaneously resulting in a further increase in the hardware costs. Fiber-optic sensors can be applied throughout the blade only if the installation is performed during the manufacturing stage in the factory. The system cannot be easily applied to existing turbines.

In this thesis, two non-contact optical measurement systems (photogrammetry and laser interferometry), which do not require any sensors to be installed in the structure, are proposed to be promising and cost efficient alternatives for measuring the vibration response of wind turbines. A different type of non-contact measurement technique has already been in use in wind turbine industry for measuring the noise generated by wind turbines and/or farms [35]. The source and the level of the noise are determined by using an array of microphones and acoustic cameras. The obtained data is then analyzed to check whether the noise is within the allowable limits prescribed by the standards or not. However, the optical methods proposed in this work are intended to be used for a wider field of application such as dynamic testing and modal analysis of wind turbines, structural health (condition) monitoring and damage detection.

Photogrammetry is a proven measurement technique based on determination of the 3D coordinates of the points on an object by using two or more images taken from different positions and orientations [36]. Although photogrammetry is efficiently used at smaller scales by a wide variety of disciplines, it was applied for the very first time to a multi-MW scale wind turbine during this research project [20-22,37].

Within the scope of the work, the 3D dynamic response of a 2.5 MW - 80 m diameter- wind turbine was captured at 33 different locations simultaneously by using 4 CCD (charge coupled device) cameras while the turbine was rotating. The results show that deformations on the turbine can be measured with an average accuracy of ± 25 mm from a measurement distance of 220 meters. It is also possible to identify some of the important rotor vibration modes (first flapwise and edgewise modes) from the acquired data. The main features of this measurement method and evaluation of the accuracy obtained are discussed in Chapter 2.

Similarly, laser interferometry, another optical measurement method utilizing laser as light source, was successfully applied to the same test turbine and was proven to provide very accurate information on the vibration characteristics of the structure. Chapter 3 and 4 present a more detailed explanation about the laser interferometry measurements and the obtained results.

2. Analyzing the vibration data recorded on a multi-MW scale wind turbine by using some state of the art identification tools and investigating the system parameters (e.g. eigenfrequencies, damping ratios) that can be extracted from the analyzed time histories:

Wind turbines have very specific characteristics and challenging operating conditions. Since they are designed and optimized to provide maximum power production for changing wind speeds and directions, they are expected to adapt to the rapidly varying environmental factors. Depending on their types and sizes, wind turbines are usually intended to be operational for wind speeds between 5 and 25 m/sec. In order to reach this goal, most of the turbines utilize active pitch control mechanisms where angle of the blade (pitch angle) is changed as a function of wind

speed. Similarly, the whole rotor is rotated towards the effective wind direction by using the yaw mechanism.

The ability of the turbine to adapt to the changes plays a crucial role in ensuring maximum energy production and the safety of the structure during extreme wind loads. This on the other hand, makes it more difficult to investigate the system from dynamic analysis point of view. Some important system characteristics (e.g. stiffness and damping) governing the vibration response change considerably depending on operating conditions (wind speed, rotor speed and blade pitch angle). Thus, time invariant system assumption, which is a significant prerequisite of system identification methods, is not easily fulfilled for these structures. Besides, wind turbines have both moving (rotor) and fixed (tower) components and simultaneous processing of the signals acquired from different parts requires some mathematical transformations (multi-blade coordinate transformation).

Conventional dynamic testing techniques based on exciting the structure at several locations with sufficient force amplitudes cannot be easily applied to these challenging structures due to their size and the technical difficulties in providing very large forces required for the excitation.

Standard wind turbine testing includes estimation of the frequencies and damping of the turbine modes from manual peak-picking from frequency response spectra of measured vibration data, or from the decaying response after exciting the structure through step relaxation or clamping of the brake [10-13]. These estimations are often performed on turbines at parked condition. Therefore, estimated modal parameters do not include aerodynamic effects that dominate the aeroelastic modes of an operating turbine and are mostly related to the turbine structure. On the other hand, even pure structural damping measured at parked condition may slightly vary depending on the force applied on the turbine because the changes in instantaneous wind speed and direction affect the behavior of bearings and the joints connecting different components. However, frequencies and damping ratios of the lower turbine modes are still important for tuning and validation of numerical models and for the verification of the prototype design [14,38].

Step relaxation is easily applied on wind turbines at parked condition but, it is relatively difficult and time consuming to use the same method for rotating turbines. The system involves specific mechanisms to be installed on the turbine to ensure the sudden release of pretensioned cables. The forces needed to excite a MW size turbine with sufficient energy can be very large. Besides, the device has to be reloaded for every input, which means bringing the turbine down to parked condition, reloading the device and waiting for the turbine to reach a certain rotation speed. If numerous tests are planned to be performed for several wind speeds, this method can be very costly and time consuming [38].

Researchers [14,25] also tried to use different excitation techniques for rotating turbines assuming that a vibration mode can be excited by a harmonic force at its natural frequency, whereby the decaying response after the end of excitation gives an estimate of damping. Several simulations and experiments were performed to verify whether turbine modes can be excited by blade pitch and generator torque variations and eccentric rotating masses placed on the nacelle or not. Results of the in-field feasibility tests showed that it is not technically possible to excite the modes with high modal frequency or high damping due to the limited capacity of the actuators. Besides, excited turbine vibrations are not pure modal vibrations and the estimated damping is therefore not the actual modal damping. Especially for systems having vibration modes with similar frequencies (e.g. fore-aft and side to side tower modes), but different damping ratios, it is not possible to isolate a certain mode and aerodynamic damping values cannot be estimated well because of the energy transfer between different modes [14].

OMA (Operational Modal Analysis) tools, a common denomination used for several analysis methods, which do not require the forces acting on the system to be measured, provide great opportunities to overcome these drawbacks. Since estimation of the modal parameters is solely based on the use of measured response signals, these methods can easily and efficiently be used to extract the dynamic properties of wind turbines excited by natural environmental inputs (winds). Indeed, early versions of OMA tools were specifically developed to solve the

problems encountered during dynamic testing of wind turbines and have been in use since early 90's [15-18]. Several researchers [10,12,13] successfully used OMA methods and reported that they obtained very good coherence between the modal parameters identified by OMA and the conventional experimental modal analysis techniques (EMA).

Although there are numerous studies conducted on wind turbines at parked condition, the information related to dynamic testing and modal analysis of MW scale large wind turbines during operation is quite limited. This thesis aims at making a contribution to this challenging field of experimental and operational modal analysis by presenting the results of the in-field vibration tests performed on a 2.5 MW – 80 meter diameter - wind turbine and the corresponding data analyses.

For this purpose, the dynamic response of the test turbine was monitored by using 3 different measurement systems namely, conventional strain gauges, photogrammetry and laser interferometry, while the turbine was both at parked condition and rotating. The recorded data was analyzed by using an OMA algorithm based on NExT (Natural Excitation Technique) and LSCE (Least Square Complex Exponential) methods and several turbine parameters (eigenfrequencies and damping ratios) were extracted. The obtained system parameters were then qualitatively compared with the results presented in a study from literature [14], which includes both aeroelastic simulations and in-field measurements performed on a similar size and capacity wind turbine.

Within the scope of the research, twelve different turbine modes were successfully extracted from the measurements taken on the parked turbine by using strain gauges and LDV (laser Doppler vibrometer). Similarly, seven different turbine modes could be identified from in-operation measurements by using strain gauges and photogrammetry. Only four of these in-operation vibration modes have been previously reported to be identified in literature. During the analyses reported in this thesis, three additional modes could be extracted from the measured vibration response for the very first time in literature. The main features of the dynamic tests performed and the results of the analyses are described in more detail in Chapter 3.

3. Determination of the challenges in testing and monitoring the in-operation vibration characteristics of wind turbines and investigating possible reasons of uncertainty in the estimated modal parameters by using simulation data.

Identification of the in-operation vibration characteristics of wind turbines is a very challenging task that requires several factors to be taken into account during different steps of the structural investigation such as measurement, data analysis and evaluation of the results.

Performing modal analysis on a rotating turbine is much more difficult than performing the same analysis on a parked turbine due to several reasons [14,19,39]. As mentioned before, some important prerequisites such as time invariant system and steady state random excitation assumptions, which form the basics of almost all types of system identification methods, are not always easily fulfilled for rotating turbines. The violation of these assumptions causes at least a large scatter in the extracted system parameters (eigenfrequencies, damping ratios and mode shapes).

The excitation resulting from aerodynamic forces contains significant components of P harmonics (the integer multiples of the rotational frequency P). These P harmonics usually have very high energy levels and dominate the recorded response up to $4-5 P$. Although their amplitudes get smaller for higher frequencies, they can still be effective up to $24P$. These frequencies may coincide with the eigenfrequencies of the system and affect the estimated parameters. Especially the frequencies which have a weak modal participation in the overall motion can be concealed by these P harmonics.

Stiffness and damping properties of the turbine structure change significantly depending on the operating conditions (wind speed, rotor speed and pitch angle). Centrifugal forces which are proportional to the square of the rotation speed generate geometric stiffening on the blade. Besides, aerodynamic stiffness (change of aerodynamic forces with deformation) and rotor stiffness vary depending on the blade angle and rotor speed. Considering that cyclic change in azimuth angle during rotation also causes some variations in the rotor stiffness, several researchers suggest that wind turbine structure should be considered as an LTP (linear time

periodic) system rather than an LTI (linear time invariant) system and should be analyzed by using algorithms taking the effects of this periodicity into account [40,41].

Unlike most structures, the damping identified for wind turbines is not purely structural; it is mainly aeroelastic. Aeroelastic damping is due to the combined effect of both structural deformations and aerodynamic forces. The aerodynamic damping originates from the fact that apparent angle of attack on the blade is related to flapping speed, rotational speed and wind speed. Therefore, the overall damping is not constant and changes significantly depending on operating conditions. For a rotating wind turbine, some important turbine modes have very high aeroelastic damping ratios changing from 10% to 60% (in terms of critical damping ratio), which make them very difficult (if not impossible) to be detected by most of the identification algorithms currently in use. Therefore, attention should be paid to whether operating conditions of the turbine stay constant during the measurements or not.

Several researchers conducting infield dynamic tests on wind turbines report that state of the art OMA methods seem very promising in extracting modal parameters accurately. However, applicability limits of these identification tools and the extent to which their main assumptions are fulfilled in case of analyzing the in-operation vibration data are still being investigated [42-44]. Nevertheless, these techniques are continuously being improved and optimized to overcome the problems that may be encountered due to the complicated nature of the turbine structure and wind loading [41,45,46].

The scatter in the estimated modal parameters can be caused not only by physical factors such as change in operating conditions but also by the mathematical uncertainty related to the applied analysis methods. The efficiency of the utilized identification techniques and the reliability of the extracted system parameters cannot easily be evaluated by using the in-field vibration measurement data which itself includes significant uncertainty due to the sudden and uncontrollable variations in wind speed, rotor speed and pitch angle. Besides, practical shortcomings such as

measurement noise and insufficient length of the recorded time signal make it very difficult to acquire accurate results even by using theoretically perfect algorithms. Therefore, in order to investigate specifically the performance of the identification methods, numeric response data is used.

In this thesis, the main challenges in testing and monitoring the in-operation vibration characteristics of wind turbines are discussed by presenting the results of the analyses performed using analytical models, aeroelastic simulations and infield vibration measurements. For this purpose, several modal analyses, which are very similar to those applied to the vibration data taken on the test turbine, were also conducted on the time histories generated by using an analytical mass – spring – damper model and an aeroelastic simulation tool (MBDyn-AeroDyn).

In order to determine the problems that may be related to the utilized identification methods, the numeric data series were analyzed by using two separate OMA algorithms LSCE (Least Square Complex Exponential) and SSI (Stochastic Subspace Identification) which are based on different mathematical approaches. The modal parameters estimated by these two methods were then compared with the known real values.

In Chapter 4, the main difficulties in analyzing the dynamic properties of wind turbines, possible reasons for the uncertainty in the estimated modal parameters, and the applicability limits of the utilized system identification algorithms are discussed based on the results of these investigations.

4. *Modifying and optimizing the utilized analysis techniques to overcome some of the problems resulting from the complicated nature of turbine structure and wind loading:*

The results presented in this thesis were obtained by using NExT (Natural Excitation Technique). The technique is well proven to provide accurate frequency and damping estimations for eigenmodes with low damping ratios. However, the analyses performed in our research showed that NExT has some limitations in identifying the dynamics of systems with high modal damping. As a matter of fact,

wind turbines, for which the method was particularly developed, are one of the typical examples of these systems [20-22,37] because for rotating turbines the flapwise rotor modes are known to have very high aeroelastic damping.

During the analysis of data series generated by using analytical models, it was observed that NExT requires processing very long time histories to extract the modal parameters when highly damped modes are searched for. In system identification, data length (or measurement duration) is defined in terms of number of cycles of the lowest frequency included in the data block and is generally recommended to be greater than 500 cycles. Depending on the dynamic properties of the structure analyzed, several researchers [47] suggest using even longer measurement blocks, namely between 1000 and 2000 times the period of the structure's fundamental mode. The number of required cycles increases significantly (around 4000-5000 cycles) when the investigated modes have high damping ratios [21,48]. For a MW scale wind turbine, 5000 cycles correspond to continuous test durations of approximately 4-5 hours.

However, finding such long measurement periods, during which wind speed, rotor speed and pitch angle stay constant, is a very challenging task in practice. Accepting some changes in operating conditions may violate the time invariant system and steady state random excitation assumptions. As mentioned before, the violation of these assumptions causes at least a large scatter in the extracted system parameters. This simple but important dilemma is one of the most significant problems to be tackled in testing and monitoring wind turbines.

In this thesis a new approach, which is based on the NExT theory, is introduced to overcome these problems. The proposed method enables eigenfrequencies of the high damping modes to be estimated by using data series which are approximately 30 times shorter than those required for standard NExT. Results of the analyses performed on numerical models show that eigenfrequencies of highly damped modes can be estimated with an average accuracy of 95 %. This achievement is expected to significantly facilitate the validation of turbine models, evaluating the

aeroelastic stability of prototypes and developing in-operation control strategies. The main features of this new method are described in more detail in Chapter 5.

Finally, in Chapter 6, the thesis is concluded by highlighting the main results of our research and indicating possible research directions for the future.

References

- [1] T. Buhl, K. Thomsen, H. Markou, Design guidelines for integrated aeroelastic control of wind turbines. Technical Report Risø-R-1577(EN), Risø National Laboratory, Roskilde, Denmark, 2006, ISBN 87-550-3550-7.
- [2] T.G. Carne, D.W. Lobitz, A.R. Nord, R.A. Watson, Finite element analysis and modal testing of a rotating wind turbine in: Proceedings of the 23rd AIAA Structures, Structural Dynamics and Materials Conference, New Orleans, Louisiana, USA, 1982 AIAA Paper 82-0697.
- [3] M.H. Hansen, K. Thomsen, P. Fuglsang, Aeroelastic modeling of the NM80 turbine with HAWC. Technical Report Risø-I-2017(EN), Risø National Laboratory, Roskilde, Denmark, 2004.
- [4] M.H. Hansen, Aeroelastic stability analysis of wind turbines using an eigenvalue approach. *Wind Energy*, 7 (2004) 133-143.
- [5] M.H. Hansen, Improved modal dynamics of wind turbines to avoid stall-induced vibrations. *Wind Energy*, 6 (2003) 179–195.
- [6] M.H. Hansen, A. Hansen, T.J. Larsen, S. Øye, P. Sørensen, P. Fuglsang, Control design for a pitch-regulated, variable speed wind turbine. Technical Report Risø-R-1500(EN), Risø National Laboratory, Roskilde, Denmark, 2005, ISBN 87-550-3409-8.
- [7] T.J. Larsen, M.H. Hansen, F. Iov, Generator Dynamics in Aeroelastic Analysis and Simulations, Technical Report Risø-R-1395(EN), Risø National Laboratory, Roskilde, Denmark, 2003, ISBN 87-550-3188-9.
- [8] D.J. Malcolm, Dynamic response of a Darrieus rotor wind turbine subject to turbulent flow. *Engineering Structures* 10 (1988) 125-134.
- [9] D.J. Malcolm, Structural response of 34-m Darrieus rotor to turbulent winds, *Journal of Aerospace Engineering*, 6 (1993) 55-75.
- [10] T.G. Carne, J.P. Lauffer, A.J. Gomez, Modal testing of a very flexible 110m wind turbine structure, in: Proceedings of the 6th International Modal Analysis Conference, Kissimmee, Florida, USA, 1988.
- [11] D.P. Molenaar, Experimental modal analysis of a 750 kW wind turbine for structural model validation. in: Proceedings of the 41st Aerospace Sciences Meeting and Exhibit, Reno, Nevada, 2003.
- [12] D.T. Griffith, R.L. Mayes, P.S. Hunter, Excitation methods for a 60 kW vertical axis wind turbine, in: Proceedings of the 28th International Modal Analysis Conference, Jacksonville, Florida, USA, 2010.
- [13] R. Osgood, G. Bir, H. Mutha, B. Peeters, M. Luczak, G. Sablon, Full-scale modal wind turbine tests: comparing shaker excitation with wind excitation, in: Proceedings of the 28th International Modal Analysis Conference, Jacksonville, Florida, USA, 2010.

- [14] M.H. Hansen, K. Thomsen, P. Fuglsang, Two methods for estimating aeroelastic damping of operational wind turbine modes from experiments, *Wind Energy* 9 (2006) 179-191.
- [15] G.H. James, T.G. Carne, J.P. Lauffer, Modal testing using natural excitation, in: *Proceedings of the 10th International Modal Analysis Conference*, San Diego, California, 1992.
- [16] G.H. James, T.G. Carne, J.P. Lauffer, The natural excitation technique (NExT) for modal parameter extraction from operating wind turbines, Technical Report, Sandia National Laboratories, 1993. SAND92-1666.
- [17] G.H. James, T.G. Carne, J.P. Lauffer, The Natural Excitation Technique (NExT) for modal parameter extraction from operating structures, *Journal of Analytical and Experimental Modal Analysis* 10 (4) (1995) 260-277.
- [18] G.H. James, T.G. Carne, P. Veers, Damping measurements using operational data, *ASME Journal of Solar Energy Engineering* 118 (1996) 190-193.
- [19] M. Ozbek, D.J. Rixen, T.W. Verbruggen, Remote monitoring of wind turbine dynamics by laser interferometry: Phase1, in: *Proceedings of the 27th International Modal Analysis Conference*, Orlando, Florida, 2009.
- [20] M. Ozbek, D.J. Rixen, Operational modal analysis of a 2.5 MW wind turbine using optical measurement techniques and strain gauges, *Journal of Wind Energy* (2012) (Article in Press).
- [21] M. Ozbek, F. Meng, D.J. Rixen, M.J.L. van Tooren, Identification of the dynamics of large wind turbines by using photogrammetry, in: *Proceedings of the 28th International Modal Analysis Conference*, Jacksonville, Florida, 2010.
- [22] M. Ozbek, D.J. Rixen, Optical measurements and operational modal analysis on a large wind turbine: Lessons learned, in: *Proceedings of the 29th International Modal Analysis Conference*, Jacksonville, Florida, 2011.
- [23] T.G. Carne, A.R. Nord, Modal testing of a rotating wind turbine, Technical Report, Sandia National Laboratories, 1983. SAND82-0631.
- [24] A.D. Wright, N.D. Kelley, R.M. Osgood, Validation of a model for a two-bladed flexible rotor system: Progress to date. In: *Proceedings of 37th AIAA Aerospace Sciences Meeting*. Reno, Nevada, 1999. AIAA-1999-0060.
- [25] K.Thomsen, J.T. Petersen, E. Nim, S. Øye, B. Petersen, A method for determination of damping for edgewise blade vibrations, 3 (2000) 233–246.
- [26] C. Kong, J. Bang, Y. Sugiyama, Structural investigation of composite wind turbine blade considering various load cases and fatigue life, *Energy* 30 (2005) 2101-2114.
- [27] G.P. Corten, J.C. Sabel, Optical motion analysis of wind turbines, Delft University of Technology, SV Research Group, 1995. ISBN 90-75638-01-9.
- [28] G.P.Corten, Optical Motion analysis of wind turbines in, *Proceedings of European Union Wind Energy Conference*, Bedford UK, 1996.
- [29] Y. Tamura, M. Matsui, L.C. Pagnini, R. Ishibashi, A. Yoshida, Measurement of wind-induced response of buildings using RTK-GPS, *Journal of Wind Engineering Industrial Aerodynamics* 90 (2002) 1783–1793.

- [30] S. Nakamura, GPS measurement of wind-induced suspension bridge girder displacements, *ASCE Journal of Structural Engineering* 126 (12) (2000) 1413–1419.
- [31] P. Breuer, T. Chmielewski, P. Gorski, E. Konopka, Application of GPS technology to measurements of displacements of high-rise structures due to weak winds, *Journal of Wind Engineering and Industrial Aerodynamics* 90 (3) (2002) 223–230.
- [32] A. Nickitopoulou, K. Protopsalti, S. Stiros, Monitoring dynamic and quasi-static deformations of large flexible engineering structures with GPS: Accuracy, limitations and promises, *Engineering Structures* 28 (2006) 1471-1482.
- [33] L.W.M.M Rademakers, T.W. Verbruggen, P.A. van der Werff, H. Korterink, D. Richon, P. Rey, F. Lancon, Fiber optic blade monitoring. in: *European Wind Energy Conference*, London, 2004.
- [34] K. Schroeder, W. Ecke, J. Apitz, E. Lembke, G. Lenschow, A fiber Bragg grating sensor system monitors operational load in a wind turbine rotor blade. *Measurement Science and Technology*, 17 (2006) 1167-1172.
- [35] Website, Brüel & Kjær Measurement Systems, <http://www.bksv.com/Products/analysis-software/acoustics/sound-power-determination/wind-turbine-sound-power-7914.aspx?sortOrder>, [accessed March 2013]
- [36] E.M. Mikhail, J.S. Bethel, J.C. McGlone, *Introduction to modern photogrammetry*, Wiley & Sons, New York, 2001.
- [37] M. Ozbek, D.J. Rixen, O. Erne, G. Sanow, Feasibility of monitoring large wind turbines using photogrammetry, *Journal of Energy* 35 (12) (2010) 4802-4811.
- [38] T.G. Carne, G.H. James, The inception of OMA in the development of modal testing technology for wind turbines, *Mechanical Systems and Signal Processing* 24 (2010) 1213-1226.
- [39] S. Chauhan, M.H. Hansen, D. Tcherniak, Application of Operational Modal Analysis and Blind Source Separation / Independent Component Analysis Techniques to Wind Turbines in: *Proceedings of the 27th International Modal Analysis Conference*, Orlando, Florida, 2009.
- [40] M.S. Allen, S. Chauhan, M.H. Hansen, Advanced operational modal analysis methods for linear time periodic system identification in; *Proceedings of the 29th IMAC International Modal Analysis Conference*, Jacksonville, Florida, 2011.
- [41] M.S. Allen, M.W. Sracic, S. Chauhan, M.H. Hansen, Output-only modal analysis of linear time-periodic systems with application to wind turbine simulation data, *Mechanical Systems and Signal Processing* 25 (2011) 1174-1191.
- [42] D. Tcherniak, S. Chauhan, M.H. Hansen, Applicability limits of operational modal analysis to operational wind turbines, in: *Proceedings of the 28th International Modal Analysis Conference*, Jacksonville, Florida, 2010.
- [43] D. Tcherniak, S. Chauhan, M. Rossetti, I. Font, J. Basurko, O. Salgado. Output-only Modal Analysis on Operating Wind Turbines: Application to Simulated Data in: *Proceedings of European Wind Energy Conference*, Warsaw, Poland, 2010.
- [44] S. Chauhan, D. Tcherniak, M.H. Hansen, Dynamic Characterization of Operational Wind Turbines using Operational Modal Analysis in: *Proceedings of China Wind Power 2010*, Beijing, China, 2010.

Chapter 1

- [45] P. Mohanty, D.J. Rixen, Operational modal analysis in the presence of harmonic excitation, *Journal of Sound and Vibration* 270 (2004) 93-109.
- [46] P. Mohanty, D.J. Rixen, Modified SSTD method to account for harmonic excitations during operational modal analysis, *Mechanism and Machine Theory* 39 (12) (2004) 1247-1255.
- [47] C. Gentile, A. Saisi, Ambient vibration testing and condition assessment of the Paderno iron arch bridge (1889), *Construction and Building Materials*,25 (2011), 3709-3720.
- [48] F. Meng, M. Ozbek, D.J. Rixen, M.J.L. Tooren, Comparison of system identification techniques for predicting dynamic properties of large scale wind turbines by using the simulated time response, in: *Proceedings of the 28th International Modal Analysis Conference*, Jacksonville, Florida, 2010.

CHAPTER 2

Feasibility of Monitoring Large Wind Turbines Using Photogrammetry

Muammer Ozbek^{a,*}, Daniel J.Rixen^a, Oliver Erne^b, Gunter Sanow^b

^a, Delft University of Technology, Faculty of Mechanical Engineering, Mekelweg 2, 2628CD, Delft, the Netherlands

^b, GOM mbH (Optical Measuring Techniques), Mittelweg 7-8, 38106 Braunschweig, Germany

Abstract

Photogrammetry, which is a proven measurement technique based on determination of the 3D coordinates of the points on an object by using two or more images taken from different positions, is proposed to be a promising and cost efficient alternative for monitoring the dynamic behavior of wind turbines. The pros and cons of utilizing this measurement technique for several applications such as dynamic testing or health monitoring of large wind turbines are discussed by presenting the results of the infield tests performed on a 2.5 MW - 80 meter diameter - wind turbine.

Within the scope of the work, the 3D dynamic response of the rotor is captured at 33 different locations simultaneously by using 4 CCD (charge coupled device) cameras while the turbine is rotating. Initial results show that the deformations on the turbine can be measured with an average accuracy of ± 25 mm from a measurement distance of 220 meters. Preliminary analyses of the measurements also show that some of the important turbine modes can be identified from photogrammetric measurement data.

This work was published in Energy (2010) 35: 4802-4811.

1. Introduction

It is state of the art to use accelerometers and/or strain gauges placed inside the blade or tower for dynamic measurements performed on wind turbines [1-10]. However, these measurement systems are sensitive to lightning and electro-magnetic fields. Besides, some extra installations inside the blades such as placement of cables for power supply and data transfer are required for these applications. The signals from rotating sensors on the blades are transferred to stationary computer via slip rings or by radio/wireless transmission. For large commercial turbines the required installations and preparations (sensor calibration) might be very expensive and time consuming [11].

Moreover, the frequency range of the vibrations to be measured also limits the use of these sensors. Accelerometers cannot provide very accurate measurements for low frequency vibrations (0.3 - 1 Hz) that are expected to dominate the response of large wind turbines. Therefore only the higher frequency (greater than 1Hz) vibrations can be captured accurately. The complicated nature of wind loads also makes the efficient use of these sensors on these specific structures very difficult. Since the deflections under the action of wind loading can be considered as the sum of a slowly changing static part and a rapidly changing dynamic part, identification of low frequency vibrations plays a crucial role in predicting the wind response of structures [12]. Several researchers reported that in wind response measurements, accelerometers should be used together with other systems such as GPS (Global Positioning System) which are able to detect these low frequency motions accurately [13-15]. However, it is also not practical to place the GPS sensors in the blade structure.

Fiber optic strain gauges are proposed to be a promising alternative to accelerometers and conventional strain gauges since optical sensors are not prone to electro-magnetic fields or lightning. However, it is reported that some additional feasibility tests are still needed to ensure the effective and cost efficient use of this measurement system. The factors affecting the performance of the fiber optic sensors such as sensitivity to humidity and temperature variations and the required error compensation methods should also be investigated further [16,17].

This work aims at investigating the feasibility of applying photogrammetry to large wind turbines and the accuracy that one can expect with current state-of-the-art software and hardware. The final goal is to use the measurements for model verification and health monitoring of wind turbines. Hence, as a following study after the estimation of the measurement accuracy, the applicability of Operational Modal Analysis on the measurements to identify the modal behavior of wind turbines will be discussed as the next research step.

2. Photogrammetric measurement techniques

Photogrammetry is a measurement technique where 3D coordinates or displacements of an object can be obtained by using the 2D images taken from different locations and orientations. Although each picture provides 2D information only, very accurate 3D information related to the coordinates and/or displacements of the object can be obtained by simultaneous processing of these images as displayed in Figure 2.1.

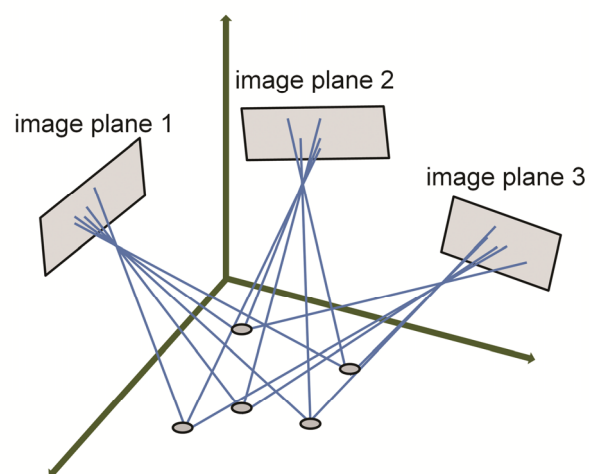


Figure 2.1. Simultaneous process of 2D images taken from different locations

Several applications of photogrammetric measurements are currently in use and proven to provide very accurate measurements for a wide variety of disciplines. The method is sometimes called “videogrammetry” (which implies that sequences of the pictures are used to monitor the dynamic response of an object) or “stereo-photogrammetry” (indicating that two or more cameras are employed simultaneously). Despite these

minor differences, all the methods are based on similar mathematical relationships established between the 3D position of an object and its 2D representations [18].

Although photogrammetry is widely used in measuring the coordinates and displacements of the objects, its use is limited to small measurement volumes and the measurements are usually performed in laboratories or similar controllable environments. Within this small measurement volume it can be efficiently used for different purposes such as;

- 3D shape determination, modeling and reverse engineering [19-21]
- Static or dynamic deformation measurements [22-30]
- Modal analysis and system identification [31-36].

Photogrammetry can also be used within large volumes but these measurements are typically static. 3D modeling and reverse engineering are usually the only application fields. However, efficient use of photogrammetry in large measurement volumes for dynamic measurements is still an unknown. There are some important issues to be considered before utilizing this technique for monitoring of large structures such as wind turbines which have very specific characteristics and challenging operating conditions.

The size of the object to be tracked is usually restricted due to the problems such as insufficient illumination, difficulties in calibration, or low resolution of the cameras. If the target to be tracked (for instance the tip of the blade) experiences large displacements and rotations throughout the measurement volume, this can result in significant changes in reflection angles and the orientation of the targets during the measurements. Besides, these targets should also be illuminated sufficiently during the entire measurement, and the only possible solution is to illuminate the whole measurement volume.

For rapidly moving objects, the shutter time (i.e. the period during which the image is created by the light entering through the shutter) should be small enough to limit blurring caused by the motion of the object during the formation of the image. However, if the shutter time is very small, proper illumination becomes more important and a stronger

light intensity is needed to provide sufficient contrast. In addition to these problems, since the number of pixels (resolution) of the utilized camera systems is limited, the pixel per area is significantly reduced if the area to be viewed is very large.

Corten and Sabel [11, 37] were the first in applying this measurement method to a wind turbine. They performed several vibration measurements on a 2 bladed wind turbine (10 meters diameter) while the turbine was in operation. For this purpose, they placed several markers both on the blades and on the tower. In order to increase the measurement accuracy they located the camera systems on tripods whose heights were approximately one third of the height of the tower. Such an approach would certainly improve the accuracy of the photogrammetric measurements but at the same time makes the applicability of the method to larger turbines more difficult. Based on the results of the consistency checks, the authors reported that the measurement error was directly related to the size of the observed object or field and in the range of 0.043% (or 1/2,500) of field of view. Corten and Sabel also aimed at comparing the measured 3D coordinates with the strain measurements taken by strain gauges installed in the blades but they could only compare the two data sets for a qualitative confirmation of the method. Quantitative comparisons showed large differences. The authors concluded that both systems in fact measure different physical quantities, and that some motions such as bending of the rotor axis, small tilt and yaw motion of the nacelle and teeter cannot be detected by strain gauges. Even detectable motions might not have a linear relationship with the strains measured locally. However, the authors also reported that photogrammetry would be a very promising method to monitor wind turbine dynamics if the hardware and software technology progressed.

The photogrammetric measurements presented in this article were performed similarly to Corten and Sabel [11, 37] in terms of using reflective round markers and post-processing the image. In the present work however, state-of-the-art software and hardware were used, all the measurement systems were located on the ground and a very large turbine was measured in operation.

3. Measurement setup

3.1 The test turbine

Our tests were conducted on a pitch controlled, variable speed Nordex N80 wind turbine with a rated power of 2.5 MW. The turbine has a rotor diameter and tower height of 80 meters and can be considered as one of the largest wind turbines that are commercially available at the time the tests were conducted. Detailed information about the technical properties of the wind turbine can be obtained through the website of the manufacturer [38]. The measurements were performed by GOM mbH [39] (GOM Optical Measuring Techniques) at the ECN (Energy Research Center of the Netherlands) wind turbine test site located in Wieringermeer, the Netherlands. More detailed information about the facilities of the test site can be found through the related website [40].

3.2 Camera layout and marker placement

Figure 2.2 shows the measurement setup and the layout of the camera-flash systems. A modified GOM PONTOS system consisting of four CCD cameras was used to monitor the dynamic behavior of the turbine in operation. The whole turbine structure was captured in all the pictures taken which resulted in a very large area (120 m high - 80 m wide) to be viewed by each camera continuously during the entire measurement period. The distance between the camera-flash light systems and the turbine was 220 meters.

The cameras and the high intensity LED (light emitting diode) based flashes were synchronized by a central PC. This central PC controlled all the communication between the data acquisition system and the cameras, and also the triggering signals and power transferred to the flashes. The sampling frequency of the measurements was 28 Hz which can be considered sufficient compared to the frequency range (0.3- 5 Hz) of the vibrations expected to be observed.

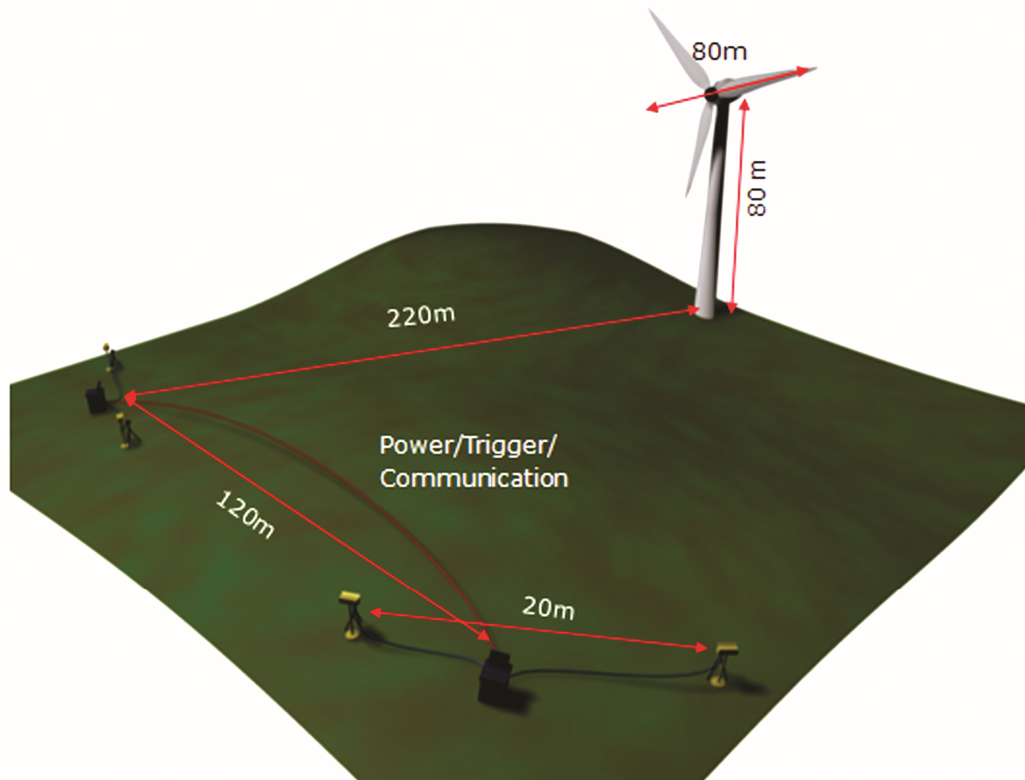


Figure 2.2. The measurement setup and camera locations (provided by GOM mBH [39])

Photogrammetry requires some markers to be placed on the object to be tracked. The camera systems follow the motion of these markers from different orientations and construct the 3D deformation vectors. These markers are made up of retro-reflective materials (1000 times more reflective than the background material) to increase the reflectivity of the target and to provide a better visibility. In our testing, a total of 55 markers (11 markers on each blade and 22 markers on the tower) were placed on the turbine. Since they are in the form of very thin stickers (round shaped - 400 mm diameter), they are not expected to affect the structural or aerodynamic properties of the blade. Figure 2.3 a-b shows the placement of the markers on the turbine.



Figure 2.3 a-b. Installation of markers on the wind turbine

It should be noted that it only took 2 professional people 6 hours to place 55 markers on the turbine. Considering the fact that each marker acts as an independent sensor, it can be concluded that it is almost impossible to reach such a high sensor installation speed by using conventional sensor technologies (accelerometers, piezoelectric or fiber-optic strain gauges). The final distribution of the markers on the turbine can be seen in Figure 2.4 a-b. Although the pictures shown in Figure 2.3 and Figure 2.4 were captured by a handheld digital camera using its flash light only, the markers can be seen easily. The displacement data obtained by using the tower markers are not presented or used in this article since tower measurements were interrupted each time a blade passed in front of it.

3.3 Illumination requirements

Proper illumination plays a crucial role in obtaining high quality images. Initial computer simulations and feasibility tests showed that the use of conventional flash-light systems would require a large amount of power for the flashes. In order to prevent the technical problems that can be encountered due to this high power requirement, a different high intensity LED based flash system was used for the measurements. For this LED illumination system a power supply of 2 kW (provided by a small size commercial generator) was sufficient to illuminate the turbine throughout the measurements.

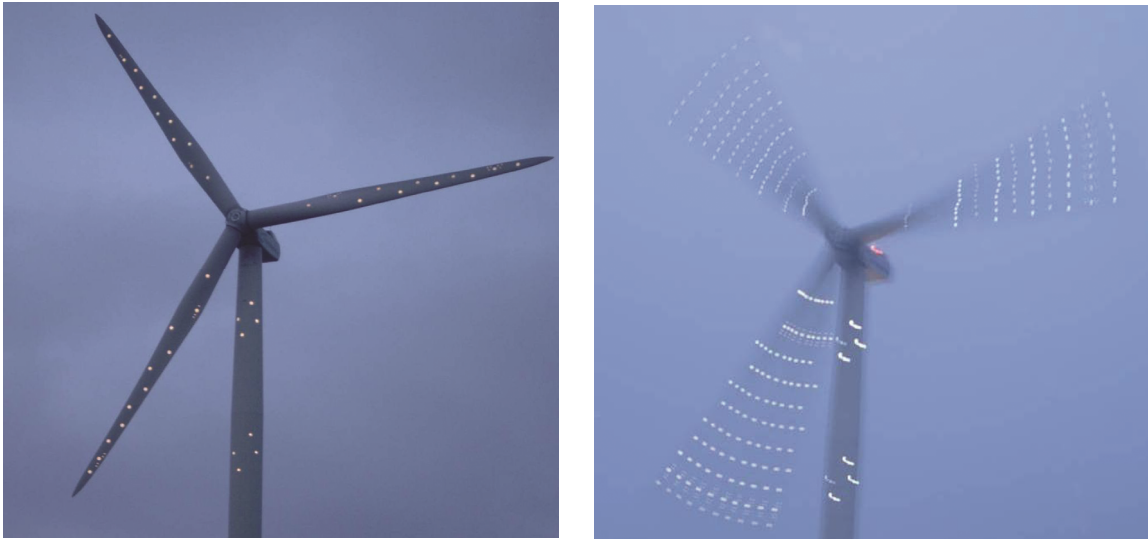


Figure 2.4. a-b: The Layout of markers on the turbine

However, the use of this new flash system during daytime is limited. In photogrammetry, the contrast between the marker and the background material is very important. If a weak flash is used during daytime, the difference between the reflection of the flash light from the marker and the reflection of the sun light from the background material is not so high. The advantage of the retro-reflective material is that it directly reflects the light beam back to its source and it is 1000 times more reflective than the blade material but despite all these advantages sun light will always be more dominant. Therefore to get a high contrast without using a powerful flash light the experiments were conducted during night time.

As the size of the object to be tracked increases, illumination and the required power become a more critical problem. Several researches [21] reported that they had to perform the photogrammetric measurements in a dark laboratory environment because the sufficient contrast levels could only be reached when the ambient lighting was off and the LED based flashes were used as the only light source in the experiment.

3.4 Camera calibration

Calibration of the cameras is one of the most important factors that directly affect the accuracy obtained and can be investigated in 2 groups namely intrinsic and extrinsic calibration. The intrinsic calibration is required to determine the geometrical and optical

characteristics of the cameras whereas; the extrinsic calibration parameters describe the camera positions and orientations with respect to a predefined global coordinate system.

Conventional camera calibration techniques can be roughly classified into two categories: photogrammetric calibration and self-calibration. For photogrammetric calibration, a calibration object having similar dimensions with the measured structure is used. This calibration object can be either a 3D object or a 2D planar pattern with precisely known geometry and dimensions. Although this technique is widely used for the measurements taken in the laboratory environment, for the tests performed on large structures the use of these calibration tools is highly impractical.

On the other hand, self-calibration (bundle adjustment method) is performed using a set of highly convergent overlapping images only. Any photogrammetric network comprising two or more camera stations and sufficient number of control points (common to each image) constitutes an over-determined nonlinear observation equation system, the parameters for which can be obtained via a least-squares estimation process [28]. This method also enables both extrinsic and intrinsic calibration parameters to be determined simultaneously.

In this study, the camera calibration was performed by using the markers distributed throughout the turbine structure and the mentioned least square based calibration algorithm. A small 2D planar pattern was also utilized to provide supplementary information related to the internal camera optical parameters.

4. Acquiring vibration data and post processing

Since the turbine was not kept at a fixed yawing angle during the measurements, the relative angle between the normal of the rotation plane and the 4 camera axes changed during the measurements. In order to prevent possible sources of error, rotation plane and the corresponding axes attached to this plane were continuously updated throughout the measurements. The deformations shown below were defined with respect to this continuously updated rotation plane and coordinate axes.

The first step in calculating the rotation plane is the determination of center of rotation. Since the markers on the rotor are moving on a circular path, this can easily be done by observing the path travelled by a marker and fitting a circle to it by using a least square based algorithm. This operation is performed for several markers. The resultant center coordinates can be slightly different depending on the marker chosen. Therefore the average of the coordinates are calculated and used to minimize the error.

Following the calculation of rotation center and plane, a rigid body correction (also called as de-rotation) is applied to the actual deformation vectors measured. A marker selected to be tracked experiences very large displacements during a complete cycle of the blade. Hence, the displacement component coming from rigid body motion of the rotor is subtracted from the measured real displacement of each marker to provide a better visualization and interpretation of the data. Therefore, although the results displayed below include rotational effects they can be evaluated as if they were measured on a stationary (parked) turbine vibrating under the action of wind loads.

A typical displacement time history measured in flapwise direction for the tip markers of 3 blades can be seen in Figure 2.5. It should be noted that these displacements are calculated with respect to the initial coordinates of the markers described by the first picture taken during rotation. Since the blades are already deformed under the action of wind loads at this instant, the first image used as the reference is not expected to represent the exact undeformed shape of the rotor. However, the selection of initial coordinates does not have an effect on the amplitudes of the calculated relative displacements or the accuracy of the measurements. In Figure 2.5 the horizontal axis represents the number of rotation cycles in the recorded data. The maximum (peak to peak) amplitudes of the relative displacements measured during 5 different measurements are displayed in Table 2.1. It can be seen that the tip of the blade can experience a relative displacement up to 102.4 cm during rotation.

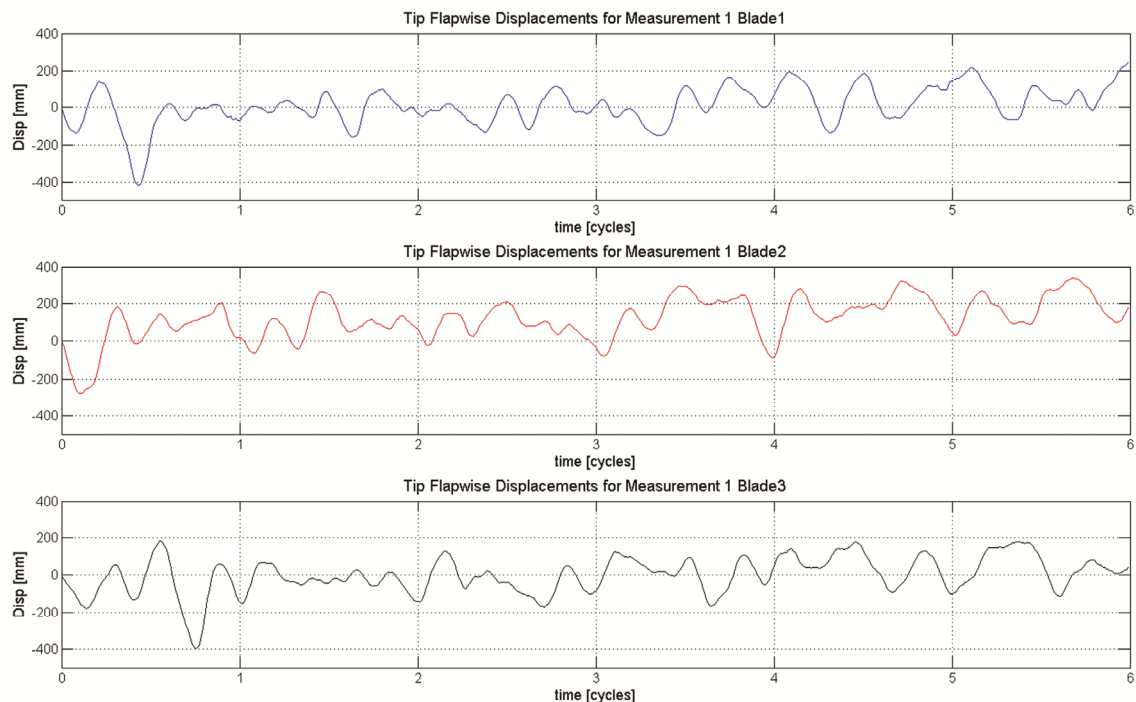


Figure 2.5. Time normalized tip flapwise displacements recorded during measurement 1

Relative Tip Disp. (mm)	M1	M2	M3	M4	M5
Blade 1 - tip marker	659	605	670	1024	1005
Blade 2 - tip marker	617	594	703	895	898
Blade 3 - tip marker	576	695	699	1007	961

Table 2.1. The flapwise displacements (peak to peak) calculated for tip marker through measurement 1-5

5. Estimation of the measurement accuracy

In photogrammetry, the measurement accuracy is usually described either in terms of pixel or the ratio of the absolute measurement error to the field of view. The accuracy is mainly related to the type and resolution of the cameras, illumination intensity, the size and visibility of the targets, and camera calibration.

Very high accuracies such as 1/50,000 (1 part in 50,000) of the observed field of view can be reached in controllable laboratory environments by using 3D calibration tools, 3D control targets and powerful illumination systems, but these ideal conditions are generally not met for infield tests performed on large wind turbines.

Several researchers performing indoor photogrammetric measurements similar to those described in this work, report average accuracies varying between 1/8,000 and 1/15,000, [28-31]. An extensive research program has been recently conducted by NASA to investigate the feasibility of using photogrammetry to measure the dynamic behavior of ultra light weight membrane-type space structures. Results indicate that the coordinate measurement errors calculated for X, Y and Z axes may differ significantly depending on the locations and the orientations of the cameras and the direction of the observed motion [21, 26]. In-plane coordinates and displacements can generally be measured with accuracies changing between 1/28,000 and 1/14,000 of field of view. However, the errors calculated for out-of-plane direction (depth) are much larger and in the range of 1/5,000. The researchers also reported that these values represent random measurement errors and can only be used for the overall measurement accuracy if systematic or gross errors are negligible [26]. It should be noted that these accuracies are computed for test objects having dimensions varying between 5-15 meters and test setups in which no major systematic measurement errors are expected. However, wind turbines have very distinct features (large dimensions, components rotating at very high speeds and continuously changing reflection angles) which make photogrammetric measurements much more challenging.

A common method to determine the measurement accuracy is to compare the 3D target coordinates reconstructed from photogrammetry with those measured by more accurate surveying systems such as theodolites, “total stations” (used in monitoring of civil engineering structures) or laser measurement devices. However, these systems measure the marker coordinates not simultaneously but sequentially. Since the markers on a wind turbine in the field are never fully at standstill, such measurements would not be suitable to validate the calibration parameters and to determine the measurement accuracy. Therefore, all the critical pre or post processing operations and the corresponding error estimation analyses have been done by using the measurements themselves i.e. by verifying the consistency of the data recorded.

In our tests, the error was estimated by checking whether or not the distance between target points remains constant throughout the measurement. In particular, we will use

the fact that the distance between the calculated center of rotation and a marker should barely change in time and can thus be used to estimate the accuracy of the measurements. Negligible length changes are expected in the blades due to centrifugal or gravity forces acting on the rotor and the out-of-plane deformation is small compared to the distance between selected points. If any difference (called as elongation or contraction in this text) is observed, it can mainly be attributed to the inaccurate measurement of the marker coordinates and therefore, can be used to estimate the accuracy.

The measurement errors revealed by the change of distance between markers and the center of rotation are expected to be mainly caused by calibration problems, reflection quality changing during the rotation and some other physical factors affecting the visibility of the markers. Depending on these factors, the measurement errors can be classified in two groups, namely *random* and *systematic* errors.

Figure 2.6 displays the labeling of the markers used to compute elongations and thereby estimate the error. It can be seen from this figure that the markers are placed on surfaces having different curvatures, which directly affects the intensity of the reflected light and the shape seen by the cameras. The markers close to the tip were placed on a relatively flat surface whereas the ones close to the hub are placed on a more curved surface. It should be noted that the marker located between 1 and 2 was dysfunctional and not used in the analyses.

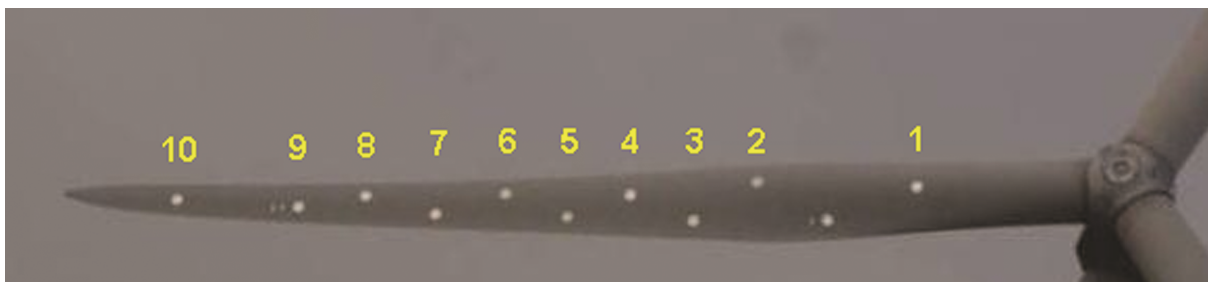


Figure 2.6. The locations and corresponding labeling of the markers used in error estimation.

The light reflected by the marker and their recorded shape will also vary during the rotation of the rotor of the turbine, inevitably affecting the quality of the measurements.

Figure 2.7 displays how the horizontal reflection and camera view angles change during a complete cycle of rotation. It should be noted that the effective view or reflection angle is a combination of horizontal and vertical angles and cannot be fully represented in a 2D plot. As can be seen from Figure 2.7 the horizontal reflection angles can vary between 0 and 30 degrees for the tip marker. Similarly, the vertical reflection angles can change between 15 and 35 degrees.

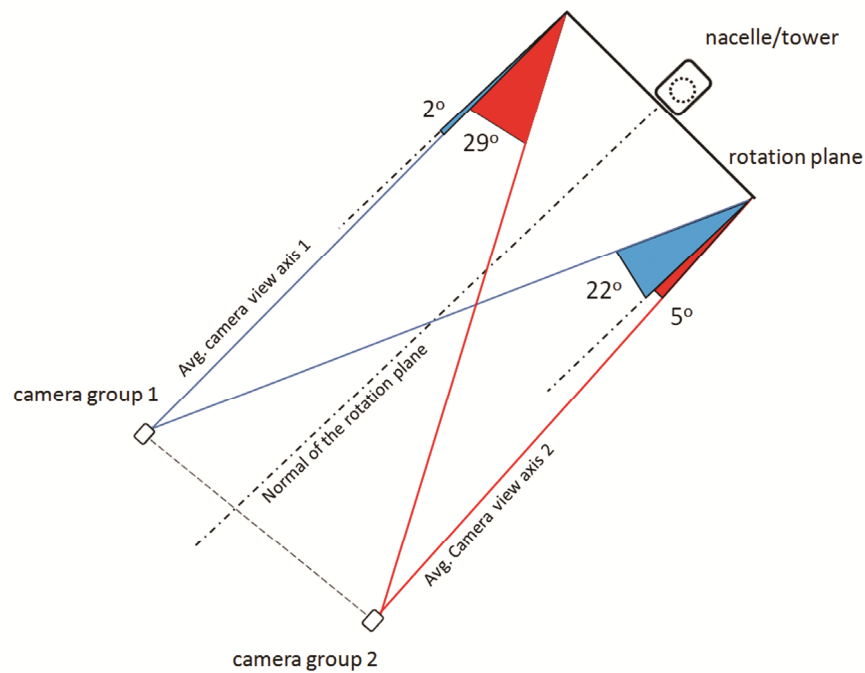


Figure 2.7. The change of horizontal reflection angles (for tip marker) during rotation

Figure 2.8 and Figure 2.9 display the change of the distance (also called as elongation) between the center of rotation (c.o.r) and markers 10 and 1 respectively. It should be noted that the original data blocks include 6 complete cycles of rotation. In order to see the repeating pattern of the change, the analyzed record was divided into 6 parts and these cycles were superposed in the plots of Figure 2.8 and Figure 2.9, as a function of the azimuth angle (zero when the blade is at the top). For Figure 2.8 the legend G1 B1 M10 C1 stands for **(G1)** Measurement1 - **(B1)** Blade1 – **(M10)** Marker10 – **(C1)** Cycle1. These figures show the elongation values obtained by applying a low-pass filter with a cut-off frequency of 5 P (P being the rotation frequency of the rotor) on the raw data.

The high frequency component, which is attributed to the random measurement error, has only a minor contribution (± 5 mm) and will be eliminated by the applied low-pass filter.

In Figure 2.8 and Figure 2.9 the polar plots on the right show where the maximum elongation points are reached for markers 5 to 10. It can easily be noticed from the figures that the elongation is highly periodic and azimuth-angle dependent, which implies that it is mainly caused by repeating systematic errors. In order to check the reliability of the elongation information, these analyses were conducted for different measurements and for the entire set of 33 markers placed on the rotor. The comparisons showed that, although the 3D displacements experienced by the markers may differ depending on the test number, the graphs of the calculated elongations were almost identical for the markers that are placed on similar locations on the blade, which strongly reinforces the fact that there is a systematic measurement error whose amplitude is determined by the location of the marker only.

Repeating systematic errors can be caused by different physical factors, which have different periodic effects on the system. A variation in the reflection quality is expected to appear once per cycle and will thus cause a dominant $1P$ component, where P denotes the rotational frequency of the rotor. On the other hand, calibration problems (either internal or external), or miscalculation of the rotational plane can cause a harmonic elongation twice a cycle and have a dominant $2P$ component. Similarly, a measurement error of $2P$ is likely to occur when the tracked marker passes through the regions where the view and reflection angles approach to the limit values. During the rotation, the markers move on a circular path, which should be fully captured in each one of the 2D images analyzed. For the outermost markers the horizontal and vertical view angles approach to critical values twice a cycle.

The instantaneous location of the traced marker in the 2D image i.e. its distance to the edges of the 2D picture can be related to the amplitude of the elongation measured at that location. As can be seen in Figure 2.8, the amplitudes of the elongations calculated at around 90 and 270 degrees of azimuth angles are not the same. Normally, the same

amount of error would be expected for these locations. Since the center of rotation does not exactly coincide with the center of the image, the markers are closer to the edge of the 2D image around 270° azimuth than they are at around 90° azimuth. The rotor which is eccentrically located in the 2D image causes the systematic measurement errors to differ at those locations.

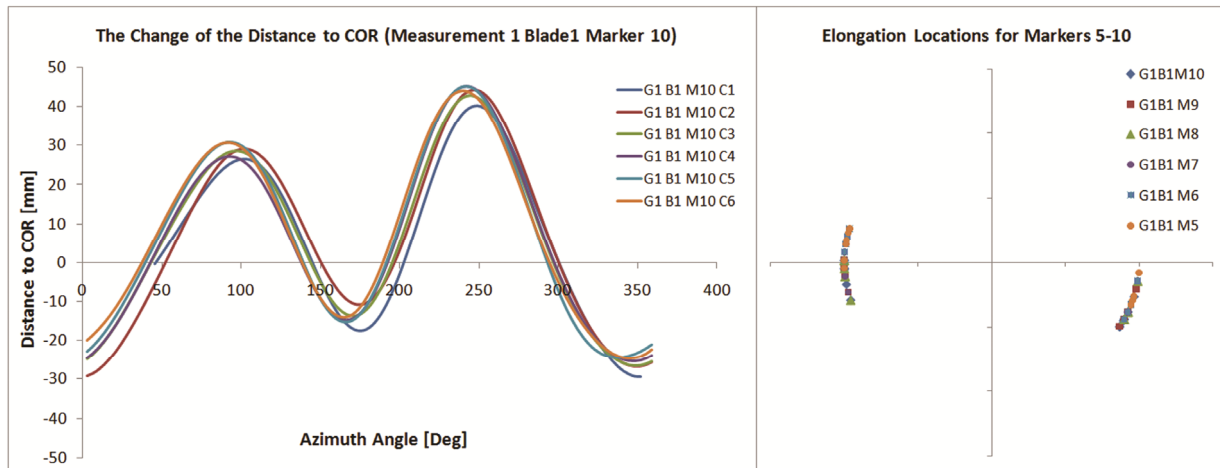


Figure 2.8. Elongation between marker 10 and c.o.r. Polar locations of maximum elongation for M5-M10

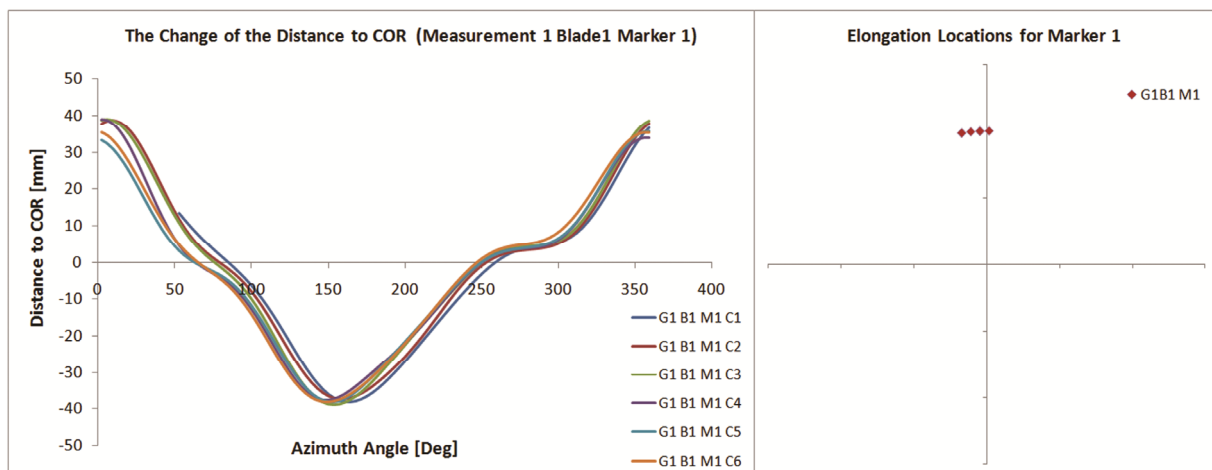


Figure 2.9. Elongation between marker 1 and c.o.r. Polar locations of maximum elongation for M1

6. Order analysis of the elongation error

The frequency domain analysis of the elongation data provides important information to be used in determining the source of the error. Figure 2.10 aims at showing the

important frequencies identified in the corresponding length changes. The frequencies, normalized with respect to the rotational frequency, are displayed along the X-axis. The Y-axis represents the marker number. The numbering of the markers was depicted in Figure 2.6. The Z-axis represents the amplitude of the Fourier transform. As can be seen from the figure the change of the distance calculated for marker 10 has a strong 2P and a relatively weaker 1P component whereas the one calculated for marker 1 has a very dominant 1P and a much weaker 2P component. 1P and 2P components always exist in the Fourier transforms of the elongation data but their relative amplitudes differ depending on the location of the marker.

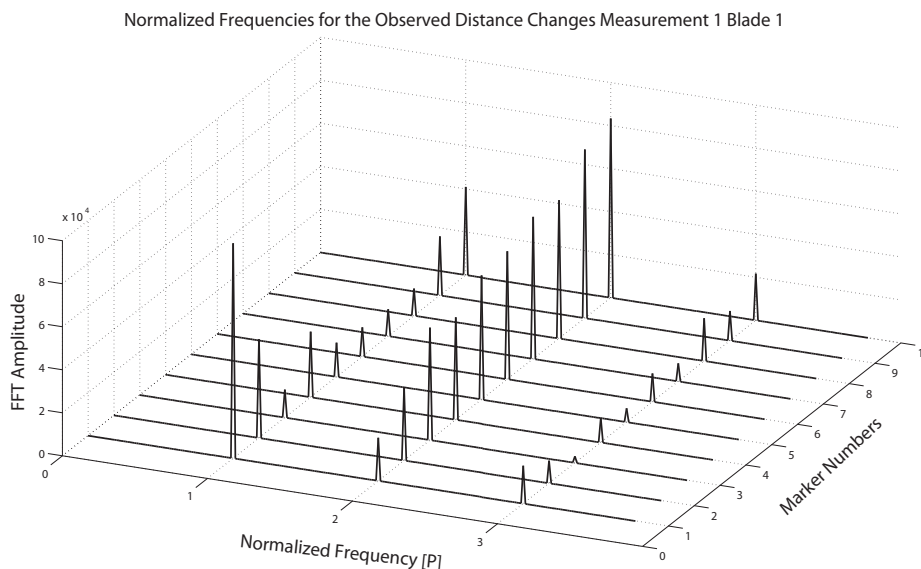


Figure 2.10. Frequency distribution of the observed distance changes (Measurement 1, Blade 1)

Markers 1 and 2 are placed on curved surfaces close to the root of the blade. The measurement errors calculated for these markers are expected to be mainly related to the reflection quality and marker orientation varying during the rotation. Although 1 P component of the error can be seen in all the 10 series its contribution in the overall error is dominant for Markers 1 and 2 only. As the distance from the center of rotation increases the contribution of 2P component gradually becomes more important, probably because those markers are closer to the boundaries of the field of view where

calibration errors and artifacts due to projection on the plane of rotation become more dominant.

Let us observe in Figure 2.10 that the contribution of order of 3P (as well as all higher orders) is significantly lower than the components of order 1P and 2P, and they will not be further discussed.

7. The possibility of correcting the systematic measurement errors

From the discussion in the previous section, it is clear that the causes of systematic errors can be traced back to geometry and optical effects varying along the circular path of the markers in the field of view of the cameras. Hence one could be tempted to use this knowledge to correct the measurements for those errors, such that the only remaining errors would be the random errors (arising from unavoidable pixel quantization and fitting errors).

Three different approaches can be potentially used for performing such a correction in future research.

- a. Properly calibrating the measurement setup by identifying the systematic error for all locations of the field of view. This would require either a very detailed theoretical analysis of optical errors and marker orientation effects, or a reference measurement using lasers for instance. Such an approach seems however difficult and unpractical.
- b. Estimating the error using the computation of elongations as described in the previous two sections, one could try to reconstruct the error in the 3D coordinates of the markers. Assuming for instance that the position of the center of rotation is estimated without error, and having good knowledge on the statistical distribution and correlation of the coordinate error at the different locations of the field of view, one could estimate the most likely position of the marker.
- c. One could also use a priori knowledge about the expected deformation of the blades. As an example, consider the components of order 1P of the systematic error in Figure 2.10. Such a contribution to the deformation of the blade in the low frequency range is not expected. Hence projecting the measurements on a small

set of expected deformation modes (obtained for instance from simple beam theory) could lead to a procedure to filter out part of the measurement error. Note however that the 2P contribution to the systematic error will probably not be removed by such a spatial filtering approach since, as can be seen in Figure 2.10, the 2P components exhibit a spatial distribution along the blade that is similar to the expected deformation. This is due to the very origin of the 2P as explained in the previous section. Hence such an approach would mainly smooth out the errors observed on markers 1 and 2.

8. Frequency Domain Investigation of Measured Vibration Data

Figure 2.11 and Figure 2.12 show typical examples of PSD (Power Spectral Density) graphs of edgewise and flapwise vibrations measured by photogrammetry. It should be noted that all the frequencies displayed below are normalized with respect to the rotational frequency. In order to protect the manufacturer's interests, the real frequencies are not given explicitly in this article. Figure 2.11 and Figure 2.12 are presented to provide a 3D frequency distribution which also includes the information related to the measurement location. The X-axis represents the normalized frequencies identified from the analyzed data; the Y-axis corresponds to the marker number (defined in Figure 2.6) and the Z-axis represents the computed PSD amplitude. The 1P and 2P components, and first edgewise mode can be recognized from Figure 2.11.

As can be seen from Figure 2.12, flapwise vibration data enables more frequencies to be identified. The integer multiples of rotation frequency up to 4P can be detected from the corresponding PSD graph. The contribution of these P components in the overall motion is consistent with those reported by several researchers [41, 42]. Besides these P components, first flapwise mode can also be seen in Figure 2.12.

Since the response is mainly dominated by the integer multiples of rotational frequency (P components) the other turbine modes which have relatively weaker participations in the overall response and which can also exhibit significant damping cannot be identified easily from PSD plots only. However, several system identification methods enable weaker frequencies to be detected. A more detailed investigation [43] of the measured

turbine response carried out by utilizing these identification methods showed that the second edgewise, second and third flapwise modes of the blades can also be identified. However, further analyses and measurements are needed for validation of observability of these high frequency modes from photogrammetric measurements.

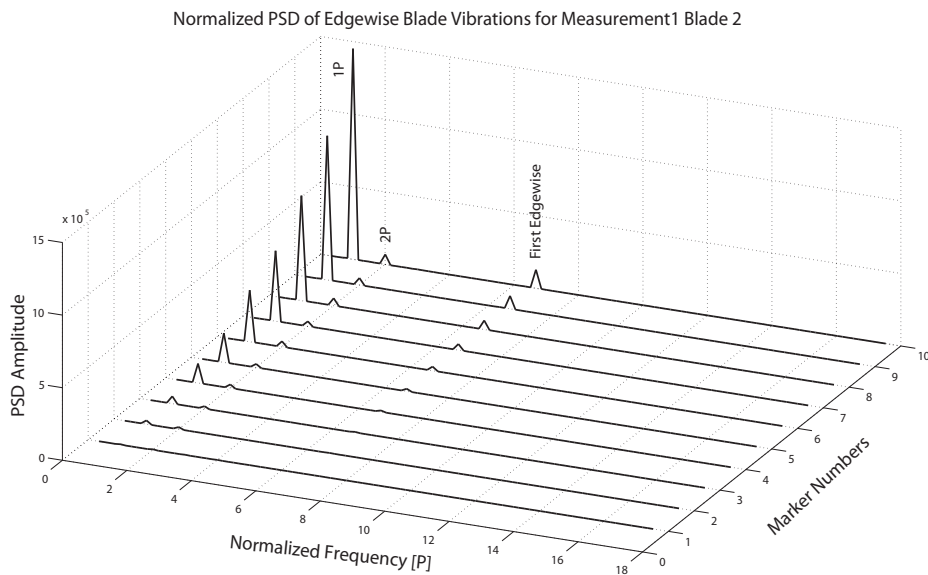


Figure 2.11. Normalized PSD of edgewise blade vibration for measurement 1 Blade 2

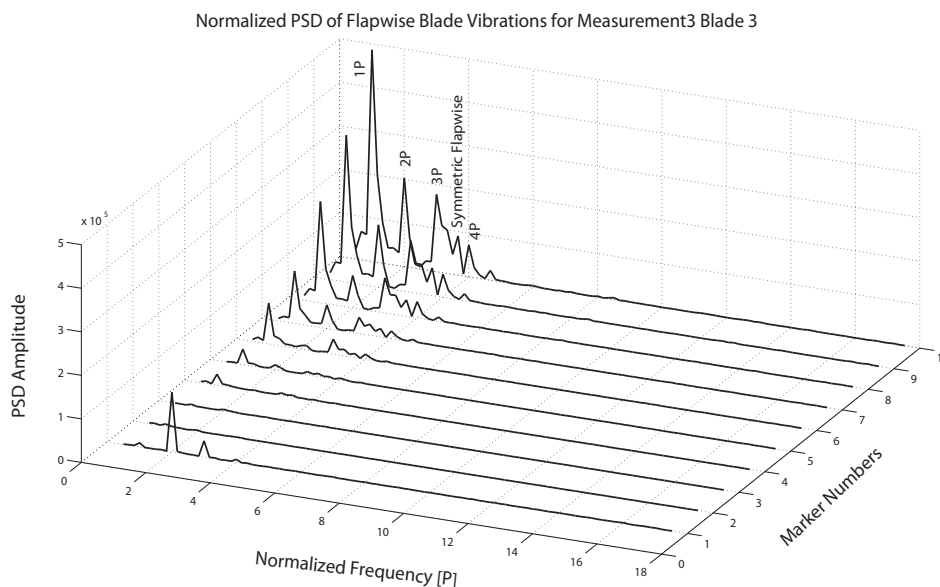


Figure 2.12. Normalized PSD of flapwise blade vibration for Measurement 3 Blade 3

9. Conclusion

Based on the results of the analyses reported in this paper, it can be concluded that the random component of the coordinate measurement error is in the range of ± 5 mm or $1/16,000$ of field of view. This amount is consistent with the random measurement errors reported in literature. If compared to the amplitudes of the deformations (summarized in Table 2.1) that are expected, this accuracy can be considered to be high and even be improved further by using higher resolution cameras.

Initial results show that the deformations on the turbine can be measured with an average accuracy of ± 25 mm from a measurement distance of 220 meters, which is the overall error including both the systematic and the random errors. The maximum value of the systematic error (2P component) was found to be of the order of ± 30 mm in our calculations, the maximum being found for the outermost markers. Since the random error component is usually in the range of ± 5 mm, independent of the marker location, the maximum overall error could reach 35 mm for the tip marker. However, using more sophisticated camera calibration, data processing and comparison techniques can reduce the systematic error further. These ideas are at the center of current research.

Although 1P component of the error can even have higher amplitudes, this can easily be eliminated by spatial filtering, therefore it is ignored.

Even though the measurement error was found to be of the order of 10 percent of the recorded deformations (displayed in Figure 2.5 and summarized in Table 2.1), the data obtained from photogrammetry appeared to be suitable to identify the 1P - 4P modes, as well as some of the lower eigenmodes and eigenfrequencies of the blades in operation. First edgewise and first flapwise modes can easily be identified from Figure 2.11 and Figure 2.12, respectively.

Some other turbine modes having relatively weaker participations can also be identified by using more sophisticated identification algorithms which were not explained in detail in this article. A more comprehensive discussion about the identification of these modes can be found in [43]. The accuracy of the identified modal properties can be increased by reducing the measurement errors (as explained above), performing longer measurements and improving the operational modal analysis methods as pointed out in [43].

Developments over the last decade have resulted in higher resolution and more sensitive cameras, and in efficient software for photogrammetry, so that we believe that photogrammetry can be a versatile and cost-effective technique for health monitoring and dynamic validation of wind turbines.

The markers which are used as displacement sensors can easily be placed on an existing turbine. No extra cable installations for data transfer and power supply are required inside the turbine. Therefore, compared to the conventional sensors (accelerometers, piezoelectric or fiber optic strain gauges), marker installations are very cost efficient and can be completed within very short periods of time. Retro-reflective paints applied on the turbine components during the manufacturing stage in the factory can substitute these markers which may result in a further decrease in the installation costs.

A photogrammetric measurement system which consists of several CCD cameras, flashes and a central PC can be re-used for monitoring several turbines. If continuous

monitoring is not required, all the turbines in a wind farm can be observed by using a single system. The measured data can be stored and used to build a condition monitoring archive. Since all the measurement systems are located on the ground, a possible technical problem can be detected and solved easily.

Wind turbines have very specific characteristics and challenging operating conditions. Although the photogrammetric measurement systems (including both the hardware and image processing software), calibration methods and utilized operational modal analysis techniques were not specifically designed and optimized to be used for monitoring large wind turbines, the accuracy reached in this feasibility study is very promising. It is believed that this accuracy can easily be increased further by utilizing more specialized hardware and data processing methods.

Acknowledgements

This research project was partly funded by the We@Sea research program, financed by the Dutch Ministry of Economical Affairs.

The authors would like to thank ECN (Energy Research Center of the Netherlands) for providing the tests turbine and other technical equipment.

The authors also acknowledge the extensive contribution of Pieter Schuer (GOM mbH), Wim Cuypers (GOM mbH), Theo W. Verbruggen (ECN) and Hans J. P. Verhoef (ECN) in organizing and performing the field tests.

References

- [1] Carne TG, Nord AR. Modal testing of a rotating wind turbine. Sandia National Laboratories, 1983. SAND82-0631.
- [2] Malcolm DJ. Dynamic response of a Darrieus rotor wind turbine subject to turbulent flow. *Engineering Structures* 1988; 10:125-134.
- [3] James GH, Carne TG, Lauffer JP. The natural excitation technique (NExT) for modal parameter extraction from operating wind turbines. Sandia National Laboratories, 1993. SAND92-1666.
- [4] Malcolm DJ. Structural response of 34-m Darrieus rotor to turbulent winds. *Journal of Aerospace Engineering* 1993; 6(1):55-75.
- [5] James GH, Carne TG, Veers PS. Damping measurements using operational data. *ASME Journal of Solar Energy Engineering* 1996; 118:190–193.

- [6] Wright AD, Kelley ND, Osgood RM. Validation of a model for a two-bladed flexible rotor system: Progress to date. In: 37th AIAA Aerospace Sciences Meeting. Reno, Nevada: 1999. AIAA-1999-0060.
- [7] Thomsen K, Petersen JT, Nim E, Øye S, Petersen B. A method for determination of damping for edgewise blade vibrations. *Wind Energy* 2000; 3:233–246.
- [8] Molenaar DP. Experimental modal analysis of a 750 kW wind turbine for structural model validation. In: 41st Aerospace Sciences Meeting and Exhibit. Reno, Nevada: 2003. AIAA-2003-1047.
- [9] Hansen MH, Thomsen K, Fuglsang P. Two methods for estimating aeroelastic damping of operational wind turbine modes from experiments. *Wind Energy* 2006; 9:179-191.
- [10] Kong C, Bang J, Sugiyama Y. Structural investigation of composite wind turbine blade considering various load cases and fatigue life. *Energy* 2005; 30:2101-2114.
- [11] Corten GP, Sabel JC. Optical motion analysis of wind turbines. Delft University of Technology, SV Research Group, 1995. ISBN 90-75638-01-9.
- [12] Tamura Y, Matsui M, Pagnini LC, Ishibashi R, Yoshida A. Measurement of wind-induced response of buildings using RTK-GPS. *Journal of Wind Eng Ind Aerodyn* 2002; 90:1783–93.
- [13] Nakamura S. GPS measurement of wind-induced suspension bridge girder displacements. *ASCE Journal of Structural Engineering* 2000 ; 126(12):1413–1419.
- [14] Breuer P, Chmielewski T, Gorski P, Konopka E. Application of GPS technology to measurements of displacements of high-rise structures due to weak winds. *Journal of Wind Eng Ind Aerodyn* 2002; 90(3):223–230.
- [15] Nickitopoulou A, Protopsalti K, Stiros S. Monitoring dynamic and quasi-static deformations of large flexible engineering structures with GPS: Accuracy, limitations and promises. *Engineering Structures* 2006; 28:1471-1482.
- [16] Rademakers LWMM, Verbruggen TW, van der Werff PA, Kortterink H, Richon D, Rey P, Lancon F. Fiber optic blade monitoring. In: *European Wind Energy Conference*. London: 2004.
- [17] Schroeder K, Ecke W, Apitz J, Lembke E, Lenschow G. A fiber Bragg grating sensor system monitors operational load in a wind turbine rotor blade. *Measurement Science and Technology* 2006; 17:1167-1172.
- [18] Mikhail EM, Bethel JS, McGlone JC. *Introduction to modern photogrammetry*. New York: Wiley; 2001.
- [19] Pauwels S, Debille J, Komrower J, Lau J. Experimental modal analysis: Efficient geometry model creation using optical techniques. *Journal of the IEST* 2006; 49(2):104-113.
- [20] Armesto J, Lubowiecka I, Ordóñez C, Rial FI. FEM modeling of structures based on close range digital photogrammetry. *Automation in Construction* 2009; 18(5):559-569.
- [21] Meyer CG, Jones TW, Lunsford CB, Pappa RS. In-vacuum photogrammetry of a 10-meter solar sail. In: *Collection of Technical Papers - AIAA/ASME/ASCE/AHS/ASC Structures, Structural Dynamics and Materials Conference 2*. 2005. p. 1004-1015 AIAA-2005-1889.
- [22] Schmidt T, Tyson J, Galanulis K. Full-field dynamic displacement and strain measurement using advanced 3D image correlation photogrammetry: Part I. *Experimental Techniques* 2003; 27(3):47-50.

Chapter 2

- [23] Schmidt T, Tyson J, Galanulis K. Full-field dynamic displacement and strain measurement - Specific examples using advanced 3D image correlation photogrammetry: Part II. *Experimental Techniques* 2003; 27(4):22-26.
- [24] Schmidt T, Tyson J, Galanulis K, Revilock D, Melis M. Full-field dynamic deformation and strain measurements using high-speed digital cameras. In: *Proceedings of SPIE - The International Society for Optical Engineering*. 2005.
- [25] Haritos N, Hira A, Mendis P, Perera U. Repair and strengthening of reinforced concrete structures using CFRPs. *Advances in Structural Engineering* 2006; 9(1):1-9.
- [26] Pappa RS, Lassiter JO, Ross BP. Structural dynamics experimental activities in ultralightweight and inflatable space structures. *Journal of Spacecraft and Rockets* 2003; 40(1):15-23.
- [27] Grytten F, Fagerholt E, Auestad T, Førre B, Børvik T. Out-of-plane deformation measurements of an aluminium plate during quasi-static perforation using structured light and close-range photogrammetry. *International Journal of Solids and Structures* 2007; 44(17):5752-5773.
- [28] Chang CC, Ji YF. Flexible videogrammetric technique for three-dimensional structural vibration measurement. *ASCE Journal of Engineering Mechanics* 2007; 133(6):656-664.
- [29] Chang CC. From photogrammetry, computer vision to structural response measurement. In: *Proceedings of SPIE - The International Society for Optical Engineering*. 2007. 652903 .
- [30] Simpson A, Smith SW, Jacob J. Aeroelastic behavior of inflatable wings: Wind tunnel and flight testing. In: *Collection of Technical Papers - 45th AIAA Aerospace Sciences Meeting*. 2007.
- [31] Ji Y, Chang CC. Identification of structural dynamic behavior for continuous system based on videogrammetric technique. In: *Proceedings of SPIE - The International Society for Optical Engineering*. 2006. 617311.
- [32] Black JT, Pappa RS. Photogrammetry and videogrammetry methods for solar sails and other gossamer structures. In: *Collection of Technical Papers - AIAA/ASME/ASCE/AHS/ASC Structures, Structural Dynamics and Materials Conference*. 2004.
- [33] Pappa RS, Black JT, Blandino JR, Jones TW, Danehy PM, Dorrington AA. Dot-projection photogrammetry and videogrammetry of Gossamer space structures. *Journal of Spacecraft and Rockets* 2003; 40(6):858-867.
- [34] Helfrick M, Niezrecki C, Avitabile P, Schmidt T. 3D Digital image correlation methods for full field vibration measurement. In: *the 26th IMAC, International Modal Analysis Conference Proceedings*. Orlando, Florida: 2008.
- [35] Helfrick M, Niezrecki C, Avitabile P. Optical non-contacting vibration measurement of rotating turbine blades. In: *the 27th IMAC, International Modal Analysis Conference Proceedings*. Orlando, Florida: 2009.
- [36] Warren C, Niezrecki C, Avitabile P. Applications of digital image correlation and dynamic photogrammetry for rotating and non-rotating structures. In: *the 7th International Workshop on Structural Health Monitoring*. Stanford, CA: 2009.
- [37] Corten GP. Optical motion analysis of wind turbines. In: *European Union Wind Energy Conference*. Bedford UK: 1996.
- [38] Website 1: Nordex Wind Energy, <http://www.nordex-online.com/en/products-services/wind-turbines/n80-25-mw/> [accessed April 2010]

[39] Website 2: GOM Optical Measuring Techniques, <http://www.gom.com> [accessed April 2010]

[40] Website 3: ECN Energy Research Center of the Netherlands, <http://www.ecn.nl/units/wind/wind-turbine-testing/> [accessed April 2010]

[41] Murtagh PJ, Basu B, Broderick BM. Mode acceleration approach for rotating wind turbine blades. *Proc. Inst. Mech. Eng. Multi-body Dynamics* 2004; 218:159-167.

[42] Murtagh PJ, Basu B, Broderick BM. Along-wind response of a wind turbine tower with blade coupling subjected to rotationally sampled wind loading. *Engineering Structures* 2005; 27:1209-1219.

[43] Ozbek M, Meng F, Rixen DJ, van Tooren MJL. Identification of the dynamics of large wind turbines by using photogrammetry. In: the 28th IMAC, International Modal Analysis Conference Proceedings. Jacksonville, Florida: 2010.

CHAPTER 3

Operational Modal Analysis of a 2.5 MW Wind Turbine Using Optical Measurement Techniques and Strain Gauges

Muammer Ozbek*, Daniel J. Rixen

Delft University of Technology, Faculty of Mechanical Engineering, Mekelweg 2, 2628 CD, Delft, the Netherlands

Abstract

This work presents the results of in-field tests performed on a 2.5 MW - 80 meter diameter - wind turbine. During the two test campaigns, dynamic response of the structure was monitored by using 3 different measurement systems namely, conventional strain gauges, photogrammetry and laser interferometry, while the turbine was both at parked condition and rotating. The recorded data was analyzed by using an OMA (Operational Modal Analysis) algorithm based on the LSCE (Least Square Complex Exponential) method while several turbine parameters (eigenfrequencies and damping ratios) were extracted. The obtained system parameters were then qualitatively compared with the results presented in a study from literature, which includes both aeroelastic simulations and in-field measurements performed on a similar size and capacity wind turbine.

Keywords

wind turbine; dynamic testing; operational modal analysis; optical measurement techniques; photogrammetry; laser interferometry

This work was published in Wind Energy (2012) ISSN: 10954244 DOI: 10.1002/we.1493

1. Introduction

Growing energy demands require wind turbine manufacturers to design more efficient and higher capacity wind turbines which inevitably results in larger and larger new models to be put into service. However, an important consequence of this increase in size and flexibility of the structure is the complicated dynamic interaction between different parts of the turbine. Motion of the blades interacts with aerodynamic forces, electro-magnetic forces in the generator and the structural dynamics of several turbine components (drive train, nacelle and tower). Understanding these dynamic interactions, the corresponding structural behavior and response characteristics is essential for optimizing the energy produced, ensuring safe and reliable operation and increasing the life-time of the system. This requires improving the design methodologies and in-operation control strategies. Therefore, more attention is paid to developing theoretical models for estimating the behavior of new wind turbines.

Contemporary aeroelastic simulation tools coupled with structural dynamics models enable designers to detect, understand and solve most of the possible problems at very early stages and optimize their designs.¹⁻⁹

Considering the fact that only the models based on real response measurements are able to represent the complicated interactions among different parts of the structure, several tests have been applied on both parked and rotating turbines. However, conventional dynamic testing techniques based on exciting the structure at several locations with sufficient force amplitudes cannot be easily applied to these challenging structures due to their size and the technical difficulties in providing very large forces that are required to reach sufficient excitation levels.

Standard wind turbine testing includes estimation of the structural frequencies and damping of the turbine modes from manual peak-picking from frequency response spectra of measured response signals, or from the decaying response after exciting the structure through step relaxation or clamping of the brake.¹⁰⁻¹³ However, estimations are often performed on turbines at parked condition. Although these estimated modal parameters are mostly related to the turbine structure and do not include aerodynamic

effects that dominate the aeroelastic modes of an operating turbine, frequencies and damping ratios of the lower turbine modes are important for tuning and validation of numerical models and for the verification of the prototype design.^{14,15}

Carne and Nord¹ extracted natural frequencies and damping ratios of operational turbine modes by applying the step relaxation method on a small (2 meters tall) rotating vertical axis wind turbine. The measured input excitation together with the recorded response enabled the authors to calculate FRF's (frequency response functions) and to estimate modal parameters for both parked condition and several rotation speeds.

Carne et al.¹⁰ also tested a 110 meter tall vertical axis wind turbine at parked condition by using the same step relaxation technique. The step excitation included input forces of 45 kN and 135 kN applied on one of the blades and the tower, respectively. As in the previous example, the authors calculated FRF's by using the measured input forces and response. However, in this work Carne et al. also applied an initial approach of OMA (Operational Modal Analysis) where the forces acting on the structure are not required to be measured and modal analyses are solely based on the recorded response. The authors compared the results obtained by using conventional FRF's and OMA approach and reported that they obtained a good coherence between the modal parameters extracted by the two different methods.

In following years, several researchers also applied step relaxation technique to test turbines at parked condition. Molenaar¹¹ performed similar tests on a 750 kW - 50 meters tall - horizontal axis turbine by exciting the structure at parked condition with sudden release of a pretensioned cable loaded up to 40kN.

Griffith et al.¹² also conducted in-field tests on a 60 kW - 25 m tall - vertical axis wind turbine at parked condition by using impact hammer, step relaxation and ambient wind excitation and compared the results obtained from various excitation methods.

Osgood et al.¹³, in a recent study, performed similar tests on a 600 kW - 37 m tall – horizontal axis turbine by exciting the structure at parked condition through shakers which are connected to the tower by cables. Extracted modal parameters were then compared with those obtained by OMA methods while turbine was vibrating under the

action of ambient wind forces. Although step relaxation is successfully applied on wind turbines at parked condition, it is relatively difficult and time consuming to use the same method for rotating turbines. The system involves specific mechanisms to be installed on the turbine to ensure the sudden release of pretensioned cables. The forces needed to excite a large commercial MW size turbine with sufficient levels of energy can be very large (even larger than the 135 kN forces mentioned above). Besides, the device has to be reloaded for every input, which means bringing the turbine down to parked condition, reloading the device and waiting for the turbine to reach a certain rotation speed. If numerous tests are planned to be performed for several wind speeds, this method can be very costly and time consuming.¹⁴ In fact it is this time requirement that motivated researchers to look for alternatives to step relaxation, finally resulting in the development of new OMA methods.

Researchers^{15,16} also tried to use different excitation techniques by assuming that a turbine mode can be excited by a harmonic force at its natural frequency, whereby the decaying response after the end of excitation gives an estimate of the damping. Simulations show that turbine vibrations related to several modes can be excited by blade pitch and generator torque variations and eccentric rotating masses placed on the turbine. However, results of the in-field tests performed on wind turbines showed that it is not possible to achieve the required pitch amplitudes to excite the modes with high modal frequency or high damping ratio due to the limited capacity of electrical pitch actuators. On the other hand, excited turbine vibrations are not pure modal vibrations and the estimated damping is therefore not the actual modal damping. Especially for systems having vibration modes with similar frequencies, but different damping ratios, it is not possible to isolate a certain mode only and aerodynamic damping values cannot be estimated well because of the energy transfer between different modes.¹⁵

OMA (Operational Modal Analysis) tools, a common representation used for several analysis methods which do not require the forces acting on the system to be measured, can be a solution to all these problems. Since estimation of the modal parameters is solely based on the use of measured response signals, these methods can be easily and efficiently used to extract the dynamic properties of these large structures excited

by natural environmental inputs (winds). Indeed, early versions of OMA tools were specifically developed to overcome the problems mentioned above and have been in use since early 90's.¹⁷⁻²⁰ Some of the researchers^{10,12,13} mentioned above have also successfully used OMA methods and have reported that they have obtained very good coherence between the modal parameters identified by OMA and the conventional experimental modal analysis techniques. A more comprehensive review of the history and development of this technique can be found in the work by Carne and James.¹⁴

Applicability limits of the current analysis tools and the extent to which the main assumptions of OMA methods are fulfilled in case of analyzing the real wind turbine data are still being investigated.²¹⁻²³ However, these techniques are continuously being improved and optimized to overcome the problems that may be encountered due to the complicated nature of the turbine structure and wind loading.²⁴⁻²⁶

This paper does not aim at focusing on the theoretical background of the utilized identification algorithms, but on the system parameters which can be obtained by applying these methods to the vibration data measured on a large scale wind turbine while turbine is both at parked condition and rotating. The article is structured as follows. First the main features of the test turbine and utilized measurement systems are described. Analysis results and identified system parameters are then investigated in two sections namely, tests on the parked and rotating turbine, followed by conclusions. In these sections, applied test techniques and data processing methods are discussed as well, to provide information on how the demonstrated results were obtained. In the article, extracted modal parameters are also qualitatively compared with the results presented by Hansen et al.¹⁵, which include both aeroelastic simulations and in-field measurements performed on a similar size and capacity wind turbine.

2. Test Turbine

Tests were conducted on a pitch controlled, variable speed Nordex N80 wind turbine with a rated power of 2.5 MW. The turbine has a rotor diameter and tower height of 80m. Detailed information on technical properties of the wind turbine can be obtained at the website of the manufacturer.²⁷

Measurements were performed at ECN (Energy Research Center of the Netherlands) wind turbine test site located in Wieringermeer, the Netherlands. More detailed information about the facilities of the test site can be found at the related website.²⁸

The reference turbine used for qualitative comparison, General Electric NM80, is also a pitch-regulated, variable speed wind turbine with a rotor diameter of 80 meters. This turbine has a rated power of 2.75 MW and is used as a test case for validation of new aeroelastic stability tools developed within the scope of European Commission supported STABCON project.¹⁵

3. Measurement Systems

One of the main objectives of the research project is to investigate how optical measurement systems (photogrammetry and laser interferometry) can be used to measure the dynamic response of large wind turbines.

Unlike conventional measurement systems (accelerometers, piezo-electric or fiber-optic strain gauges), optical measurement techniques do not require any sensors to be placed on the turbine. Therefore, no additional preparations such as cable installations for power or data transfer are needed inside the blade or the tower. However, some reflective markers should be placed (or painted) on the structure. These markers are made up of a retro-reflective material, which is 1000 times more reflective than the background blade material. Since the markers are in the form of very thin stickers (with a diameter of 400mm) they do not have any effect on aerodynamic performance of the blades. During the tests, a total of 55 markers were placed on the turbine (11 markers for each blade and 22 markers on the tower). Placement of the markers on the blade and their final distribution throughout the structure can be seen in Figure 3.1 a and b, respectively. These pictures were taken from a very recent work of the authors which includes a more comprehensive explanation of the photogrammetric measurement setup and evaluation of the obtained measurement accuracy.²⁹



Figure 3.1 a-b. Placement of markers and their final layout on the turbine²⁹.

These markers are essential for both photogrammetry and laser interferometry but, they are used for different purposes in each method. Photogrammetry is a proven measurement technique based on the determination of 3D coordinates of the points on an object by using two or more images taken from different orientations and positions. Although each picture provides 2D information only, very accurate 3D information related to the coordinates and/or displacements of the object can be obtained by simultaneous processing of these images. In photogrammetry, markers are used as targets to be tracked by the camera systems and all the targets can be tracked simultaneously.

During in-field tests, dynamic behavior of the turbine was monitored from a measurement distance of 220 meters by using a modified PONTOS system consisting of four CCD cameras. Photogrammetric measurements were performed by GOM mbH³⁰ (GOM Optical Measuring Techniques). Although photogrammetry is efficiently used in smaller scales by a wide variety of disciplines, this method was applied for the very first time to a MW scale wind turbine within the scope of this research project. Initial results showed that the deformations of the turbine can be measured with an average accuracy of ± 25 mm from a measurement distance of 220 m.²⁹ Considering the fact that for a rotating turbine deformations measured in flapwise direction can be as high as

± 1000 mm, this accuracy can be considered as high. This measurement error is observed to be mainly caused by calibration problems due to the rotation of the turbine. Therefore, their magnitudes are frequency dependent. For frequencies greater than $5P$ where P denotes the rotational frequency (0.28 Hz for the test turbine), measurement accuracy is much higher and in the range of ± 5 mm.²⁹

In laser interferometry, a laser vibrometer continuously sends a laser beam to the target and receives the beam reflected from its surface. If the object is moving, this causes a frequency change and phase shift between the sent and reflected beams. By detecting this frequency change (Doppler principle), velocity of the moving object can be found. If the object itself has a reflective surface, no extra retro-reflective markers are needed. However, since the blade material was not reflective enough and the distance between the laser source and the turbine was very long, high quality laser signals could only be acquired if the laser was targeted to the markers. Once the quality of reflected laser beam is assured, laser vibrometer can measure the vibration of the blade with very high accuracy (in micron level).

During the tests, laser interferometry measurements were taken by using a Polytec OFV 505 laser head and OFV 5000 controller with VD06 velocity decoder. These systems were located in the field at a distance of 200 meters from the turbine. An SLR (Super Long Range) lens which enables an increased measurement range up to 300 meters was also required to take measurements from this distance. Figure 3.2 shows the reflection of laser beam from the marker on the blade.

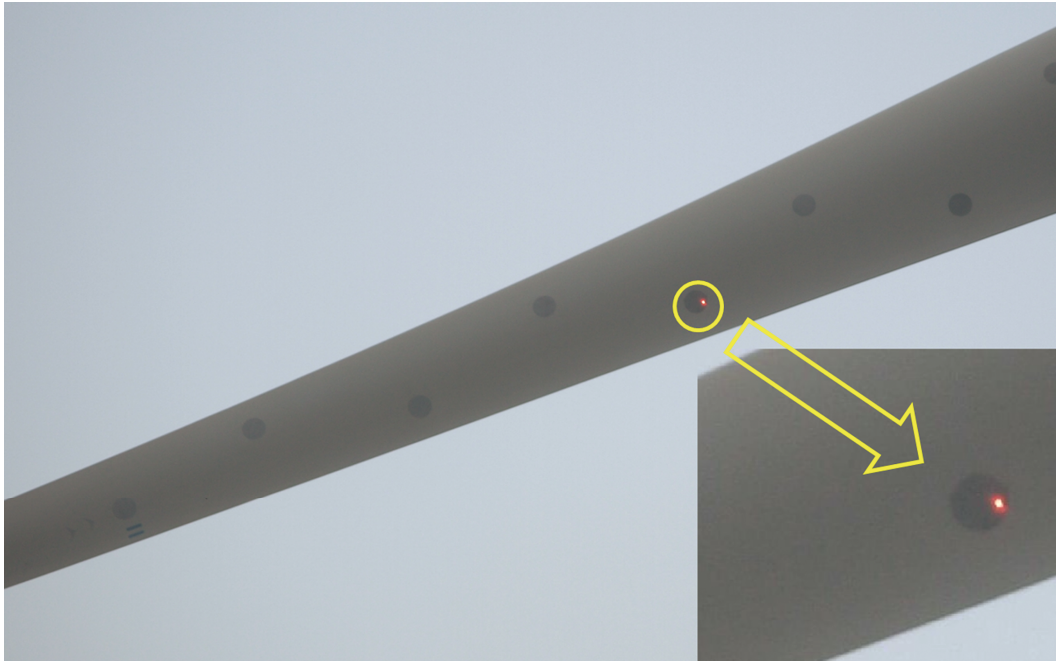


Figure 3.2. Reflection of laser beam from the marker on the blade.

Different from photogrammetry, laser vibrometer can only measure the motion of a single point at a time. However, it is still possible to measure all the markers distributed throughout the blade successively. Although this approach increases test duration, it enables vibration characteristics of the structure to be acquired with the same spatial resolution as provided by photogrammetry. If needed, laser measurements taken at different times and locations can easily be analyzed together by scaling the recorded laser signal with respect to a reference signal taken by another data acquisition system installed on the turbine. It is also possible to process the laser signals together with those obtained from different measurement systems /sensors. These issues will be discussed in more detail in following sections.

A third system, which has already been installed in the turbine as a part of a long term wind load monitoring campaign conducted by ECN, consists of 6 strain gauges placed at the root region of the three blades (2 strain gauges per blade) and 2 strain gauges located at the tower base.

These strain gauges are used to measure flapwise and edgewise vibration of the blades and fore aft and side to side vibration of the tower at a sampling frequency of 32 Hz. All

the data recorded by 3 different systems were then synchronized by using a GPS clock whose absolute time accuracy is approximately 10 milliseconds. Considering the fact that frequencies that are expected to dominate the response of the wind turbine are mostly in low frequency range [0 - 5 Hz], this accuracy can be considered as sufficient. Table 3.1 summarizes the main features of measurements taken by these 3 different measurement systems.

Measurement Type	Strain Gauge	Photogrammetry	Laser Interferometry
Measurement Block [Sec]	continuous	21	294
Measurement Accuracy	-	± 25mm	In micron scale
Measurement Distance	On the turbine	220 m	200 m (max 300 m)
Sampling Frequency [Hz]	32	28	1280
Number of Sensors	8	33	1
Parked Turbine Tests	X	-	X
Rotating Turbine Tests	X	X	-

Table 3.1. The main features of measurements.

It should be noted that since it is very difficult to keep the laser on the same marker while turbine is rotating, LDV (Laser Doppler vibrometer) was only used for the measurements taken on parked turbine. Similarly, photogrammetric measurements could not be conducted when the turbine was at parked condition because low wind speeds could not excite the structure sufficiently resulting in high noise to signal ratios.

4. Analysis Results and Identified System Parameters

Researchers^{15,31,32} agree on the fact that performing modal analysis on a rotating turbine is much more challenging than performing the same analysis on a parked turbine due to the facts that;

- For a rotating wind turbine some of the important turbine modes have very high aeroelastic damping ratios ranging between 10% and 30% (in terms of critical damping ratio) which makes them very difficult to be detected by most of the

identification algorithms that are currently in use. Aeroelastic damping is a combination of both structural and aerodynamic dampings but mostly dominated by the aerodynamic component caused by rotation of the blades. However, for a parked turbine the aerodynamic component is small (at low wind speeds) therefore, identified damping is generally considered to be composed of only structural damping which is usually less than 1%. On the other hand, some exceptions to this are also described in this section.

- For a rotating turbine, integer multiples of rotational frequency (also called P harmonics where P denotes the rotational frequency) always dominate the response of the structure. These frequencies can be effective up to 24P and sometimes coincide with the real eigenfrequencies of the system.³³
- Besides, for rotating turbines, these P harmonics cause violation of steady state random excitation assumption which is one of the most important requirements of OMA algorithms.
- Another important assumption, time invariant system requirement, is also difficult to accomplish for rotating wind turbines because of the rotation of the blades and yawing, pitching motion of the turbine. However, for parked turbines all these motions of the different components are prevented which makes the time invariant system assumption much easier to fulfill.

4.1 Tests on parked turbine: Strain and LDV

This section summarizes the results of the analyses of strain gauge and laser interferometry measurements taken on the parked turbine. During the measurements, the turbine was kept at a fixed orientation and yawing motion was prevented by application of the yaw brakes. Blade pitch angles were fixed at zero degree where flapwise blade vibration exactly corresponds to motion out of the rotor plane. This is the same as the angle of the blade during rotation below rated wind speeds (<15 m/sec for the test turbine). Similarly, the brakes were applied to prevent the movement of the rotor. Several measurement blocks changing between 240 and 4500 secs were recorded by strain gauges while the turbine was kept in this configuration. For laser measurements, data block length was 294 secs.

During the measurements, average wind speed was below 5 m/sec. Optimum wind speed for the tests is usually selected by taking various factors into account. Due to safety reasons (not to damage the bearings), turbine is not allowed to be kept braked at zero pitch for wind speeds above 5 m/sec. Besides, for higher wind speeds, several aerodynamic interactions between air flow and the blade can be encountered resulting in a scatter in the identified damping values. This phenomenon is also known as aerodynamic drag effect and reported to cause some fluctuations in the extracted modal parameters by several researchers.^{14,18} These factors limit the maximum allowable wind speed. Similarly, the minimum value is related to the amplitude of the forces required to excite the turbine sufficiently. Wind loads are the only sources of dynamic excitation so very low wind speeds may not be able to produce the required force amplitudes.

Table 3.2 summarizes the modal parameters (frequencies and damping ratios) calculated by using strain gauge and LDV measurements. LDV measurements were taken on the markers that were close to the tip of the blades. Frequencies and damping ratios were extracted by using the NEXt approach¹⁸⁻²⁰ together with the LSCE time domain identification method. When the turbine starts rotating, the name of the mode changes to the one indicated in parentheses. The abbreviations FW and BW stand for forward and backward whirling, respectively. Damping ratios are given in terms of critical damping ratio.

These modal parameters are important for tuning and validation of numerical models and for the verification of prototype designs. They can also be used for health monitoring applications. As can be seen in the table, frequency values are relatively stable and do not change depending on the measurement block analyzed. However, damping values may differ slightly. The damping scatter encountered in the 1st flapwise and side to side tower modes is mostly related to the drag phenomenon mentioned above.^{14,18}

Since the turbine is kept at a fixed orientation during the tests, the relative angle between the effective wind direction and the normal of the rotation plane continuously changes depending on the instantaneous wind direction resulting in a different

aerodynamic coupling for each measurement. This also shows that it is not possible to completely eliminate the aerodynamic component of damping even for low wind speeds.

Mode	Frequency [Hz]	Damping	S_F	S_E	S_T	S_L
1 st Fore Aft Tower	0.345	0.003	X		X	X
1 st Side to Side Tower	0.347	0.003 - 0.009		X	X	X
1 st Yaw (BW Flapwise)	0.902	0.010 - 0.020	X		X	X
1 st Tilt (FW Flapwise)	0.974	0.011 - 0.020	X		X	X
1 st Symmetric Flapwise	1.077	0.010 - 0.020	X		X	X
1 st Vertical Edgewise (BW)	1.834	0.004		X	X	X
1 st Horizontal Edgewise (FW)	1.855	0.004		X	X	X
2 nd Tilt (FW Flapwise)	2.311	0.005	X	X	X	X
2 nd Yaw (BW Flapwise)	2.430	0.004	X	X	X	X
2 nd Symmetric Flapwise	3.00	0.005	X		X	X
2 nd Edgewise	6.36	0.005	X	X		X
Tower Torsion Mode (Needs further verification)	6.154	0.005	X			X

Table 3.2. Modal parameters calculated for the parked turbine.

One important point to be mentioned is that at a first glance, the two frequencies of 6.36 and 6.154 Hz can be considered as the 2nd vertical and horizontal edgewise frequencies. Although the frequency of 6.36 Hz can be identified from both edgewise and flapwise blade vibrations, its amplitude is higher in the edgewise direction. Therefore, it is considered to correspond to the 2nd edgewise mode. However, the frequency of 6.154 Hz can only be identified from flapwise vibrations. For that reason, it can also be considered to be related to a tower mode (most probably the tower torsion

mode) which can be identified from the blades. Since the measurements on the tower have a low spatial resolution and are only taken in the fore aft and side to side directions, torsion mode of the tower may not be visible from the recorded tower strain measurements. However, it can still be possible to detect this mode from strain measurements taken on the blades. Tower torsion mode also results in blade motion in the flapwise direction which can be detected by the blade sensors oriented in the same direction. It should be noted that these estimations can only be confirmed by calculating the mode shapes of the identified frequencies which requires several measurements taken at different locations throughout the structure.

As mentioned before, one of the main objectives of the research project is to investigate whether or not LDV can be used to monitor the dynamic properties of wind turbines. However, in this work, LDV was only used for the measurements taken on parked turbine due to the difficulties in keeping the laser on the same marker while the turbine is rotating. In order to verify that this method can effectively be used in measuring the vibration response of the structure, it is required to demonstrate that all the modes, which are identified from strain gauge data, can also be extracted from laser measurements.

Strain gauges installed in the turbine are placed at some specific locations (rotor, tower and nacelle) and orientations (flapwise, edgewise) to ensure that all the modes can be observed. Indeed, gauges placed on the rotor may not detect the frequencies related to the tower modes. Similarly, blade sensors oriented in edgewise direction may not provide accurate information about vibration in flapwise direction. Complete description of the dynamic characteristics of the structure can only be obtained by combining the information coming from different sensors. Since LDV can measure the vibration of a single point at a time, this can only be provided by taking measurements at different locations on the turbine.

Following the validation of the observability of all the frequencies through laser measurements, it is also required to confirm that modal parameters estimated from laser measurements are in good coherence with those estimated from strain gauges installed on the turbine. Estimated parameters (especially damping) may change

depending on the signals selected. Analyzing all the available signals together is a widely used approach in system identification. However, this approach can also increase the noise level in the measurements and prevent the detection of some modes. Especially the modes that have very low modal participation in the response can only be detected when the signals, which specifically include the investigated frequency, are used. Therefore, before performing operational modal analysis reference signal combinations should be determined for each frequency. This can be done by examining PSD (Power spectral density) plots or by applying OMA methods on each signal separately.

The signals, which do not contain any information related to the investigated mode, should be eliminated not to add extra noise to the analysis. This situation is usually more critical for rotating turbines where some frequencies (P harmonics of rotational frequency) have very high energy levels and dominate the measured response. Consequences of inappropriate signal selection will also be discussed in the following sections describing the results of the analyses performed on the rotating turbine.

In system identification, it is recommended to use at least two different signals in the analyses. Using only one signal may cause the obtained results to be excitation dependent. Since one LDV was used during the test campaign, laser signal had to be accompanied with one strain gauge measurement in this work. The same analyses can also be made by using 2 different laser systems simultaneously. In this case, no additional strain gauge measurement would be needed as a reference. These ideas are at the center of our ongoing research projects.

In order to make a quantitative comparison between laser and strain gauge measurements, depending on the sensor location and the direction of the measured vibration, the measurements were investigated in 4 groups namely;

- Edgewise direction (in-plane direction) blade strain measurements shown as S_E and recorded by sensors 1, 3 and 5
- Flapwise direction (out of plane direction) blade strain measurements shown as S_F and recorded by sensors 2, 4 and 6

- Tower strain measurements shown as S_T and recorded by sensors 7 and 8
- Laser measurements on the blade shown as S_L and recorded by sensor 9.

These signal combinations were analyzed separately to find whether or not they can be used to identify each one of the frequencies given in Table 3.2. Results enabled the authors to decide on the best reference signals to investigate a specific frequency. Selected reference signals are also displayed in Table 3.2. In the table, the symbol “X” is used to show the frequencies that can be extracted from a certain signal combination. Similarly, the frequencies that cannot be extracted from the investigated signal combination are represented by the symbol “-”.

As shown in the table, all the frequencies can be identified by analyzing LDV signals. However, these frequencies cannot be detected from a single data block only. LDV measurement contains a single channel data recorded on a specific marker at a time. The targeted marker may not be at a suitable location to detect some of the modes (or frequencies). Therefore, it is required to try several locations (markers) and time series to identify all the modes.

Following the determination of appropriate signal combinations (through investigation of PSD plots and/or preliminary OMA results), laser measurements were analyzed together with one of these reference signals (the signal corresponding to the blade on which the laser measurement was taken). Modal parameters calculated by using laser and one strain gauge data were then compared with those calculated by using all the selected reference signals. Two results of this comparison were given as an example below in Table 3.3.

As can be seen in Table 3.3, for each of the frequencies (0.974 and 1.077 Hz), damping values were calculated by using two different measurements. Damping of the 1st tilt mode at 0.974 Hz was identified by using measurements 17 and 19 (M17, M19). The same damping identification was performed for the 1st symmetric flapwise mode at 1.077 Hz by using measurements 16 and 19 (M16, M19). For each measurement, analyses were repeated for 2 different reference signal groups namely, Reference Groups A and B. Reference Group A consists of all possible signals that can be used to

identify a certain frequency and therefore can be considered to provide the most reliable and accurate results for the investigated mode. As shown in Table 3.2, both frequencies are observable in tower and flapwise direction blade vibrations. Thus, Reference Group A consists of 5 signals obtained from flapwise blade S_F (2, 4, 6) and tower S_T (7, 8) strain gauges. Similarly, Reference Group B consists of two signals namely; the laser measurement S_L (9) and one flapwise direction strain measurement. This flapwise signal was selected as one of the signals 2, 4, 6 depending on the blade which the laser was aimed at.

Frequency	Measurement	Blade with laser	Ref. Group A (5 signals)	Damping A	Ref. Group B (2 Signals)	Damping B
0.974	M17	Blade 1	2-4-6-7-8 ($S_F + S_T$)	0.020	9 – 2 (on Blade1)	0.020
0.974	M19	Blade 2	2-4-6-7-8 ($S_F + S_T$)	0.010	9 – 4 (on Blade2)	0.012
1.077	M16	Blade 3	2-4-6-7-8 ($S_F + S_T$)	0.010	9 – 6 (on Blade3)	0.010
1.077	M19	Blade 1	2-4-6-7-8 ($S_F + S_T$)	0.020	9 – 2 (on Blade1)	0.019

Table 3.3. Damping values calculated for different reference signals.

Results show that the damping identified for a specific frequency may change depending on the data series analyzed. Even if the same reference signals are used (2, 4, 6, 7, 8), two different damping values are obtained by using two different time series (M17 and M19 for 0.974 Hz). However, this difference is not related to the measurement methods used. Reference Group A and B always give very close damping estimations, which proves that laser vibrometer measurements can be used efficiently to monitor the dynamic response of wind turbines. As mentioned before, same analyses can also be made by using 2 different laser systems simultaneously. In this case, no additional strain gauge measurement would be needed as a reference. A more detailed

explanation on the use of laser interferometry in testing wind turbines can also be found in the work by Ozbek et al.³¹

4.2 Tests on rotating turbine: Strain and Photogrammetry

This section summarizes the results of the analyses of strain gauge and photogrammetry measurements taken on the rotating turbine. During the test period, the response of the turbine was continuously measured by strain gauges. Therefore, modal parameters could be extracted for various operating conditions and wind speeds. Calculated modal parameters were then compared with the results presented by Hansen et al.¹⁵ The work mentioned includes the results of both aeroelastic simulations performed by the stability tool HAWCSstab^{5,34,35} and the real measurements taken on a wind turbine which has a similar size and capacity as the test turbine in our work. Therefore, some of the graphs presented below include the parameters extracted from our study and two additional graphs taken from the simulations and the measurements presented in the reference study¹⁵.

Figure 3.3 shows the aeroelastic frequencies we identified for different wind speeds. As can be seen in the figure, some of the modes extracted for the parked turbine (shown in Table 3.2) could not be detected for the rotating turbine. The 1st tilt (FW flapwise), 1st yaw (BW flapwise) and 1st symmetric flapwise modes could not be identified due to their very high damping ratios. Hansen et al.¹⁵ experienced the same problem and reported that these three flapwise modes have too high aerodynamic dampings for identification in response to the excitation by turbulence. Similarly, the 2nd BW flapwise mode, which has a lower damping, could not be observed in the rotation data due to its weak modal participation in the overall motion. It should be noted that for the range of wind speeds given in Figure 3.3, some pitch activity of the blades is inevitable. The rated wind speed specified for the test turbine is 15 m/sec and pitch activities start to be observed for wind speeds above 13 m/sec. Although the time invariant system assumption is not fully satisfied due to the change in pitch angle, damping estimations were also performed for these wind speeds (>13 m/sec). Identification of modal parameters for these wind speeds can only be possible by tolerating some pitch activity which definitely results in some scatter in obtained values.

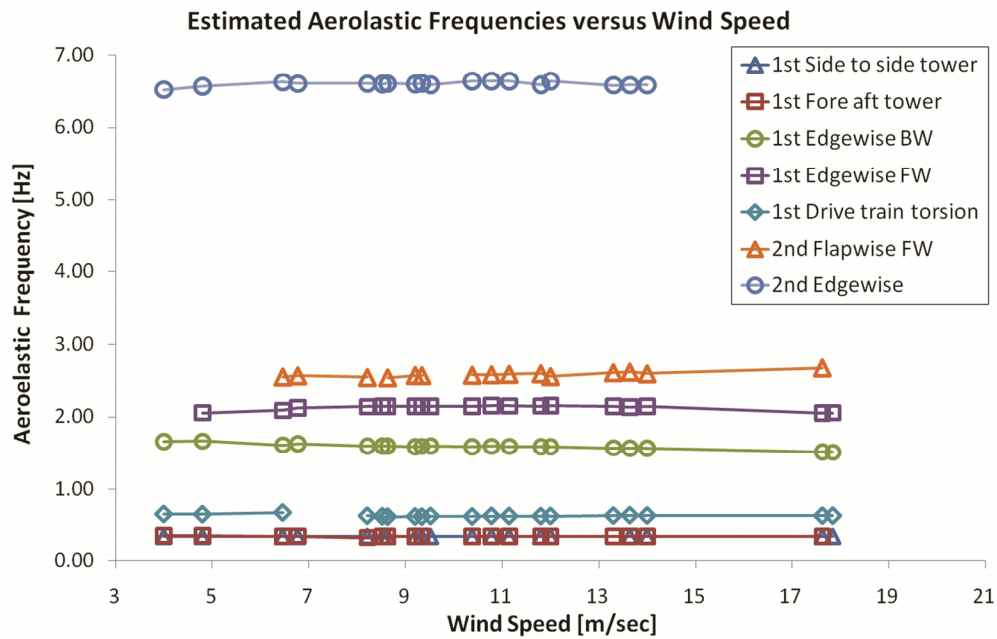


Figure 3.3. Extracted eigenfrequencies.

Figure 3.4 shows the change in aeroelastic damping ratio calculated for side to side tower mode as a function of wind speed. Identified values are in a very good agreement with the HAWCStab simulation results both in terms of trend and magnitude. The values found are less than 1% through different operating conditions and wind speeds. It should be noted that damping ratios are given in terms of critical damping ratios.

The same comparison is made for the fore aft tower mode and the results are shown in Figure 3.5. Although the two tower modes have almost the same frequencies, aeroelastic damping calculated for the fore aft mode is greater due to the motion of the tower in the direction perpendicular to rotor plane. The identified damping ratios are smaller than HAWCStab estimations, but can still be considered as close. Compared with side to side mode, analyzing the fore aft tower mode and estimating the corresponding modal parameters are more challenging. OMA tools utilized in this work are based on the use of correlation functions, which produce very accurate results in case of zero average steady state data series. However, changes in mean wind speed cause very slow variations in fore aft tower movement and bending moment. These quasi-static variations cannot be fully eliminated by using conventional data processing techniques

(such as detrending and filtering) and cause scatter in the estimated modal parameters. Therefore, the data series having a non-zero varying average should not be used in the analysis. Although such an approach limits the number of measurements that can be used in the analysis, it significantly increases the reliability of the extracted modal damping.

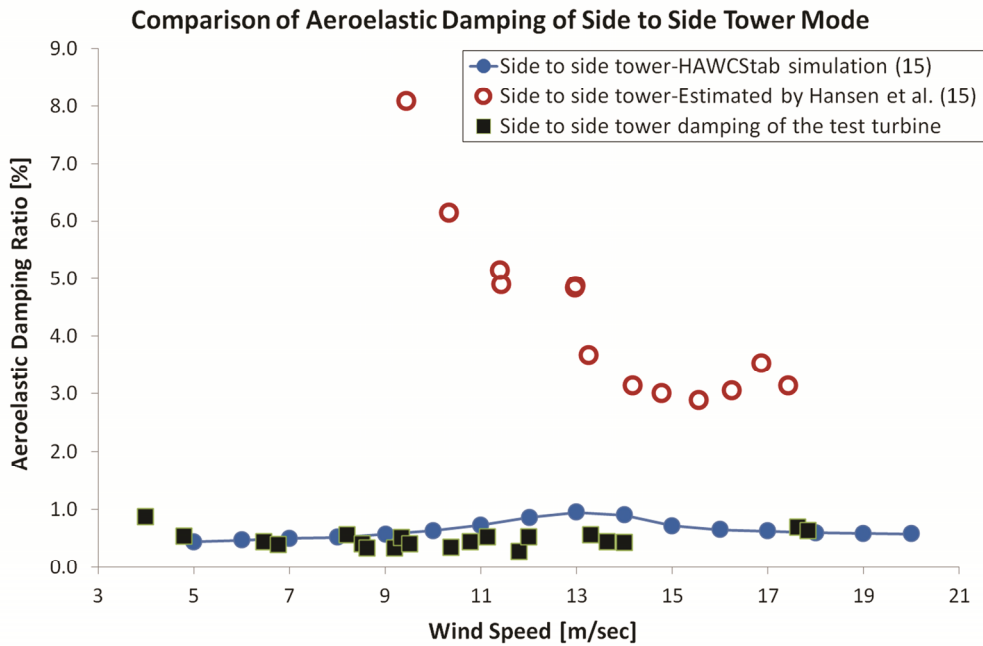


Figure 3.4. Side to side tower mode damping comparison.

Comparison of aeroelastic damping ratios found for the first BW edgewise mode is shown in Figure 3.6. The extracted damping ratios are slightly higher than the HAWCStab results, but are very close to the estimations¹⁵ made by using in-field vibration data. Edgewise modes are very straightforward to identify because they have very high modal participation in the overall response of the turbine and low aeroelastic damping.

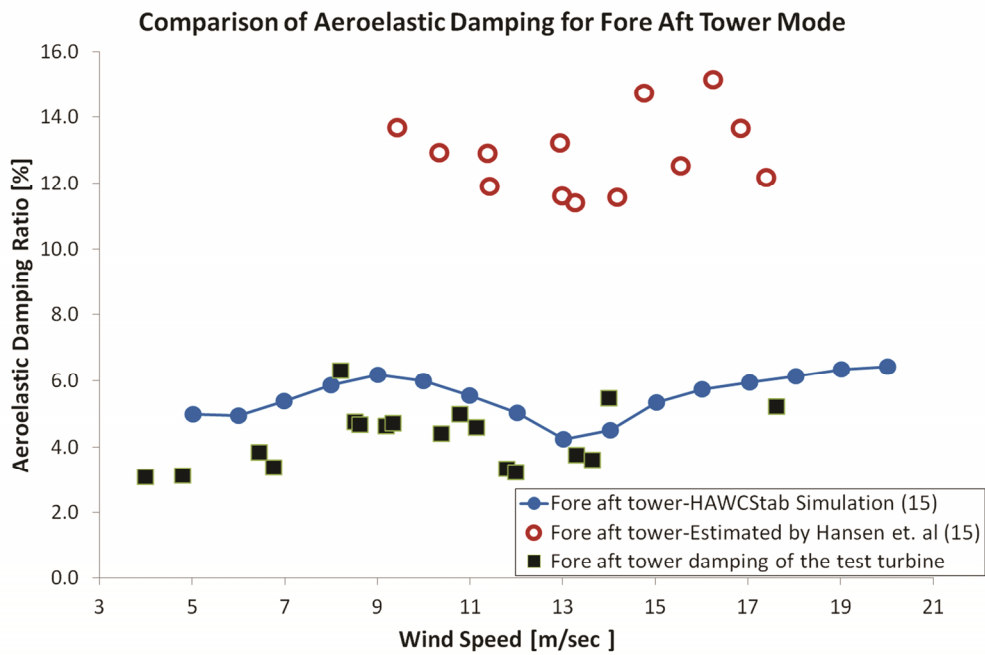


Figure 3.5. Fore aft tower mode damping comparison.

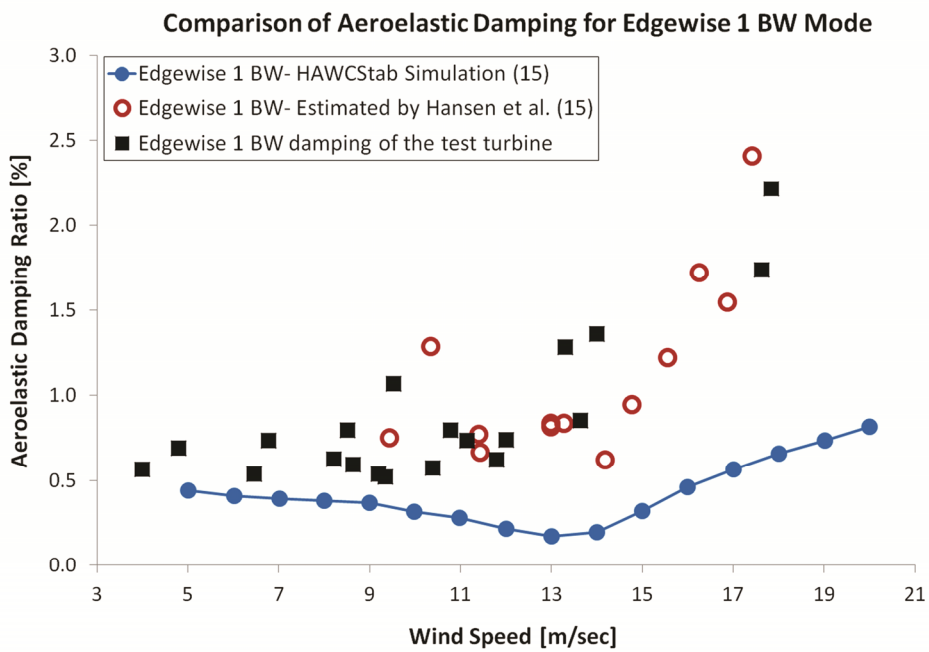


Figure 3.6. The 1st edgewise BW mode damping comparison.

Unlike tower modes, they can be detected by using the strain gauges placed both on the blades and the tower. Similarly, Figure 3.7 displays the same damping comparison for the 1st edgewise FW mode. Acquired damping ratios are again very close to both simulations and estimations given by Hansen et al.¹⁵

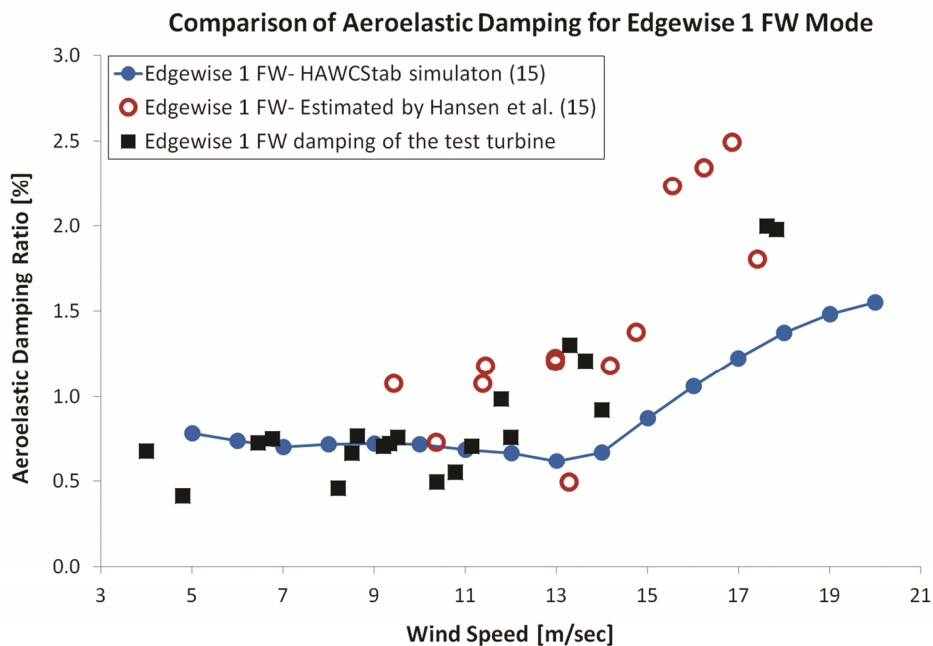


Figure 3.7. The 1st edgewise FW mode damping comparison.

It should be noted that, during the measurements that were used in modal analysis, operating conditions of the turbine (wind speed, rotor speed and pitch angle) have to stay constant. Possible variations in these parameters result in a noisy input data and a scatter in identified modal parameters. Therefore, only the measurements corresponding to very low standard deviations of wind speed and rotor speed were selected and analyzed to obtain the results presented in this work. However, it should also be noted that some pitching activity was observed starting from the wind speeds close to the rated speed. As mentioned before, identification of modal parameters for these wind speeds can only be possible by tolerating some pitch activity which definitely results in some scatter in the obtained values.

For most of the identification methods, especially for OMA tools using correlation functions, measurement duration is one of the most important factors that directly affect

the accuracy of the estimations.^{33,36,37} Measurement duration (length of the analyzed data series) is defined in terms of the number of cycles of the lowest frequency included in the data block and recommended to be greater than 200 cycles. The number of required cycles increases significantly when the investigated modes have high damping ratios.^{36,37} Since for a rotating wind turbine, some of the modes have relatively high damping ratios, long time series are needed. Nevertheless, low damping modes can still be identified from short data series. In this work, lengths of these measurement blocks change between 1800 and 6000 seconds which correspond to 500 and 1700 cycles of the lowest frequency (0.28 Hz - rotational frequency), respectively.

Figure 3.8 shows aeroelastic damping ratios identified for the drive train torsion mode. This mode could not be detected by most of the sensors placed on the rotor and the tower. Edgewise direction strain measurements taken on the blades were the only signals that could be used to analyze this mode. When these signals were combined and processed with the strain signals measured in flapwise direction, the identified mode was lost. It is believed that since it has a very weak modal participation in the overall motion, extra noise added by flapwise signals, which do not contain any information related to the torsion response of the drive train, prevented this mode from being detected accurately. Although frequencies could be identified for all the data blocks analyzed, stable damping ratios could not be extracted for most of the measurements. Estimations could only be made for some below rated wind speeds. Obtained results are similar to those predicted by HAWCStab simulations. Since any damping estimation for this mode was not given in the reference study, the identified damping ratios could only be compared with the simulation results.

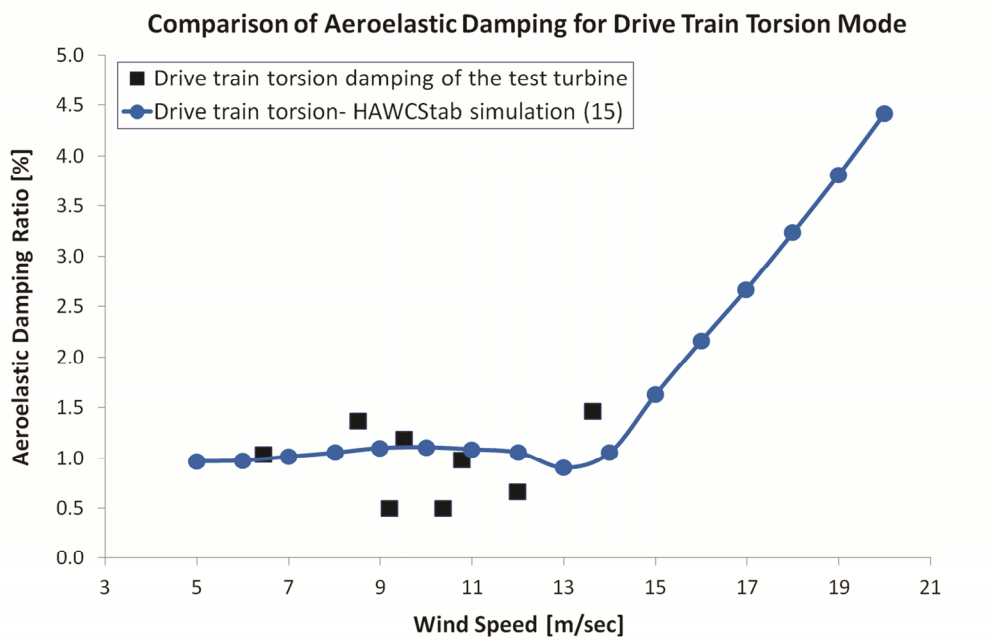


Figure 3.8. The 1st drive train torsion mode damping comparison.

Figure 3.9 shows aeroelastic damping ratios calculated for the 2nd FW flapwise and 2nd edgewise modes. Because Hansen et al. did not include the damping estimations or simulation results for these modes in their work¹⁵, the identified damping ratios could not be compared with any reference values.

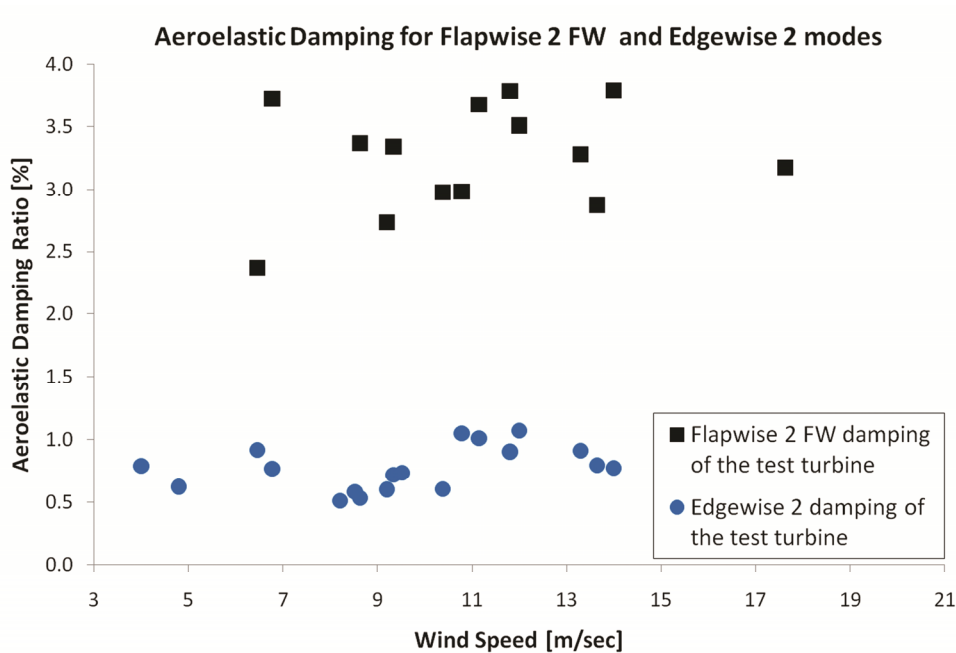


Figure 3.9. Damping ratios extracted for the 2nd FW Flapwise and 2nd Edgewise modes.

The advantage of strain gauge measurements is that they can be used to monitor the turbine continuously which enables modal parameters to be identified for various wind speeds. In addition, very long measurements can be taken by using this system, which significantly increases the accuracy of identified results. On the other hand, since the number of measurement locations is limited (6 gauges on the rotor and 2 gauges at the tower base), mode shapes cannot be obtained and some relatively weak turbine modes may not be observed. The modes that have very low modal participations in the response can only be detected if measurements are taken from specific locations where these modes have very high modal amplitudes.

Photogrammetry, which provides very detailed information on 3D deformation of the blades measured at 33 different points simultaneously, seems very promising in overcoming the drawbacks of strain gauge measurements. Initial results show that deformations of the turbine can be measured with an average accuracy of ± 25 mm from a measurement distance of 220 m.²⁹ Considering the fact that for a rotating turbine, deformations measured in flapwise direction can be as high as ± 1000 mm, this accuracy can be considered as high. Measurement errors are observed to be mainly

caused by calibration problems due to the rotation of the turbine. Therefore, their magnitudes are frequency dependent. For frequencies greater than $5P$ where P denotes the rotational frequency (0.28 Hz for the test turbine), measurement accuracy is much higher and in the range of ± 5 mm.²⁹ However, due to the limited memory capacity of the camera systems used in the tests, each photographic measurement block consists of 21 seconds or 6 cycles of rotation only.

Considering the recommended measurement durations^{36,37}, it can be concluded that it would be very challenging to get stable and reliable identification results by using such short data series that contain only 6 cycles. However, P harmonics dominating the overall response and some important turbine modes can be seen from PSD (Power Spectral Density) plots of the recorded vibration data. Figure 3.10 and Figure 3.11 show the PSD graphs of edgewise and flapwise direction blade vibration photogrammetric data, respectively. These figures are presented to provide a 3D frequency distribution that also includes information related to the measurement location. The X-axis represents the frequencies normalized with respect to rotational frequency (P) therefore it is dimensionless. The Y-axis corresponds to the marker number. Marker 1 is placed at the blade root whereas Marker 10 is located at the tip of the blade. The Z-axis represents the computed PSD amplitude. $1P$ and $2P$ components and the 1st edgewise mode can be recognized from Figure 3.10.

As can be seen in Figure 3.11, flapwise vibration data enables more frequencies to be identified. Integer multiples of rotational frequency up to $4P$ can be detected from the corresponding PSD graph. Besides these P components, the 1st flapwise mode can also be seen in Figure 3.11. Since the response is mainly dominated by P harmonics, other turbine modes, which have relatively weaker modal participations in the response, cannot be identified easily from PSD plots only.

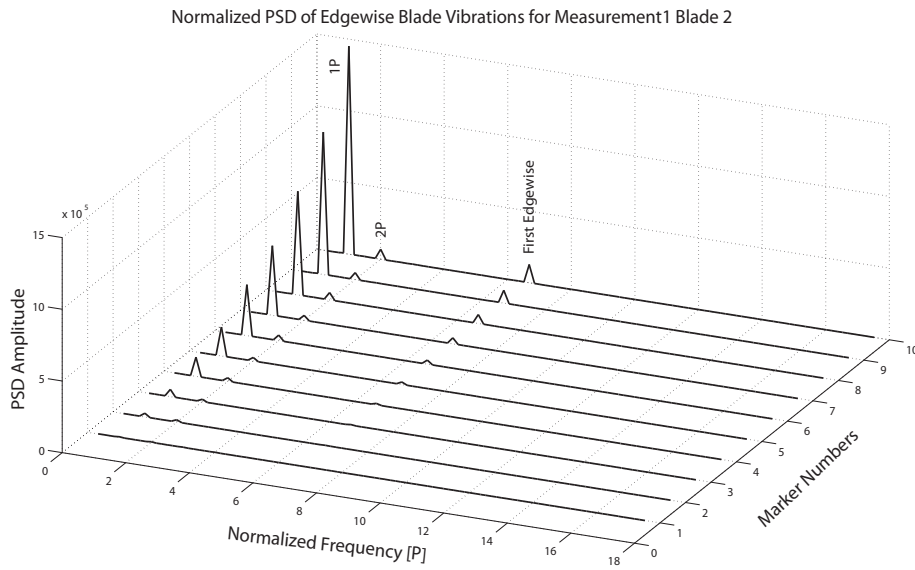


Figure 3.10. Normalized PSD of edgewise blade vibration²⁹.

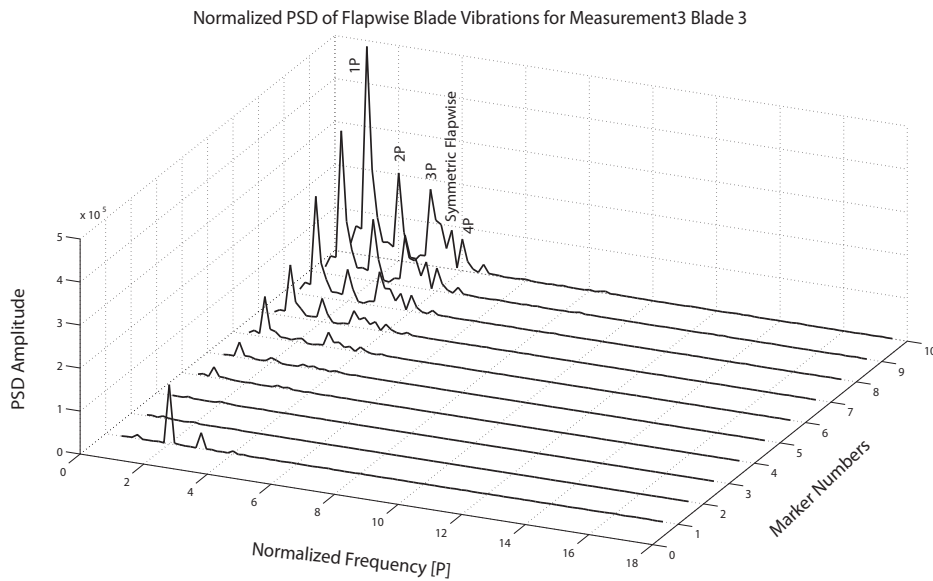


Figure 3.11. Normalized PSD of flapwise blade vibration²⁹.

A more detailed investigation³⁷ of the measured turbine response performed by utilizing several OMA methods showed that the second edgewise, the second and third flapwise modes of the blades can also be identified. However, further analyses and

measurements are needed for the validation of the observability of these high frequency modes from photogrammetric measurements. State of the art camera systems only allow relatively short measurement durations to be recorded. As the memory capacities of these systems increase, longer measurement durations are expected to be acquired soon. The progress in hardware and sensor technology will enable photogrammetry to be used as a continuous monitoring system where all the important turbine modes can be simultaneously extracted and analyzed with very high accuracy and spatial resolution.

5. Conclusions

Identification of the modal parameters of wind turbines are very important for optimizing the energy produced, ensuring safe and reliable operation and increasing the life-time of the system. However, conventional dynamic testing techniques based on exciting the structure from several locations with sufficient force amplitudes cannot be easily applied to these challenging structures due to their size and the technical difficulties in providing very large forces that are required to reach sufficient excitation levels.

OMA (Operational Modal Analysis) tools namely, the analysis methods that do not require the forces acting on the system to be measured, can be a solution to these problems. Since estimation of the modal parameters is solely based on the use of measured response signals, these methods can easily and efficiently be used to extract the dynamic properties of these large structures excited by natural environmental inputs (winds).

Analyses performed by using OMA methods seem very promising in extracting the modal parameters. Within the scope of the research, twelve different turbine modes were successfully calculated from the measurements taken on the parked turbine using strain gauges and LDV.

Similarly, seven different turbine modes could be identified from in-operation measurements using strain gauges and photogrammetry. Obtained results are in good coherence with those presented in similar studies in literature. Performing modal analysis on a rotating turbine is much more challenging than performing the same

analysis on a parked turbine due to the high aeroelastic damping of some important modes, rotational P harmonics that dominate the dynamic response and the difficulties in fulfilling some important system identification assumptions such as time invariant system and steady state random excitation.

The turbine modes (1st FW, BW and symmetric flapwise modes), known to have very high aeroelastic damping ratios, could not be detected through the analyses of the rotation data. The 2nd BW flapwise mode, which has a relatively lower damping, could not be extracted due to its low modal participation in the motion.

During the analyses, it was observed that frequency values are more easily identified and the calculated values are mostly stable and reliable. However, significant scatter can be encountered in estimated damping ratios. This scatter can be caused by physical factors such as the change in operating conditions or mathematical uncertainty related to the applied algorithms.

The three investigated measurement methods were verified to provide very valuable information on the dynamic response of the structure. Strain gauge data recorded continuously throughout the test campaign enabled modal parameters to be calculated for different operating conditions and wind speeds. Similarly, laser interferometry (applied to the parked turbine only) has been proven to be efficient in monitoring wind turbine dynamics. System parameters identified by using one strain gauge (reference) and one laser measurement were almost the same as those obtained by using 8 strain gauges. The same analyses can also be made by using 2 different laser systems simultaneously. In this case, no additional strain gauge measurement would be needed as a reference. These ideas are at the center of our ongoing research programs.

Photogrammetry was also demonstrated to provide accurate measurement of 3D deformations of the rotor. Within the scope of the work, the dynamic response of the rotor was captured at 33 different locations simultaneously by using 4 CCD (charge coupled device) cameras while the turbine was rotating. Initial results show that deformations of the turbine can be measured with an average accuracy of ± 25 mm from a measurement distance of 220 m.²⁹ This measurement error is observed to be

frequency dependent. For vibration frequencies greater than 5P, obtained accuracy is much higher and in the range of ± 5 mm.

Due to the low memory capacity of the utilized systems, the measurement duration was limited to 21 secs. However, high resolution deformation measurements simultaneously taken at 33 points made it possible to identify some important modes even for such short measurement durations. With the help of the rapid progress in hardware and the corresponding sensor technology, these technical limitations are expected to be overcome soon, enabling photogrammetry to become a versatile and cost-efficient alternative for health monitoring and dynamic testing of wind turbines.

Depending on the purpose of the investigation, different measurement techniques can be used. For the tests performed at parked condition, laser interferometry provides very accurate information on the vibration behavior of the structure. Similarly, photogrammetry is more useful in testing turbines during rotation. The high spatial resolution acquired makes it a promising alternative for some specific applications such as health monitoring and damage detection. However, state of the art hardware and camera systems allow photogrammetry to be used for short term measurement campaigns only. Conventional strain gauges, unlike optical measurement techniques, require some installations and preparations on the turbine (such as placement of cables for power and data transfer), which make them more costly both financially and in terms of installation time. However, these techniques are still expected to be used widely until the alternative measurement methods are well established to be more efficiently used in testing wind turbines.

Acknowledgements

This research project was partly funded by the We@Sea research program, financed by the Dutch Ministry of Economical Affairs. The authors would like to thank ECN (Energy Research Center of the Netherlands) for providing the test turbine and the other technical equipment. The authors also acknowledge the extensive contribution of Pieter Schuer (GOM mbH), Wim Cuypers (GOM mbH), Theo W. Verbruggen (ECN) and Hans J. P. Verhoef (ECN) in organizing and performing the field tests.

References

1. Carne TG, Lobitz DW, Nord AR, Watson RA. Finite element analysis and modal testing of a rotating wind turbine. *Proceedings of the AIAA 23rd Structures, Structural Dynamics and Materials Conference*, New Orleans, Louisiana, USA, 1982.
2. Malcolm DJ. Dynamic response of a Darrieus rotor wind turbine subject to turbulent flow. *Engineering Structures* 1988; 10: 125-134.
3. Malcolm DJ. Structural response of 34-m Darrieus rotor to turbulent winds. *Journal of Aerospace Engineering* 1993; 6: 55-75.
4. Larsen TJ, Hansen MH, Iov F. Generator Dynamics in Aeroelastic Analysis and Simulations. *Technical Report Risø-R-1395(EN)*, Risø National Laboratory, 2003.
5. Hansen MH. Aeroelastic stability analysis of wind turbines using an eigenvalue approach. *Wind Energy* 2004; 7: 133-143.
6. Hansen MH, Thomsen K, Fuglsang P. Aeroelastic modelling of the NM80 turbine with HAWC. *Technical Report Risø-I-2017(EN)*, Risø National Laboratory, 2004.
7. Hansen MH. Improved modal dynamics of wind turbines to avoid stall-induced vibrations. *Wind Energy* 2003; 6: 179–195.
8. Hansen MH, Hansen A, Larsen TJ, Øye S, Sørensen P, Fuglsang P. Control design for a pitch-regulated, variable speed wind turbine. *Technical Report Risø-R-1500(EN)*, Risø National Laboratory, 2005.
9. Buhl T, Thomsen K, Markou H. Design guidelines for integrated aeroelastic control of wind turbines. *Technical Report Risø-R-1577(EN)*, Risø National Laboratory, 2006.
10. Carne TG, Lauffer JP, Gomez AJ. Modal testing of a very flexible 110m wind turbine structure. *Proceedings of the 6th International Modal Analysis Conference*, Kissimmee, Florida, USA, 1988.
11. Molenaar DP. Experimental modal analysis of a 750 kW wind turbine for structural model validation. *Proceedings of the 41st Aerospace Sciences Meeting and Exhibit*, Reno, Nevada, 2003.
12. Griffith DT, Mayes RL, Hunter PS. Excitation methods for a 60 kW vertical axis wind turbine. *Proceedings of the 28th International Modal Analysis Conference*, Jacksonville, Florida, USA, 2010.
13. Osgood R, Bir G, Mutha H, Peeters B, Luczak M, Sablon G. Full-scale modal wind turbine tests: comparing shaker excitation with wind excitation. *Proceedings of the 28th International Modal Analysis Conference*, Jacksonville, Florida, USA, 2010.
14. Carne TG, James GH. The inception of OMA in the development of modal testing technology for wind turbines. *Mechanical Systems and Signal Processing* 2010; 24: 1213 -1226.
15. Hansen MH, Thomsen K, Fuglsang P. Two methods for estimating aeroelastic damping of operational wind turbine modes from experiments. *Wind Energy* 2006; 9: 179-191.
16. Thomsen K, Petersen JT, Nim E, Øye S, Petersen B. A method for determination of damping for edgewise blade vibrations. *Wind Energy* 2001; 3: 233–246.
17. James GH, Carne TG, Lauffer JP. Modal testing using natural excitation. *Proceedings of the 10th International Modal Analysis Conference*, San Diego, California, 1992.

Chapter 3

18. James GH, Carne TG, Lauffer JP. The natural excitation technique (NExT) for modal parameter extraction from operating wind turbines. *Technical Report SAND92-1666*, Sandia National Laboratories, 1993.
19. James GH, Carne TG, Lauffer JP. The Natural Excitation Technique (NExT) for Modal Parameter Extraction from Operating Structures. *Journal of Analytical and Experimental Modal Analysis* 1995; 10: 260-277.
20. James GH, Carne TG, Veers PS. Damping measurements using operational data. *ASME Journal of Solar Energy Engineering* 1996; 118: 190–193.
21. Tcherniak D, Chauhan S, Hansen MH. Applicability Limits of Operational Modal Analysis to Operational Wind Turbines. *Proceedings of IMAC International Modal Analysis Conference*, Jacksonville, FL, 2010.
22. Tcherniak D, Chauhan S, Rossetti M, Font I, Basurko J, Salgado O. Output-only Modal Analysis on Operating Wind Turbines: Application to Simulated Data. *Proceedings of European Wind Energy Conference*, Warsaw, Poland, 2010.
23. Chauhan S, Tcherniak, D, Hansen MH. Dynamic Characterization of Operational Wind Turbines using Operational Modal Analysis. *Proceedings of China Wind Power 2010*, Beijing, China, 2010.
24. Mohanty P, Rixen DJ. Operational modal analysis in the presence of harmonic excitation. *Journal of Sound and Vibration* 2004; 270: 93-109.
25. Mohanty P, Rixen DJ. Modified SSTD method to account for harmonic excitations during operational modal analysis. *Mechanism and Machine Theory* 2004; 39: 1247-1255.
26. Allen MS, Sracic MW, Chauhan S, Hansen MH. Output-only modal analysis of linear time-periodic systems with application to wind turbine simulation data. *Mechanical Systems and Signal Processing* 2011; 25: 1174-1191.
27. Nordex Wind Energy. <http://www.nordex-online.com/en/products-services/wind-turbines/n80-25-mw/>. (Accessed September 2011)
28. ECN Energy Research Center of the Netherlands. <http://www.ecn.nl/units/wind/wind-turbine-testing/>. (Accessed September 2011)
29. Ozbek M, Rixen DJ, Erne O, Sanow G. Feasibility of monitoring large wind turbines using photogrammetry. *Energy* 2010; 35: 4802-4811.
30. GOM Optical Measuring Techniques. www.gom.com. (Accessed September 2011)
31. Ozbek M, Rixen DJ, Verbruggen TW. Remote monitoring of wind turbine dynamics by laser interferometry:Phase1. *Proceedings of the IMAC International Modal Analysis Conference*, Orlando, FL, 2009.
32. Chauhan S, Hansen MH, Tcherniak D. Application of Operational Modal Analysis and Blind Source Separation / Independent Component Analysis Techniques to Wind Turbines. *Proceedings of the IMAC International Modal Analysis Conference*, Orlando, FL, 2009.
33. Ozbek M, Rixen DJ. Optical Measurements and Operational Modal Analysis on a Large Wind Turbine: Lessons Learned. *Proceedings of the IMAC International Modal Analysis Conference*, Jacksonville, FL, 2011.

34. Riziotis VA, Voutsinas SG, Politis ES, Chaviaropoulos PK. Aeroelastic stability of wind turbines: the problem, the methods and the issues. *Wind Energy* 2004; **7**: 373–392.
35. Marrant B, van Holten Th. System identification for the analysis of aeroelastic stability of wind turbine blades. *Proceedings of European Wind Energy Conference*, London, 2004.
36. Meng F, Ozbek M, Rixen DJ, van Tooren MJL. Comparison of System Identification Techniques for Predicting Dynamic Properties of Large Scale Wind Turbines by Using the Simulated Time Response. *Proceedings of the IMAC International Modal Analysis Conference*, Jacksonville, FL, 2010.
37. Ozbek M, Meng F, Rixen DJ, van Tooren MJL. Identification of the Dynamics of Large Wind Turbines by Using Photogrammetry. *Proceedings of the IMAC International Modal Analysis Conference*, Jacksonville, FL, 2010.

CHAPTER 4

Challenges in Testing and Monitoring the In-Operation Vibration Characteristics of Wind Turbines

Muammer Ozbek^{a*}, Fanzhong Meng^b and Daniel J. Rixen^a

^a, Delft University of Technology, Faculty of Mechanical Engineering, Mekelweg 2, 2628CD, Delft, the Netherlands

^b, Delft University of Technology, Faculty of Aerospace Engineering, Kluyverweg 1, 2629HS, Delft, the Netherlands

Abstract

This paper aims at discussing the main challenges in testing and monitoring the in-operation vibration characteristics of wind turbines by presenting the results of the analyses performed using analytical models, aeroelastic simulations and infield vibration measurements.

Within the scope of the research, the dynamic behavior of a 2.5 MW - 80 meter diameter – wind turbine was monitored by using three different measurement systems namely, conventional strain gauges, photogrammetry and laser interferometry, while the turbine was both at parked condition and rotating. The modal parameters were extracted for several operation conditions and wind speeds. Similar modal analyses were also conducted on the response time histories which were generated by using an analytical mass – spring – damper model and an aeroelastic simulation tool coupled with the structural dynamics model. The main challenges in analyzing the dynamic properties of wind turbines, possible reasons of the uncertainty in the estimated modal parameters, and the applicability limits of the utilized system identification algorithms are discussed based on the results of these investigations.

Keywords: Wind turbine, Vibration measurement, OMA, Operational Modal Analysis, Photogrammetry, Laser interferometry

This work was submitted to *Mechanical Systems and Signal Processing (MSSP)*

1. Introduction

Wind turbines have very specific characteristics and challenging operating conditions. Since they are designed and optimized to provide maximum power production for changing wind speeds and directions, they are expected to adapt to the rapidly varying environmental factors. Depending on their types and sizes, wind turbines are usually intended to be operational for wind speeds between 5 and 25 m/sec. In order to reach this goal, most of the turbines utilize active pitch control mechanisms where the angle of the blade (pitch angle) is changed as a function of wind speed. Similarly, the whole rotor is rotated towards the effective wind direction by using the yaw mechanism.

The ability of the turbine structure to adapt to the changes plays a crucial role in ensuring the maximum energy production and the safety of the turbine during extreme wind conditions. This on the other hand, makes it more difficult to investigate the structure from the dynamic analysis point of view. Some important prerequisites such as time invariant system and steady state random excitation assumptions, which form the basics of almost all types of in-operation system identification methods, are not always easily fulfilled for such systems. The violation of these assumptions causes at least a large scatter in the extracted system parameters. This unavoidable uncertainty limits the efficient use of these parameters in some important applications such as health monitoring and damage detection. Therefore, all these factors should be taken into account during the different steps of the structural investigation such as measurement, data analysis and evaluation of the results.

The factors affecting the accuracy of the estimated modal parameters are investigated in more detail in the sections below following the brief description of the test turbine, the utilized measurement systems and identification algorithms.

2. Test Turbine

The tests presented in this work were conducted on a pitch controlled, variable speed Nordex N80 wind turbine with a rated power of 2.5 MW. The turbine has a rotor diameter and a tower height of 80m. Detailed information on the technical properties of the wind turbine can be obtained at the website of the manufacturer [1]. The

measurements were performed at the ECN (Energy Research Center of the Netherlands) wind turbine test site located in Wieringermeer, the Netherlands. More detailed information about the test site can be found at the related web address [2].

3. Measurement Systems

One of the main objectives of the research project is to investigate how optical measurement systems (photogrammetry and laser interferometry) can be used to measure the dynamic response of large wind turbines.

Unlike conventional measurement systems (accelerometers, piezo-electric or fiber-optic strain gauges), optical measurement techniques do not require any sensors to be placed on the turbine. Therefore, no additional preparations such as cable installations for power or data transfer are needed inside the blade or the tower. However, some reflective markers should be placed (or painted) on the structure. These markers are made up of a retro-reflective material, which is 1000 times more reflective than the background blade material. Since the markers are in the form of very thin stickers (with a diameter of 400 mm) they do not have any effect on the aerodynamic performance of the blades. During the tests, a total of 55 markers were placed on the turbine (11 markers on each blade and 22 markers on the tower). Installation of these markers on the blades can be seen in Figure 4.1 a and b.

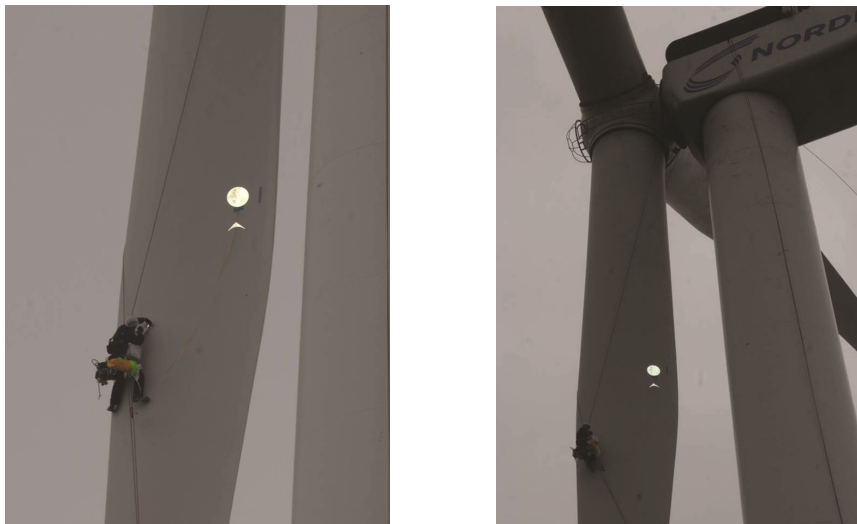


Figure 4.1 a-b. Installation of markers on the turbine [3]

Similarly, their final distribution throughout the structure can be seen in Figure 4.2 a and b. These pictures were taken from a recent work of the authors which includes a more comprehensive explanation of the photogrammetric measurement setup and evaluation of the obtained accuracy [3].

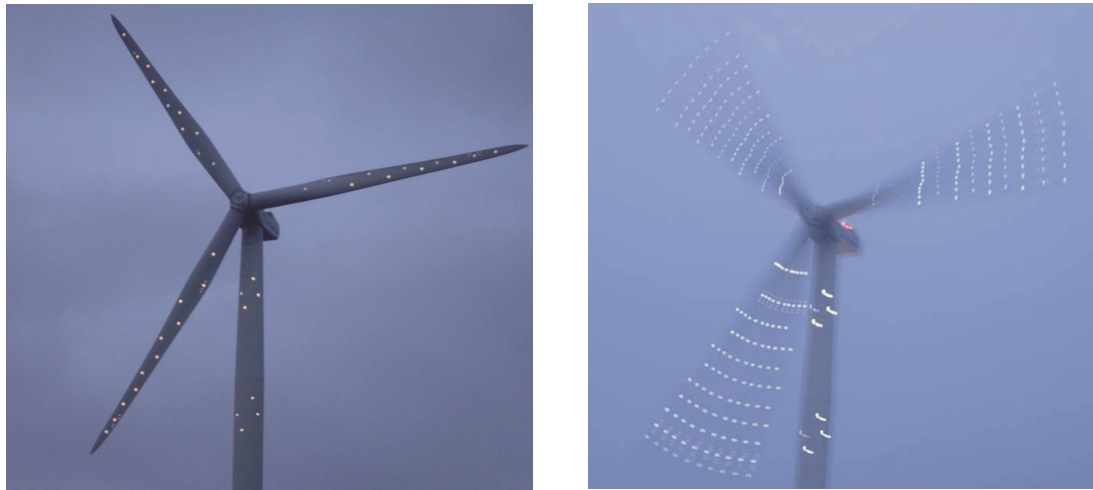


Figure 4.2 a-b. The final distribution of the markers on the turbine [3]

These markers are essential for both photogrammetry and laser interferometry but, they are used for different purposes in each method. Photogrammetry is a proven measurement technique based on the determination of the 3D coordinates of the points on an object by using two or more images taken from different orientations and positions [4]. Although each picture provides 2D information only, very accurate 3D information related to the coordinates and/or displacements of the object can be obtained by simultaneous processing of these images. In photogrammetry, markers are used as the targets to be tracked by the camera systems and all the targets can be tracked simultaneously.

During the in-field tests, the dynamic behavior of the turbine was monitored from a measurement distance of 220 meters by using a modified PONTOS system consisting of four CCD cameras. The photogrammetric measurements were performed by GOM mbH [5] (GOM Optical Measuring Techniques). Although photogrammetry is efficiently used at smaller scales by a wide variety of disciplines, this method was applied for the very first time to a MW scale wind turbine within the scope of this research project.

In laser interferometry, a laser vibrometer continuously sends a laser beam to the target and receives the beam reflected from its surface. If the object is moving, this causes a frequency change and phase shift between the sent and the reflected beams. By detecting this frequency change (using Doppler principle), the velocity of the moving object can be found. If the object itself has a reflective surface, no extra retro-reflective markers are needed. However, since the blade material was not reflective enough and the distance between the laser source and the turbine was very long, high quality laser signals could only be acquired if the laser was targeted to the markers. Figure 4.3 shows the reflection of the laser beam from the marker on the blade.

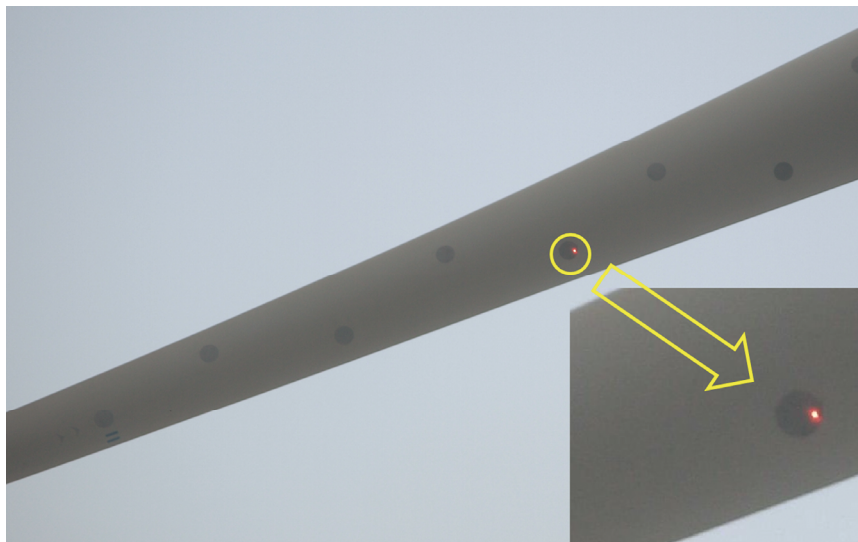


Figure 4.3. Reflection of the laser beam from the marker on the blade

Different from photogrammetry, laser vibrometer can only measure the motion of a single point at a time. However, it is still possible to successively measure all the markers distributed throughout the blade. During the tests, the laser interferometry measurements were taken by using a Polytec OFV 505 laser head and OFV 5000 controller with VD06 velocity decoder. These systems were located in the field at a distance of 200 meters from the turbine. An SLR (Super Long Range) lens which enables an increased measurement range up to 300 meters was also required to take measurements from this distance.

A third system, which has already been installed in the turbine as a part of a long term wind load monitoring campaign conducted by ECN, consists of 6 strain gauges placed

at the root region of the three blades (2 strain gauges per blade) and 2 strain gauges located at the tower base.

These strain gauges are used to measure the flapwise and edgewise vibrations of the blades and the fore-aft and side to side vibration of the tower at a sampling frequency of 32 Hz. All the data recorded by the three different systems were then synchronized using a GPS clock whose absolute time accuracy is approximately 10 milliseconds. Considering the fact that the frequencies that are expected to dominate the response of the wind turbine are mostly in the low frequency range [0-5Hz], this accuracy can be considered as sufficient.

It should be noted that since it is very difficult to keep the laser on the same marker while the turbine is rotating, LDV (Laser Doppler vibrometer) was only used for the measurements taken on the parked turbine. Similarly, photogrammetric measurements could not be conducted when the turbine was at parked condition because the low wind speeds could not excite the structure sufficiently resulting in high noise to signal ratios.

4. The Utilized Identification Algorithms

The analyses of both the vibration measurements recorded during the in-field tests and the numeric data generated by the analytical model and the aeroelastic simulations were performed by using OMA (Operational Modal Analysis) methods.

The algorithms based on this approach do not require the forces acting on the system to be measured. Since the estimation of the modal parameters is solely based on the use of the measured response signals, these methods can easily be used to extract the dynamic properties of large wind turbines excited by the natural environmental inputs (winds). Indeed, the early versions of OMA tools were specifically developed to overcome the problems encountered in the dynamic testing of wind turbines and have been in use since the early 90's [6-10].

In this work, in order to determine the possible problems that may be related to the utilized identification methods, the numeric data series (obtained from the analytical

model and the aeroelastic simulations) were analyzed by using two separate OMA algorithms which are based on different mathematical approaches.

The first method, LSCE (Least Square Complex Exponential), is a time domain analysis method requiring the use of impulse response functions [11]. However, impulse response functions cannot easily be measured on large structures like wind turbines. Therefore, this method can be utilized to identify the dynamic characteristics of the wind turbine only when applied together with NExT (Natural Excitation Technique). The NExT approach is based on the observation that the auto and cross correlations between measured output signals are comparable to impulse responses [8]. It enables LSCE and similar time domain identification methods to be used for the analyses of vibration data excited by the ambient forces such as the wind.

The LSCE method was selected in this work due to its relatively flexible structure which allows some modifications to easily be made to solve the specific problems caused by the complicated nature of the wind loads acting on the turbine [12]. However, its ability in identifying the highly damped modes should be investigated further to ensure its efficient use in the operational modal analysis of wind turbines, where some of the important modes have very high aeroelastic damping [13].

The second method, SSI (Stochastic Subspace Identification) is also a time domain analysis technique, but it does not require the impulse response functions or correlation functions to be calculated first [14, 15]. Its ability in extracting the highly damped modes has been confirmed in a recent work of the authors [13]. However, unlike LSCE, it is not possible to easily modify the SSI method to overcome the specific problems related to the wind excitation.

The applicability limits of these analysis tools and the extent to which the main assumptions of OMA methods are fulfilled in case of analyzing the real wind turbine data are still being investigated [16-19]. Some of the limitations and their possible effects on the identified system parameters are discussed in more detail in the following sections.

5. Analytical Model and Aeroelastic Simulation Tool

The reliability of the identified system parameters cannot easily be evaluated by using the in-field vibration measurement data which itself includes significant uncertainty due to the sudden and uncontrollable changes in several physical factors such as wind speed, rotor speed and pitch angle. Besides, the recorded data series are inevitably distorted by measurement errors. So in order to investigate specifically the performance of the identification algorithms, we first consider the numeric response data generated by an analytical mass - spring - damper model and an aeroelastic simulation tool MBDyn-AeroDyn [20].

By using the analytical model, it is possible to produce response data for a system whose dynamic characteristics (eigenfrequencies and damping ratios) are known a priori. The modal parameters are then estimated by applying identification algorithms on these generated data series and compared with the known values. The damping ratios of the investigated system can easily be changed to prescribed values. Figure 4.4 shows the 5 DOF (degrees of freedom) mass – spring – damper system utilized in the analyses.

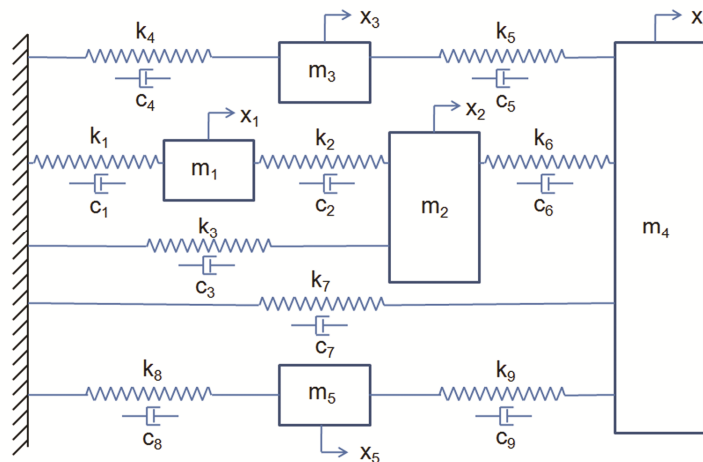


Figure 4.4. The utilized analytical model

Random white noise input forces having a flat spectrum of [0 32] Hz were applied on the system shown in Figure 4.4 at 5 different locations simultaneously. Since the

eigenfrequencies of the system are all in low frequency range ($[0\ 2]$ Hz), it is ensured that all the modes of the model are excited by sufficient levels of energy. In order to eliminate the effects of initial conditions the first 300 seconds of the generated data series were not used in the analysis.

Similarly, an aeroelastic turbine model, MBDyn-AeroDyn [20], is used to generate response time histories during which all the important parameters affecting the dynamic behavior of the turbine are kept constant. Since the simulation is performed for a specific turbine model, unlike the analytical model, the frequencies and damping ratios cannot be set to predetermined values.

The aeroelastic simulations utilized in this work were specifically generated for a 5 MW - 126 meter diameter- wind turbine and used to acquire the time domain deformation response calculated at several locations on the blade. In this model, the tower is represented by five beam elements, each containing three nodes. The rotor hub is described by a rigid body element and can rotate around a horizontal revolution hinge located at the free end of the main shaft, which is rigidly connected on the nacelle element having a tilt angle of 5 degrees. Three blades are mounted on the hub with a 1.5 meter offset from the hub center and with 2.5 degrees pre-cone angle (toward the upwind direction). They are clamped on the hub while the pitch angle can be adjusted. The blades are 61.5 meters long and have a chord length variation in span wise direction. They are modeled by five three-node beams. The final configuration of the turbine model can be seen in Figure 4.5.

The aerodynamic loads acting on the turbine were generated by using a wind speed profile which was composed of two components namely, constant mean wind speed part and zero average randomly fluctuating part having a frequency content of $[0\ 20]$ Hz. Considering the fact that the eigenfrequencies investigated are in the low frequency range ($[0\ 6]$ Hz), this loading is expected to be sufficient to excite all the modes of the system. Similar to the analytical model, the first 500 seconds of the simulation were not used in the analysis to eliminate the effects of initial conditions.

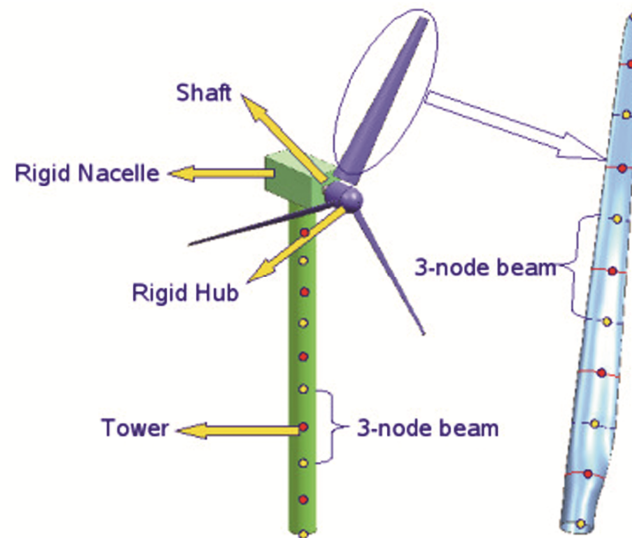


Figure 4.5. The utilized MBDyn-AeroDyn model

6. The Factors Affecting the Identified System Parameters

The following sections aim at briefly summarizing the factors affecting the reliability of the identified system properties. It should be noted that although these factors are investigated in separate sections, they are not fully independent from each other. The uncertainty in the estimated modal parameters is generally due to the combined effects of all the factors described below.

6.1 Difficulties in Fulfilling the Steady State Random Excitation Assumption

Most of the system identification methods are based on the assumption that the investigated structure is excited by steady state random white noise such that all the modes of the system can be excited with sufficient levels of energy.

Although turbulence is close to being random, the resulting excitation from the aerodynamic forces contains significant components of all P -harmonics (the integer multiples of the rotational frequency P) on the rotor frame and the $1P$, $3P$, $6P$, etc. harmonics in the fixed frame [21]. These P harmonics usually have very high energy levels and dominate the recorded response up to $4-5P$. Although their amplitudes get smaller for higher frequencies they can still be effective up to $24P$.

Depending on the operating conditions (wind speed and rotor speed), these frequencies may coincide with the eigenfrequencies of the system and affect the estimated parameters. Especially the frequencies which have a weak participation in the overall motion can be concealed by these P harmonics. Figure 4.6 shows the PSD graph of the flapwise direction blade vibration measured by photogrammetry. This figure is presented to provide a 3D frequency distribution that also includes the information related to the measurement location. The X-axis represents the frequency content normalized with respect to the rotation frequency (P) and the Y-axis corresponds to the marker number. Marker 1 is placed at the blade root whereas Marker 10 is located at the tip of the blade. The Z-axis represents the computed PSD amplitude. As can be seen in the figure, the P harmonics have very high energy levels up to 4P.

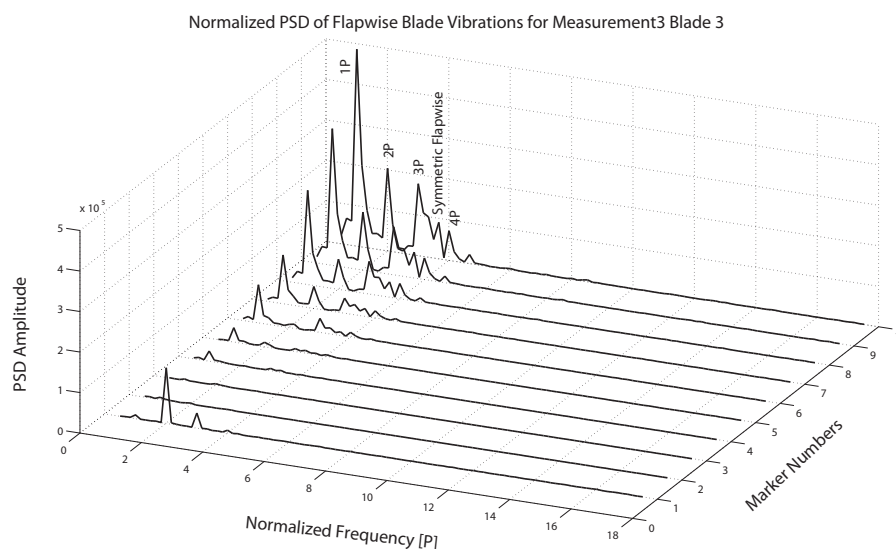


Figure 4.6. Normalized PSD of the flapwise blade vibration [3]

Similarly, the stability diagram displaying the frequencies that were identified from the strain gauge measurements taken on the blades is shown in Figure 4.7. In the figure, the X and Y axes represent the frequency and the assumed system order in the analysis, respectively. The dominant frequencies existing in the investigated data series can be recognized as the frequencies remaining nearly unchanged while the order of the identification is increased. Since these system frequencies appear as “stable” lines in the diagram, the graph is typically called as “stability diagram”.

In Figure 4.7 the rotational P harmonics are shown by the blue dash lines whereas the red lines are used for the real eigenfrequencies of the system. As indicated in the figure, the P harmonics seem to be effective up to 10P (2.76 Hz). It should be noted that in the graph, the maximum frequency is limited to 3 Hz not to make the plot too confusing and difficult to interpret. The two eigenfrequencies, the 1st FW (forward whirling) and BW (backward whirling) edgewise modes, can also be recognized in the graph at 1.869 and 1.881 Hz. Since these two modes have very high participation in the recorded vibration response, they are not influenced by the 7P harmonics (1.938 Hz) which is closely located. On the other hand, it can be noticed that the 2nd FW flapwise mode of 2.3 Hz is affected by the 8P component located at 2.215 Hz. These two frequencies combine and appear to be a single frequency when the order of the identification is approximately 200 and then separated again into two frequencies. Therefore, some scatter can be encountered in the parameters estimated for this mode. The real eigenfrequencies and the P harmonics can be closer or they can even coincide. In this case, it is highly difficult to properly recognize the eigenmode or to determine its damping.

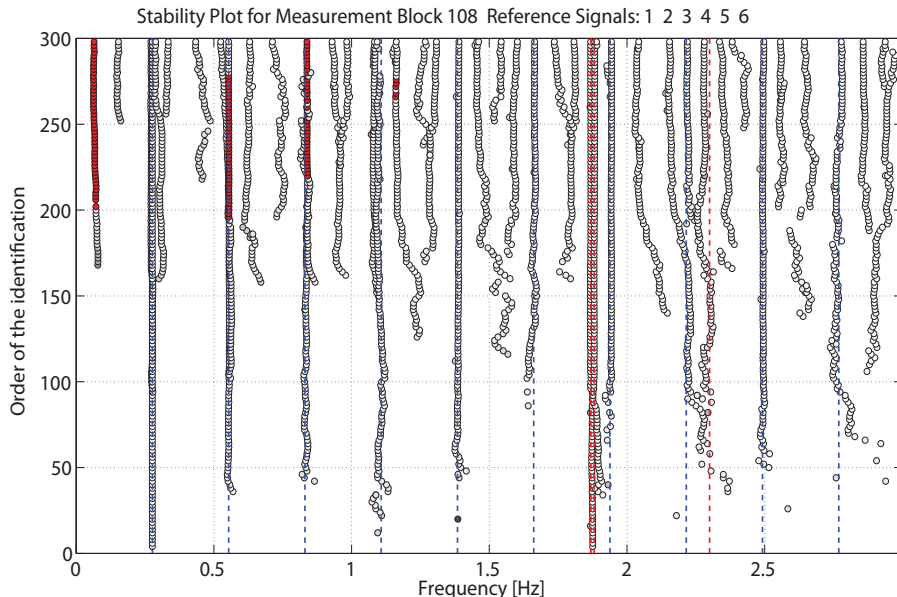


Figure 4.7. P harmonics identified in the blade vibrations

Several researchers conducting infield tests on wind turbines report that they had to discard some of their measurements and analyses since several P harmonics coincided

with the real turbine modes [21]. Such a problem can be solved in two different ways. Vibration data can be measured at a different rotational speed and used for identification. Although this solution would separate the previously coinciding real eigenfrequency and the P harmonics, it is not always easy to find such a suitable measurement period. As a second alternative, Mohanty and Rixen [12, 22] proposed a modified version of OMA which was extended to identify modal parameters in the presence of harmonic excitations even with the frequencies close to the eigenfrequencies of the system.

6.2 Difficulties in Fulfilling the Time Invariant System Assumption

Time invariant system assumption, which is another important prerequisite to be fulfilled for the identification of linear systems, requires that the dynamic properties (mass, stiffness and damping) of the analyzed system should be constant during the structural analysis. However, this assumption is not always easily satisfied for wind turbines, due to several reasons.

Unlike most civil engineering structures, the damping identified for wind turbines is not purely structural; it is aeroelastic. Aeroelastic damping is a combination of both the structural and the aerodynamic dampings, but mostly dominated by the aerodynamic component. The aerodynamic damping originates from the fact that the apparent angle of attack on the blade is related to the flapping speed, rotational speed and wind speed. Therefore, the overall damping is not constant and changes significantly depending on the operating conditions.

Similarly, the stiffness properties of the turbine structure vary with the blade angle (pitch angle). Pitch angle changes depending on the wind speed and rotor speed. Therefore, attention should be paid to whether the operation conditions of the turbine stay constant during the measurements or not.

The cyclic change in azimuth angle during rotation also causes some variations in the rotor stiffness. Therefore, the measurements taken on the rotating frame (blades) should be transformed to ground fixed reference frame to eliminate the rotational effects. This transformation can be performed by using multi-blade or Coleman

transformation. Only then, the system can be investigated as a linear time invariant system. However, some researchers report that this approach will miss some important information if the turbine is anisotropic [19]. There are also practical limitations, for example the transformation cannot be computed if measurements are taken from only one blade. Besides, the measurements on all of the blades must be taken at identical axial positions and with properly calibrated sensors. Otherwise, the transformation will not yield the expected results [19, 23]. These researchers also suggest that the wind turbine structure should be considered as a LTP (linear time periodic) system rather than a LTI (linear time invariant) system and should be analyzed by using algorithms taking the effects of this periodicity into account.

6.3 High Aeroelastic Damping and Measurement Duration

For a rotating wind turbine, some important turbine modes have very high aeroelastic damping ratios changing from 10% to 60% (in terms of critical damping ratio) which make them very difficult (if not impossible) to be detected by most of the identification algorithms that are currently in use.

However, for a parked turbine the aerodynamic component is very small therefore, the identified damping is generally considered to be composed of only structural damping which is usually less than 1%. On the other hand, some exceptions to this are also described in this work.

Damping is always the most difficult parameter to identify from the analysis of vibration data. Although frequency estimations are mostly reliable and stable, significant scatter can be encountered in damping estimations. This scatter can be caused by both the physical factors such as the change in the operating conditions and the mathematical uncertainty related to the applied algorithms. Especially, extracting the high damping modes is a challenge for almost all system identification methods. Since the utilized algorithms are based on different mathematical approaches, the reasons for increased uncertainty for high damping modes should be investigated separately for each method.

For the OMA tools using correlation functions (NExT approach), it was observed that measurement duration is one of the most important factors in the estimation of these

high damping modes [13]. In theory, the calculation of the correlation function is founded on infinite time series and can be considered, in the simplest form, as a mathematical averaging operation. Therefore, increasing the length of the analyzed data series (the number of data points) will definitely increase the accuracy of the averaging or the correlation function. However, measurement duration is more critical in the estimation of the high damping modes. Low damping modes can still be identified from the short data series. This is directly related to the theory of Natural Excitation Technique (NExT) which suggests that correlation functions can be used to represent impulse response functions. It can be stated that very long data series are needed to create correlation functions which can accurately represent the impulse response functions of these high damping modes.

In system identification, the measurement duration is defined in terms of the number of cycles of the lowest frequency included in the data block and recommended to be greater than 200 cycles. The number of required cycles increases significantly when the investigated modes have high damping ratios [13, 24]. Since for a rotating wind turbine, some of the modes have relatively high damping ratios, very long time series are needed. However, finding long measurement periods during which wind speed, rotor speed and pitch angle stay constant is a very challenging task. Accepting some changes in the operating conditions may violate the time invariant system assumption. This simple but important dilemma is one of the most important problems to be solved in testing and monitoring wind turbines.

Since SSI (Stochastic Subspace Identification) algorithms are not based on the NExT approach, they do not require very long measurements. However, similar limitations related to the number of cycles (minimum 200 cycles), that should be included in the investigated data block, are also valid for this method.

In this work, it is also aimed to investigate the efficiencies of the selected methods in identifying the high damping modes. The numeric data generated by the analytical model is used for this purpose. The damping estimations are performed by using data series of different measurement durations. Figure 4.8 shows the estimated damping ratio as a function of the measurement duration. It can be seen from the graph that the

estimations become stable and reliable after 200 cycles. This value is consistent with those recommended in the literature for the identification of low damping modes.

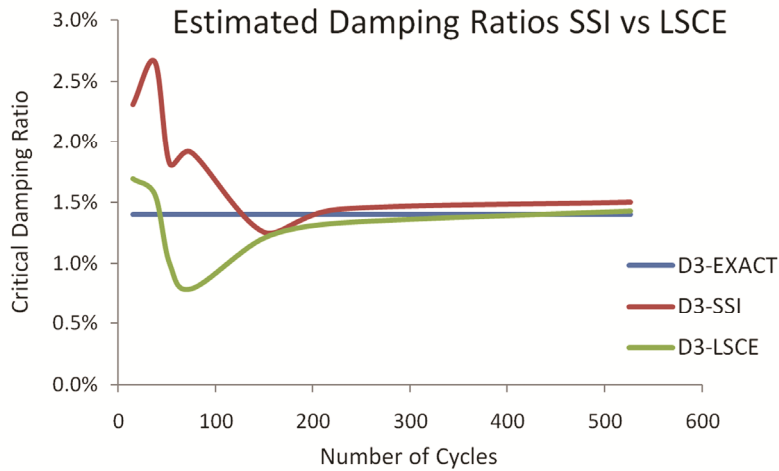


Figure 4.8. Change in damping ratio estimated for Mode 3

Similarly, Table 4.1 displays the system parameters estimated for the measurement duration of 500 cycles. As can be seen in the table, all the modes having low damping ratios could be identified by both of the methods utilized. However, LSCE did not succeed in detecting the highly damped mode (mode 2). The length of the analyzed data series was increased until the highly damped mode appeared in the stability plot. LSCE could extract this mode only when the measurement duration was extended up to 5000 seconds (3750 cycles).

By using the ratio of the lowest frequency (0.752 Hz) of the analyzed model to the one measured for the test turbine (0.28 Hz - rotation frequency), it was found that for the 2.5 MW turbine, the minimum measurement duration required to detect the highly damped flapwise modes should be approximately 4 hours. However, it is generally very difficult to obtain such a data block during which the operating conditions of the turbine remain constant.

According to the results of the analyses, SSI method seems to be more efficient in detecting the high damping modes. However, several researchers using this technique for the operational modal analysis of large wind turbines reported that they could not

extract some important turbine modes (the 1st FW, BW and symmetric flapwise modes) which are known to have high aeroelastic damping ratios [21]. The authors concluded that these three flapwise modes have too high aerodynamic damping for identification in response to the excitation by turbulence.

Mode	Frequency	Damping	Frequency	Damping	Frequency	Damping
	Exact [Hz]	Exact	SSI [Hz]	SSI	LSCE [Hz]	LSCE
1	0.752	0.010	0.752	0.008	0.750	0.009
2	0.920	0.300	0.917	0.298	-	-
3	1.286	0.014	1.282	0.015	1.282	0.014
4	1.650	0.009	1.649	0.010	1.650	0.010
5	1.884	0.017	1.886	0.016	1.884	0.016

Table 4.1. System parameters extracted for the analytical model

The analytical model enables the prescribed values to be assigned to the damping ratios of the selected modes. However, it cannot efficiently represent the complicated nature of wind loading (like the P harmonics) and its possible effects on the structure. Therefore, similar analyses were also performed using an aeroelastic simulation tool which was specifically designed to model the behavior of wind turbines. Unfortunately, in this case the dynamic parameters of the system are not known a priori. They can only be calculated from the generated data series.

Table 4.2 shows the modal parameters identified from the MBDyn-AeroDyn simulations performed for the 5 MW -126 m diameter- wind turbine. The results are quite similar to those obtained for the mass-spring-damper analytical model. For low damping modes, both LSCE and SSI methods extract frequencies that are very close to each other. However, slight differences are encountered in the estimated damping ratios. Although relatively long simulations (4500 sec) were analyzed, once again the highly damped 1st flapwise mode could not be detected by the LSCE method. The analyses of the simulated response confirm that the estimated modal parameters may slightly change depending on the utilized identification technique and that some methods can be considered to be more advantageous in analyzing the highly damped aeroelastic turbine

modes. On the other hand, this difference can also be explained by the fact that the response may not be fully comparable to the one of a linear system since the aeroelastic simulation tool performs a full non-linear analysis not exhibiting genuine linear modes.

Mode	Frequency (SSI) [Hz]	Frequency (LSCE) [Hz]	Damping (SSI)	Damping (LSCE)
1 st Side to side Tower	0.27	0.27	0.007	0.008
1 st Flapwise	0.72	-	0.64	-
1 st Edgewise	1.07	1.07	0.026	0.020
2 nd Flapwise	2.05	2.05	0.035	0.026
3 rd Flapwise	4.37	4.38	0.047	0.011
2 nd Edgewise	-	5.43	-	0.013
Blade Torsion	5.62	-	0.028	-

Table 4.2. System parameters extracted for the 5MW turbine simulation

6.4 Selection of the Reference Frame

Depending on the measurement location, the vibration data recorded on a rotating wind turbine can be investigated in two different reference frames (or coordinate systems) namely, fixed reference frame (tower, nacelle) and rotating reference frame (blades). When selecting the data to be analyzed, it is important to choose the signals from the same frame. The analyses, which contain the signals from both of the coordinate systems simultaneously, violate the time invariant system assumption due to the change in the azimuth angle during rotation [21]. The measurements taken on the blades can be transformed to the fixed reference frame by using multi-blade or Coleman transformation [25], but this requires the instantaneous orientation of the blades (azimuth angles) to be determined by using accurate tachometer recordings, which were synchronized with the vibration measurements.

Two different frequency values are calculated for the same mode (except symmetric ones) by using two different reference frames. Although these two frequencies represent the same mode physically, the one found by using the ground fixed reference

frame includes all the rotational effects and changes with the rotor speed. On the other hand, the vibration information coming from the blade sensors enables the frequencies to be analyzed without being modified by the rotational effects. Therefore, the frequencies obtained by using the rotating frame are stable and do not change for different rotor and/or wind speeds (except centrifugal stiffening).

The fixed coordinate system is crucial in the dynamic testing of wind turbines because the Campbell diagram, which shows the changes in aeroelastic frequencies (as a function of wind speed) and possible resonance problems, is constructed by using this coordinate system. However, depending on the purpose of the analysis, using a rotating coordinate system can also be useful. If the investigated mode coincides with P harmonics in the ground fixed frame, it can still be detected from the rotating reference frame.

6.5 The complex characteristics of the measured deformations

All system identification methods, especially the algorithms, which are based on the use of correlation functions, produce very accurate results in case of analyzing zero or constant average steady state data series. However, the change in the mean wind speed causes very slow variations in the deformations measured along the effective wind direction. The overall response is usually a varying average time-series that can result in some scatter in damping estimation. Therefore the analyses of the vibrations measured along the wind direction (rotor flapwise modes and fore aft tower mode) are always more difficult than the analyses of those (blade edgewise modes and side to side tower mode) measured in the direction perpendicular to wind flow. Figure 4.9 shows the change in the tower bending moments (strains) measured in the fore aft and side to side directions. As can be seen from the graph, the change in the mean wind speed causes a very slow variation in the tower strains measured in the fore aft direction. This variation cannot be fully eliminated by using the conventional data processing techniques (such as detrending and filtering) and causes scatter in the estimated modal parameters.

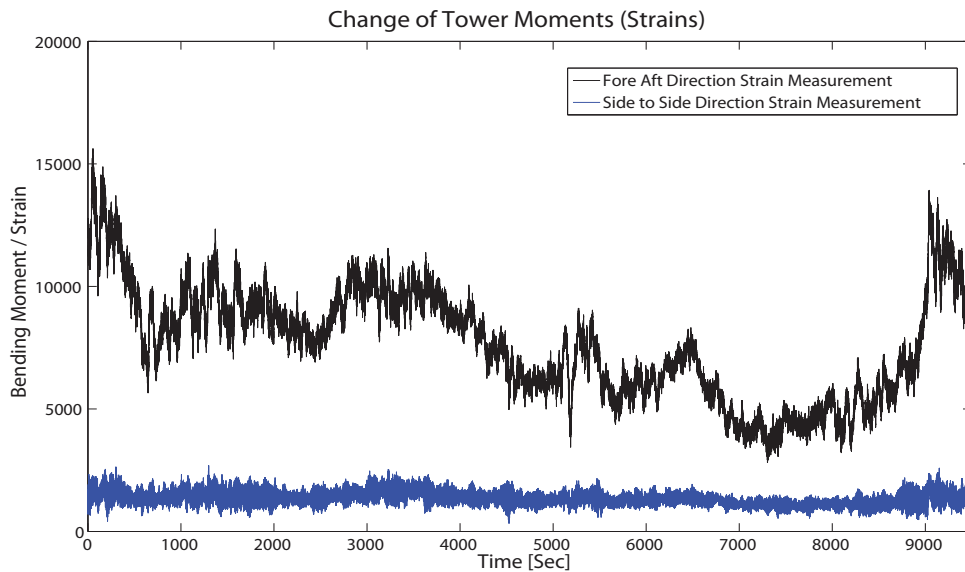


Figure 4.9. Fore aft and side to side tower strain measurements

6.6 Changing Wind Speed and Direction

As mentioned in the sections above, the dynamic characteristics of the turbine system mostly depend on the operating conditions. Especially the extracted damping ratio, which is mainly dominated by the aerodynamic component, is significantly affected by the wind speed and rotor speed. Therefore, during the measurements that will be used in the modal analysis, the operating conditions of the turbine have to stay constant.

Although wind speed and rotor speed remain constant within the selected measurement block, the change in wind direction can still cause slight changes in the extracted damping. The turbine is continuously rotated towards the effective wind direction by using the active yaw mechanism, but the calculation of the wind direction is based on averaging the anemometer recordings taken within measurement periods of typically 10 minutes. Therefore, instantaneous changes in the direction cause different aerodynamic coupling between the wind and the turbine structure.

The infield tests performed on wind turbines show that the aerodynamic coupling between the structure and the air flowing around it should be taken into account even for the measurements taken on the parked turbines where the aerodynamic component

of the damping is generally neglected. Several researchers reported that some scatter in the calculated damping ratios were encountered during the tests performed on the parked turbines at low wind speeds [7, 10]. The reported phenomenon is also known as aerodynamic drag effect. Since the turbine is kept at a fixed orientation during the tests, the relative angle between the effective wind direction and the normal of the rotation plane continuously changes depending on the instantaneous wind direction resulting in a different aerodynamic coupling for each measurement.

6.7 Selection of the Reference Signal Groups

Taking measurements from several locations on the structure always increases the spatial resolution and the accuracy of the identified system parameters. However, analyzing all these signals together can also increase the noise level in the measurements and prevent the detection of some modes. Especially the modes that have very low modal participation in the response can only be detected when the signals, which specifically include the investigated frequency, are used. Therefore, before performing operational modal analysis the reference signal combinations should be determined for each frequency separately. The signals, which do not contain any information related to the investigated mode, should be eliminated not to add extra noise to the analysis.

7. Measurements on the Parked Turbine

This section presents the results of the analyses of the strain gauge and laser interferometry measurements taken on the parked turbine. During the measurements, the turbine was kept at a fixed orientation and the yawing motion was prevented by application of the yaw brakes. Similarly, the blade pitch angles were fixed at zero degree. All the measurements were performed for wind speeds of approximately 5 m/sec. More detailed information related to the measurement setup and the main features of the test campaign can be found in some recent works of the authors [3], [24], [26-28]. The present paper focuses more specifically on the challenges in acquiring and analyzing the in-operation vibration measurements of wind turbines and aims at discussing the factors affecting the reliability of the identified system parameters.

Table 4.3 summarizes the modal parameters (frequencies and damping ratios) calculated by using the strain gauge and LDV (laser Doppler vibrometer) measurements. The LDV measurements were taken on the markers that were close to the tip of the blades. The frequencies and damping ratios were extracted by using the NExT approach [7-9] together with the LSCE time domain identification method. When the turbine starts rotating, the name of the mode changes to the one indicated in parentheses. The abbreviations FW and BW stand for forward and backward whirling, respectively. Damping ratios are given in terms of critical damping ratio.

Mode	Frequency [Hz]	Damping
1 st Fore aft Tower	0.345	0.003
1 st Side to side Tower	0.347	0.003 - 0.009
1 st Yaw (BW Flapwise)	0.902	0.010 - 0.020
1 st Tilt (FW Flapwise)	0.974	0.011 - 0.020
1 st Symmetric Flapwise	1.077	0.010 - 0.020
1 st Vertical Edgewise (BW)	1.834	0.004
1 st Horizontal Edgewise (FW)	1.855	0.004
2 nd Tilt (FW Flapwise)	2.311	0.005
2 nd Yaw (BW Flapwise)	2.430	0.004
2 nd Symmetric Flapwise	3.000	0.005
2 nd Edgewise	6.360	0.005
Tower Torsion Mode (needs further verification)	6.154	0.005

Table 4.3. Modal parameters estimated for the parked turbine

In system identification, it is recommended to use at least 2 different signals in the analyses. Therefore, in this work the laser signal had to be accompanied with one strain gauge measurement. The system parameters identified by using one strain gauge (reference) and one laser measurement were almost the same as those obtained by using 8 strain gauges. The same analyses can also be made by using 2 different laser

systems simultaneously. In this case, no additional strain gauge measurement would be needed as a reference.

Vibration measurements on parked turbines are relatively easier to conduct and to analyze because most of the limitations and problems mentioned above are not encountered while testing parked turbines.

Since the rotation of the blades, pitching and yawing motions are prevented; time invariant system assumption is easily satisfied. Similarly, the steady state random excitation assumption is better fulfilled because the P harmonics, which dominate the response of the structure during rotation, are not present in the response measured at parked condition.

The aerodynamic damping, which constitutes the major part of the aeroelastic damping identified for rotating turbines, is usually neglected for the parked turbine when the wind speed is low. Therefore, the estimated damping can be assumed to be composed of only structural damping and is generally less than 1%. These low damping ratios enable the modal parameters to be extracted accurately by using very short measurement durations (approximately 100 cycles).

For a parked turbine, there is only one reference frame (ground fixed) and no coordinate transformation is needed. Low wind speeds cause a relatively smaller static component in the measured deformation values. The measured response is close to zero (or constant) average time series for which the utilized analysis methods produce accurate and reliable results. On the other hand, the vibration levels measured for the parked turbine are much smaller compared to those measured for a rotating one in nominal wind conditions. Since the measurement error to signal ratio is relatively high, photogrammetry measurements taken at parked condition could not provide the high resolution required to be used in OMA.

Proper selection of the reference signal combination is important for all kinds of vibration measurements. However, it can be more critical if some frequencies (like P harmonic) have very high energy levels and dominate the measured response. For a parked turbine, all the modes have comparable amplitudes and participation factors.

Although for low wind speeds, the aerodynamic component of the estimated damping is considered to be small, some slight differences in the extracted damping can still be

encountered due to the aerodynamic drag effect mentioned above. As can be seen in Table 4.3, especially for the 1st flapwise modes (tilt, yaw and symmetric) the estimated damping differs slightly depending on the data series analyzed. This difference can be attributed to the changes in effective wind direction. Since the turbine is kept at a fixed orientation during the tests, the changes in the instantaneous wind direction result in a different aerodynamic coupling for each measurement. This also shows that it is not possible to completely eliminate the aerodynamic component of the damping even for very low wind speeds.

8. Measurements on the Rotating Turbine

This section summarizes the results of the analyses of the strain gauge and photogrammetry measurements taken on the rotating turbine. During the test period, the response of the turbine was continuously monitored by the strain gauges. Therefore, the modal parameters could be extracted for various operating conditions and wind speeds. As in the analysis of parked turbine data, the NExT approach was used together with the LSCE time domain identification method.

Figure 4.10 shows the aeroelastic frequencies identified for different wind speeds. As can be seen in the figure, some of the modes extracted for the parked turbine (shown in Table 4.3) could not be detected for the rotating turbine. The 1st tilt (FW flapwise), 1st yaw (BW flapwise) and 1st symmetric flapwise modes could not be identified due to their very high damping ratios. Hansen et al. [21] experienced the same problem and reported that these three flapwise modes have too high aerodynamic dampings for identification in response to the excitation by turbulence. Similarly, the 2nd BW flapwise mode, which has a relatively lower damping, could not be observed in the rotation data due to its weak participation in the recorded motion.

Figure 4.11 shows the aeroelastic damping ratios estimated for the first fore aft and side to side tower bending modes. Although the two tower modes have almost the same frequencies, aeroelastic damping calculated for the fore aft mode is greater due to the motion of the tower in the direction perpendicular to the rotor plane. Compared with the side to side tower mode, analyzing the modal parameters of the fore aft mode is more

challenging. As previously shown in Figure 4.9, the response of the tower in fore aft direction is usually a varying average time series due to the slowly changing mean wind speed, which results in some scatter in the damping.

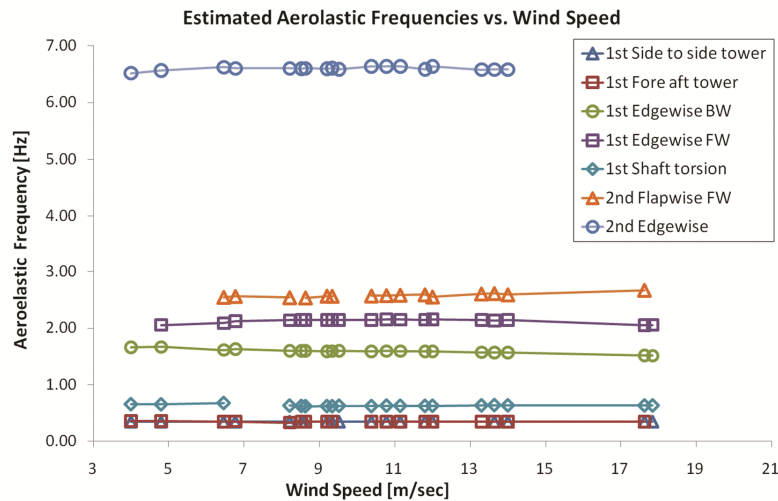


Figure 4.10. The extracted aeroelastic modes

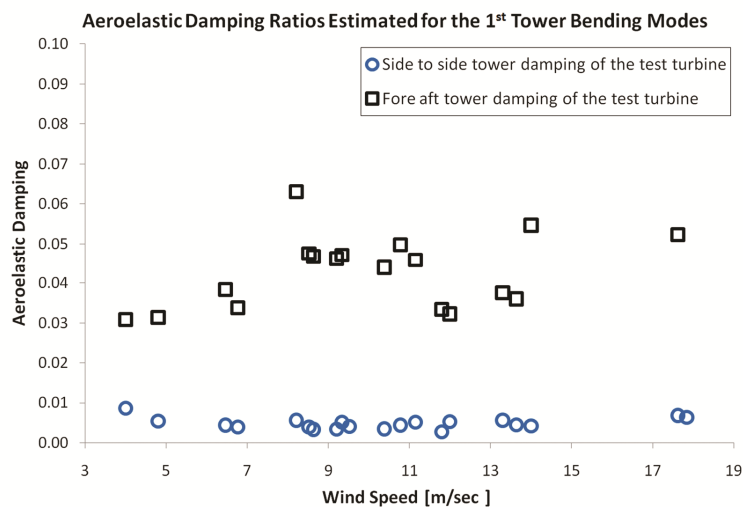


Figure 4.11. Aeroelastic damping ratios of the 1st tower modes

Similarly, Figure 4.12 shows the damping ratios estimated for the 1st edgewise modes. These modes are very straightforward to identify because they have very high modal participation and low aeroelastic damping. Since the measured response is perpendicular to the effective wind direction, the recorded motion does not have a static component due to the mean wind speed. The vibration time histories obtained are in the

form zero average time series for which identification algorithms (especially those utilizing correlation functions) produce very accurate results. Therefore, edgewise direction vibration data can easily be processed resulting in a relatively low scatter.

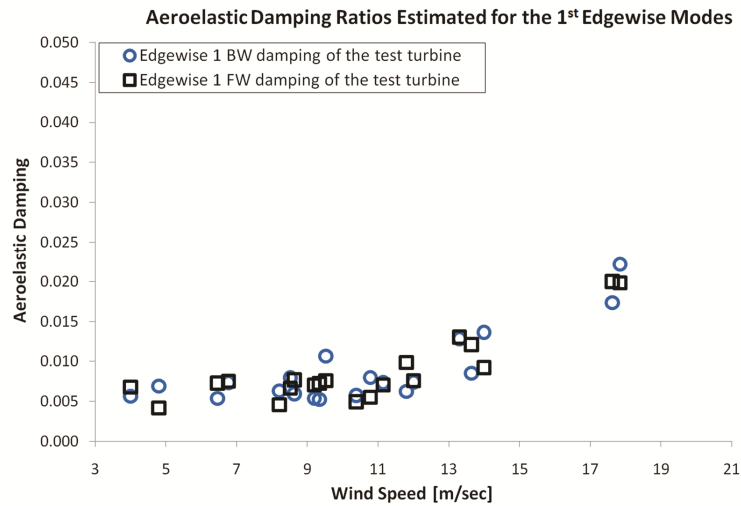


Figure 4.12. Aeroelastic damping ratios of the 1st edgewise modes

Figure 4.13 shows the aeroelastic damping ratios identified for the shaft torsion mode. This mode is very difficult to detect and analyze. Most of the sensors could not measure this frequency. The edgewise direction strain gauge measurements taken on the blades were the only signals that could be used to extract this mode.

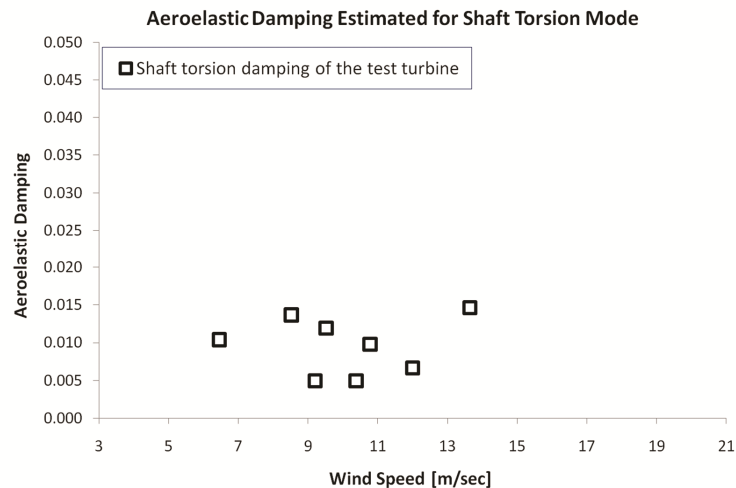


Figure 4.13. Aeroelastic damping ratios of the shaft torsion mode

Several signal combinations were tested to determine the best reference signals to be used in the analysis of the shaft torsion mode. When the edgewise signals were combined and processed with the flapwise direction strain signals, the identified mode was lost. Since it has a very low participation in the response, the extra noise added by the flapwise signals, which do not contain any information related to the shaft response, prevented this mode from being detected accurately. Although the frequencies could be identified for all the data blocks analyzed, damping ratios could not be extracted for most of the measurements. Estimations could only be made for some wind speeds lower than the rated wind speed.

Figure 4.14 shows the damping estimations made for the 2nd FW flapwise mode. Similar to the shaft torsion mode, several reference signal combinations are required to be tested to make accurate damping estimations. Since its modal contribution is relatively higher, this mode could be detected in most of the measurements. For each measurement, the analyses were repeated by using the fixed and rotating reference frames separately. When the investigated frequency coincided with some P harmonics in one of the coordinate systems, the other coordinate system enabled the modal parameters to be determined.

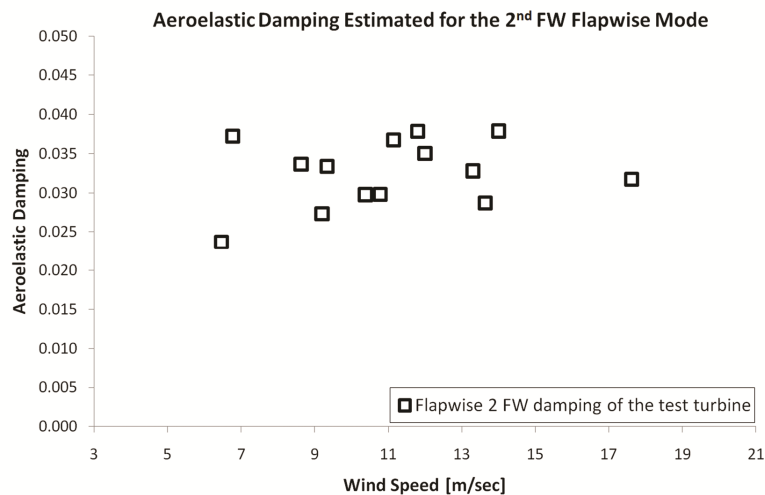


Figure 4.14. Damping ratios estimated for the 2nd FW flapwise

The aeroelastic damping ratio estimated for the 2nd edgewise frequency is shown in Figure 4.15. Similar to the 1st edgewise mode, this mode has a low damping and a high modal contribution. Since the measured vibration is perpendicular to the effective wind direction, it does not have a slowly changing static component. Therefore, it can easily be processed and analyzed resulting in a low scatter.

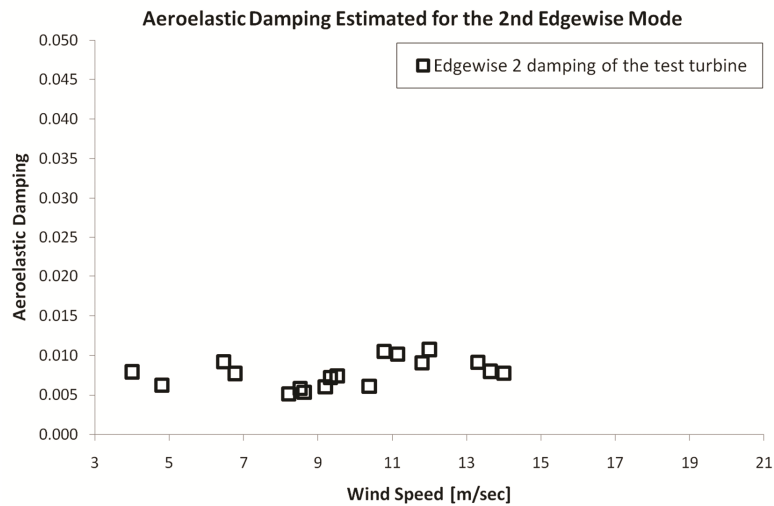


Figure 4.15. Damping ratios estimated for the 2nd FW edgewise

As mentioned before, one of the main objectives of the research project is to investigate how optical measurement systems (photogrammetry and laser interferometry) can be used to measure the dynamic response of large wind turbines. Due to the difficulties in keeping the laser on the same marker while the turbine is rotating, LDV was only used for the tests performed on the parked turbine.

During rotation, the dynamic response of the turbine was simultaneously monitored at 33 different locations on the rotor by using photogrammetry. Initial results show that the deformations of the turbine can be measured with an average accuracy of ± 25 mm from a measurement distance of 220 m [3]. Since the amplitudes of the measured vibrations vary between 600 and 1000 mm, this accuracy can be considered to be high. However, due to the limited memory capacity of the camera systems used in the tests, each photographic measurement block consists of 21 seconds or 6 cycles of rotation.

Considering the recommended measurement durations, it can be concluded that it would be very challenging to get reliable identification results by using such short data series that contain only 6 cycles. However, the P harmonics dominating the overall response and some important turbine modes can clearly be detected from the PSD plots of the recorded vibration data (please see Figure 4.6). On the other hand, PSD plots are not sufficient alone to accurately display the highly damped modes or the modes which have very low modal contributions in the response. The observability of some higher modes by using OMA methods (the 2nd edgewise, the 2nd and 3rd flapwise blade modes) was also demonstrated in a recent work of the authors [24]. However, further investigations, which require longer measurement durations and more detailed analyses, are needed to verify these estimations.

9. Conclusions

Identification of the in-operation vibration characteristics of wind turbines is a very challenging task that requires several factors to be taken into account during different steps of the structural investigation such as measurement, data analysis and evaluation of the results.

The conventional dynamic testing techniques based on exciting the structure at several locations with sufficient force amplitudes cannot be easily applied to wind turbines due to their size and the technical difficulties in providing very large forces that are required to reach sufficient excitation levels. Therefore, testing and monitoring the dynamic behavior of large wind turbines should preferably be performed by applying OMA (Operational Modal Analysis) methods where it is not required to measure the forces acting on the structure.

Several researchers conducting infield dynamic tests on wind turbines report that these methods seem very promising in extracting the modal parameters accurately. However, the applicability limits of these identification tools and the extent to which the main assumptions of OMA methods are satisfied in case of analyzing the real turbine data are still being investigated. Although the complex characteristics of the wind loads acting on the structure cause the efficient use of OMA methods for monitoring these

structures to be challenging, most of the important turbine modes can still be extracted accurately.

The wind excitation due to the aerodynamic forces contains significant components of all P-harmonics on the rotor frame and of the 1P, 3P, 6P, etc. harmonics in the fixed frame. These P harmonics usually have very high energy levels and dominate the recorded response up to 4-5 P. Although their amplitudes get smaller for higher frequencies they can still be effective up to 24P. These frequencies may coincide with the eigenfrequencies of the system and affect the estimated parameters.

For a rotating wind turbine, the identified modal parameters (especially the damping) are significantly affected by the wind speed and rotor speed. Therefore, during the measurements, the operating conditions of the turbine have to stay constant. Possible variations in these parameters result in noisy input data and scatter of the identified parameters. Although frequency estimations are mostly reliable and stable, significant scatter can be encountered in damping estimations. This scatter can be caused by not only the change in the operating conditions but also the mathematical uncertainty related to the applied algorithms and the limited length of the measurement blocks.

For a rotating wind turbine some important turbine modes have very high aeroelastic damping ratios changing between 10% and 60% (in terms of critical damping ratio), making them very difficult to be detected by most of the identification algorithms that are currently in use. Although extracting the high damping modes is a challenge for almost all system identification methods, some methods can be considered to be more advantageous in analyzing these highly damped modes. Therefore, attention should be paid to selecting the identification tool to be used in the structural investigation. However, it can still be required to use several techniques together and compare the obtained results to ensure the accuracy of the estimations.

The modes that have relatively lower modal contributions in the measured vibration response can only be determined when the appropriate signals, which specifically include the investigated frequency, are used. Analyzing all the signals together can increase the noise level in the measurements and prevent the detection of these weak

modes. Therefore, before performing operational modal analysis, the reference signal combinations should be determined for each frequency separately.

In some cases, the analyses are required to be performed in two different ways, using the fixed reference frame and using a rotating one. When the investigated frequency coincides with some P harmonics in one of the coordinate systems, the other coordinate system may enable the modal parameters to be determined.

These and other similar approaches suggested in this work will definitely increase the analysis duration, but they are expected to be very useful in solving the specific problems encountered in testing and monitoring wind turbines.

The tested optical measurement systems were verified to provide very valuable information on the dynamic response of the structure. All the modes that were identified for the parked turbine could successfully be detected in the laser measurements.

Photogrammetry was also proven to provide the accurate measurement of the 3D deformations of the rotor. Due to the low memory capacity of the utilized systems, the measurement duration was limited to 21 secs. However, the high resolution deformation measurements simultaneously taken at 33 points made some important modes possible to be identified even for such short measurement durations. Photogrammetry is expected to be a versatile and cost effective alternative for monitoring and testing wind turbines with the aid of the rapid progress in the hardware and image processing technologies.

Acknowledgements

This research project was supported by the We@Sea research program, financed by the Dutch Ministry of Economical Affairs. The authors would like to thank ECN (Energy Research Center of the Netherlands) for providing the test turbine and the other technical equipment. The authors also acknowledge the extensive contribution of Pieter Schuer (GOM mbH), Wim Cuypers (GOM mbH), Theo W. Verbruggen (ECN) and Hans J. P. Verhoef (ECN) in organizing and performing the field tests.

References

- [1] Website, Nordex Wind Energy, <http://www.nordex-online.com/en/products-services/wind-turbines/n80-25-mw/> (accessed August 2011).
- [2] Website, ECN Energy Research Center of the Netherlands, <http://www.ecn.nl/units/wind/wind-turbine-testing/> (accessed September 2011).
- [3] M. Ozbek, D.J. Rixen, O. Erne, G. Sanow, Feasibility of monitoring large wind turbines using photogrammetry, *Journal of Energy* 35 (12) (2010) 4802-4811.
- [4] E.M. Mikhail, J.S. Bethel, J.C. McGlone, *Introduction to Modern Photogrammetry*, Wiley, New York, 2001.
- [5] Website, GOM Optical Measuring Techniques, <http://www.gom.com> (accessed September 2011).
- [6] G.H. James, T.G. Carne, J.P. Lauffer, Modal testing using natural excitation, in: *Proceedings of the 10th International Modal Analysis Conference*, San Diego, California, 1992.
- [7] G.H. James, T.G. Carne, J.P. Lauffer, *The Natural Excitation Technique (NExT) for Modal Parameter Extraction from Operating Wind Turbines*, SAND92-1666, Sandia National Laboratories, Albuquerque, NM, USA, 1993.
- [8] G.H. James, T.G. Carne, J.P. Lauffer, The Natural Excitation Technique (NExT) for modal parameter extraction from operating structures, *Journal of Analytical and Experimental Modal Analysis* 10 (4) (1995) 260-277.
- [9] G.H. James, T.G. Carne, P. Veers, Damping measurements using operational data, *ASME Journal of Solar Energy Engineering* 118 (1996) 190-193.
- [10] T.G. Carne, G.H. James, The inception of OMA in the development of modal testing technology for wind turbines, *Mechanical Systems and Signal Processing* 24 (2010) 1213-1226.
- [11] N.M.M. Maia, J.M.M. Silva, J. He, N.A.J. Lieven, R.M. Lin, G.W. Skingle, W.M. To, A.P.V. Urgueria, *Theoretical and Experimental Modal Analysis*, Research Studies Press Ltd., Somerset, England, 1997.
- [12] P. Mohanty, D.J. Rixen, Operational modal analysis in the presence of harmonic excitation, *Journal of Sound and Vibration* 270 (2004) 93-109.
- [13] F. Meng, M. Ozbek, D.J. Rixen, M.J.L. Tooren, Comparison of system identification techniques for predicting dynamic properties of large scale wind turbines by using the simulated time response, in: *Proceedings of the 28th International Modal Analysis Conference*, Jacksonville, Florida, 2010.
- [14] P. van Overschee, B. De Moor, *Subspace Identification for Linear Systems: Theory - Implementation - Applications*, Kluwer Academic Publishers, London, 1996.
- [15] K.D. Cock, B. De Moor, Subspace identification methods, *Control systems robotics and automation* 1 (3) (2003) 933-979.
- [16] D. Tcherniak, S. Chauhan, M.H. Hansen, Applicability limits of operational modal analysis to operational wind turbines, in: *Proceedings of the 28th International Modal Analysis Conference*, Jacksonville, Florida, 2010.

- [17] D. Tcherniak, S. Chauhan, M. Rossetti, I. Font, J. Basurko, O. Salgado, Output-only modal analysis on operating wind turbines, application to simulated data, in: Proceedings of the European Wind Energy Conference, Warsaw, Poland, 2010.
- [18] S. Chauhan, D. Tcherniak, M.H. Hansen, Dynamic characterization of operational wind turbines using operational modal analysis, in: Proceedings of the China Wind Power 2010, Beijing, China, 2010.
- [19] M.S. Allen, M.W. Sracic, S. Chauhan, M.H. Hansen, Output-only modal analysis of linear time-periodic systems with application to wind turbine simulation data, *Mechanical Systems and Signal Processing* 25 (2011) 1174-1191.
- [20] F. Meng, P. Masarati, M.J.L. van Tooren, Free/open source multibody and aerodynamic software for aeroelastic analysis of wind turbines, in: Proceedings of the 28th ASME Wind Energy Symposium, (47th Aerospace Science Meeting and Exhibit), Orlando, Florida, 2009.
- [21] M.H. Hansen, K. Thomsen, P. Fuglsang, Two methods for estimating aeroelastic damping of operational wind turbine modes from experiments, *Wind Energy* 9 (2006) 179-191.
- [22] P. Mohanty, D.J. Rixen, Modified SSTD method to account for harmonic excitations during operational modal analysis, *Mechanism and Machine Theory* 39 (12) (2004) 1247-1255.
- [23] M.S. Allen, S. Chauhan, M.H. Hansen, Advanced operational modal analysis methods for linear time periodic system identification, in: Proceedings of the 29th International Modal Analysis Conference, Jacksonville, Florida, 2011.
- [24] M. Ozbek, F. Meng, D.J. Rixen, M.J.L. van Tooren, Identification of the dynamics of large wind turbines by using photogrammetry, in: Proceedings of the 28th, International Modal Analysis Conference, Jacksonville, Florida, 2010.
- [25] D.A. Peters, Fast floquet theory and trim for multi-bladed rotorcraft, *Journal of the American Helicopter Society* 39 (1994) 82-89.
- [26] M. Ozbek, D.J. Rixen, Operational modal analysis of a 2.5 MW wind turbine using optical measurement techniques and strain gauges, *Journal of Wind Energy* (2011) (Accepted).
- [27] M. Ozbek, D.J. Rixen, Optical measurements and operational modal analysis on a large wind turbine: Lessons learned, in: Proceedings of the 29th International Modal Analysis Conference, Jacksonville, Florida, 2011.
- [28] M. Ozbek, D.J. Rixen, T.W. Verbruggen, Remote monitoring of wind turbine dynamics by laser interferometry: Phase1, in: Proceedings of the 27th International Modal Analysis Conference, Orlando, Florida, 2009.

CHAPTER 5

An Alternative NExT (Natural Excitation Technique) Based Eigenfrequency Estimator for Analyzing Highly Damped Systems

Muammer Ozbek ^{*,a}, Daniel J. Rixen ^b

^a Delft University of Technology, Faculty of Mechanical Engineering, Mekelweg 2, 2628 CD, Delft, the Netherlands

^b Technische Universität München, Institute of Applied Mechanics, Boltzmannstr. 15 D-85748 Garching, Germany

Abstract

NExT (Natural Excitation Technique) is a well-established experimental dynamic analysis method, often used in applications where vibration frequencies and modes need to be estimated from operational data. The method is proven to provide accurate frequency and damping estimations for eigenmodes with low damping ratios. However, it requires analyzing very long time histories to extract the modal parameters when highly damped modes are searched for. Therefore, the applicability of the standard NExT algorithm to some specific structures such as wind turbines, where some of the important modes have very high aeroelastic damping, is limited.

In this work a new approach, which is based on the NExT theory, is introduced to overcome these problems. The proposed method enables eigenfrequencies of the high damping modes to be estimated with an accuracy of 95%, in the ideal case, by using data series which are approximately 30 times shorter than those required for standard NExT.

This work was submitted to *Mechanical Systems and Signal Processing (MSSP)*

1. Introduction

NExT (Natural Excitation Technique) [1-3], which enables modal parameters of a system to be estimated from in-operation response data without needing to measure the input forces acting on the structure, is a well established experimental dynamic analysis tool utilized in several disciplines. The method assumes steady state random white

noise excitation and is based on the use of auto- and cross-correlation functions of measured response signals as impulse response functions. Therefore, it allows several time domain analysis methods, which require impulse response functions as input, to be used for analyzing vibration data excited by ambient forces.

The preliminary versions of NExT have been in use since the early 90's. The method was developed to extract dynamic characteristics of wind turbines [1-3], which are very challenging structures to be tested by using conventional experimental modal analysis (EMA) techniques. Several researchers [4-6] have successfully used operational modal analysis (OMA) methods (based on NExT or similar approaches) for testing wind turbines and reported that they have obtained very good coherence between the modal parameters identified by operational and experimental modal analysis tools. A more comprehensive review of the history and development of NExT can be found in a recent work by Carne and James who are the developers of this technique [7].

The method is well known for providing accurate frequency and damping estimates in identifying the systems with low damping ratios. Unless some additional dampers are used intentionally, most structures (buildings, bridges) have relatively low structural damping varying between 0.5% and 3%. Therefore, NExT can easily be applied to extract their dynamic characteristics [8,9]. However, in case of high damping the NExT method (and Operational Modal Analysis in general) has difficulties in identifying the modal parameters adequately. As a matter of fact, wind turbines, for which the method was specifically developed, are one of the typical examples of these systems [10-13].

Unlike the civil engineering structures mentioned above, the damping identified for wind turbines is not purely structural; it is mainly aeroelastic. Aeroelastic damping is due to the combined effect of both structural deformations and aerodynamic forces. The aerodynamic damping originates from the fact that apparent angle of attack on the blade is related to flapping speed, rotational speed and wind speed. Therefore, the overall damping is not constant and changes significantly depending on operating conditions. For a rotating wind turbine, some important turbine modes have very high aeroelastic damping ratios changing from 10% to 60% (in terms of critical damping ratio), which make them very difficult (if not impossible) to be detected by most of the

identification algorithms currently in use [9]. One could say that identifying these modes properly is not critical since they will not lead to aeroelastic instabilities (i.e. flutter), but the information one can extract from those modes can be very useful for model validation and for health monitoring for instance.

For Operational Modal Analysis (OMA) tools based on NExT, it is observed that measurement duration is one of the most important factors in the estimation of these high damping modes [9, 12, 13]. In theory, the calculation of correlation function is founded on infinite time series and can be considered, in its simplest form, as a mathematical averaging operation. Therefore, increasing the length of the analyzed data series (number of data points) will definitely increase the accuracy of averaging and of the correlation function. Measurement duration is more critical in identifying high damping modes. Low damping modes can still be identified from short data series. However, very long time histories are needed to create correlation functions which can accurately represent the impulse response functions of these high damping modes.

In system identification, measurement duration is defined in terms of number of cycles of the lowest frequency included in the data block and is generally recommended to be greater than 500 cycles. Depending on the dynamic properties of the structure analyzed, several researchers [14] suggest using even longer measurement blocks, namely between 1000 and 2000 times the period of the structure's fundamental mode. The number of required cycles increases significantly (around 4000-5000 cycles) when the investigated modes have high damping ratios [9, 12]. Since for a rotating wind turbine some of the modes are highly damped, very long time series are needed. For a MW scale wind turbine, 5000 cycles correspond to test durations of approximately 4-5 hours. However, finding such long measurement periods, during which wind speed, rotor speed and pitch angle stay constant, is a very challenging task.

Changes in operating conditions affect not only damping but also stiffness properties of the structure for several reasons. First the centrifugal forces, which are proportional to the square of the rotation speed, generate geometric stiffening. Secondly when the rotation speed varies, the aerodynamic stiffness (change of aerodynamic forces with deformation) varies. Finally, when measured in the reference frame of the rotor plane,

the stiffness of the rotor varies with the blade pitch angle, which is automatically controlled depending on the wind speed and rotor speed. Therefore, attention should be paid to whether operating conditions of the turbine stay constant during the measurements or not. Accepting some changes in operating conditions may violate the time invariance assumption, which is a significant prerequisite for most system identification techniques. This simple but important dilemma is one of the major problems to be tackled in testing and monitoring wind turbines. Applicability limits of several dynamic analysis tools and the extent to which the main assumptions of OMA methods are fulfilled in case of analyzing the real wind turbine data are still being investigated [15-18]. However, these techniques are continuously being improved and optimized to overcome the problems that may be encountered due to the complicated nature of the turbine structure and wind loading [19-21].

In this work, a new method, which is also based on the NExT theory, is proposed as a possible approach to improve the capability of NExT to identify high damping modes. The results of the analyses show that eigenfrequencies related to highly damped modes can be detected by using very short data series of 150-200 cycles (instead of 5000). This achievement is expected to significantly facilitate the validation of turbine models, improving health monitoring based on operational measurements and developing better control algorithms to minimize the vibration of turbine components.

The paper is organized as follows. In section 2 we illustrate on a simple example the difficulty to identify highly damped modes in operational modal analysis. In section 3 we shortly recall the mode superposition for impulse response in order to introduce the notations and to set the basis for the analysis. In section 4 we derive the relation between the correlations computed for finite length response data and the modal responses. In section 5 we show that, due to finite signal lengths, correlations are not exactly impulse-like responses as assumed in the standard NExT method, but included a remainder that can be used to evaluate highly damped frequencies in a procedure further outlined in section 6. The application of the proposed analysis technique is also illustrated in the same section on a simulated test case.

2. Identification of a 5 DOF Analytical Model by Standard NExT Algorithms

This section aims at illustrating the limitations of using standard NExT algorithms in identifying highly damped systems. In order to investigate specifically the performance of the applied method, numeric response data generated by a 5 DOF (degree of freedom) system is used. Such an approach makes it possible to produce response data from an analytical model, of which dynamic characteristics (eigenfrequencies and damping ratios) are known a priori. The modal parameters are estimated by applying identification algorithms on these simulated data series. Extracted parameters are then compared with the known exact values. Figure 5.1 shows the 5 DOF system utilized in the analyses. In the figure, the symbols m , k and c stand for the mass, stiffness and damping of the structural components, respectively. The selected model is intended to approximate a wind turbine blade. Therefore, eigenfrequencies are chosen in accordance with those expected to dominate the response of large wind turbines. Likewise a very large damping ratio is assigned to the 1st mode similar to the aeroelastic damping of the first flapwise blade mode. Table 5.1 shows the exact and identified values of the modal parameters of the system analyzed. The estimations shown in Table 5.1 are made by using time series having durations of 500 cycles of the lowest frequency (0.55 Hz) included in the data.

For the structural configuration shown in Figure 5.1, it is not possible to obtain the modal damping ratios given in Table 5.1 by using physically meaningful lumped dampers. The modal damping assumption was thus used in order to assign a very high damping ratio to the first mode and low damping ratios to the other modes. Therefore, in this example the damping matrix has been built by a modal expansion, assuming real modes and no modal coupling through damping:

$$[C] = \sum_{s=1}^5 [M] \{\phi_s\} 2\xi_s \omega_s \{\phi_s\}^T [M] \quad (1)$$

where the damping matrix $[C]$ is built on the mass matrix $[M]$, the mass-normalized real modes $\{\phi_s\}$, the damping ratios ξ_s and the real eigenfrequency ω_s .

Uncorrelated random white noise input forces having a flat spectrum in the range [0 100] Hz were applied on the structure on all 5 degrees of freedom simultaneously. Since the eigenfrequencies of the system are all in the low frequency range ([0 4] Hz), it is ensured that all the modes are excited with sufficient energy.

In order to eliminate the effects of initial conditions and transition response, the first 300 seconds of the generated data series were not utilized in the analysis. The remaining data was used to calculate correlation functions, which as suggested by NExT, can be used as impulse response functions (see also the following sections). Obtained correlation functions were analyzed using the LSCE (Least Square Complex Exponential) method to extract the modal parameters shown in Table 5.1. LSCE is a time domain analysis method identifying the modal parameters by a fit on the impulse response functions [22-24]. As mentioned before, NExT enables LSCE and similar time domain identification techniques to be used for analyzing vibration data excited by ambient forces.

In order to investigate the effect of measurement duration on the estimated modal parameters, these calculations were repeated for correlation functions which are generated by using data series with different lengths. It was observed that at least 200-300 cycles are needed to make stable and accurate estimations for the modes with low damping ratios. These values are consistent with those mentioned in literature. However, identification of the highly damped mode is difficult (the first mode in Table 5.1 cannot be identified with 500 cycles) and requires much longer data series to be analyzed. The utilized algorithms can extract the highly damped first mode only when the measurement duration is extended up to 4000-5000 cycles.

When the LSCE identification technique is directly applied to the impulse response functions computed for the 5 DOF system, all the modes can be identified very easily and accurately. This exercise clearly shows that the limitation related to the detection of highly damped modes is not due to the LSCE identification but rather to the evaluation of impulse responses through correlation of signals in NExT. Indeed, in the milestone publications [1-3] summarizing the derivation of the method, it is clearly stated that the modes to be identified are assumed to have low damping ratios. In the current work,

calculations verify that it is also possible to extract highly damped modes provided that very long measurements are analyzed. However, in practice it is very difficult to find such long measurement durations during which the two important assumptions of NExT, i.e. time invariant system and steady state random excitation assumptions, are satisfied.

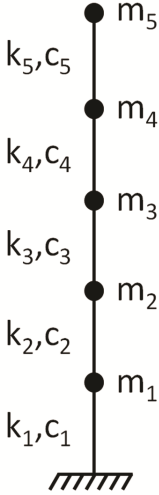


Figure 5.1. The 5 DOF system analyzed

Mode	Damped Frequency Exact [Hz]	Damped Frequency Estimated [Hz]	Damping Exact	Damping Identified
1	0.55	-	50.0%	-
2	1.78	1.78	1.00%	1.00%
3	2.78	2.78	1.40%	1.30%
4	3.58	3.59	0.90%	0.90%
5	4.02	4.02	1.20%	1.10%

Table 5.1. Modal parameters of the 5 DOF system analyzed (exact and NExT-LSCE estimated values using noise-free time signal corresponding to 500 cycles of the fundamental frequency)

The following sections describe how the standard NExT algorithm is modified to be able to detect the highly damped eigenfrequencies by using relatively shorter data. Estimation of the corresponding damping ratios is not included in this work.

3. Modal Superposition and Impulse Response

For a linear system with N degrees of freedom, the general dynamic equation of motion can be written as follows;

$$[M]\{\ddot{x}(t)\} + [C]\{\dot{x}(t)\} + [K]\{x(t)\} = \{f(t)\} \quad (2)$$

where,

$[M]$: Mass matrix

$[C]$: Viscous damping matrix

$[K]$: Stiffness matrix

$\{x(t)\}$: Displacement vector

$\{\dot{x}(t)\}$: Velocity vector

$\{\ddot{x}(t)\}$: Acceleration vector

$\{f(t)\}$: Force vector

The time response vector $\{x(t)\}$ obtained from Eq.(2) can be described as a superposition of the modal responses of the dynamic system.

$$\{x(t)\} = \sum_{s=1}^N \{\phi_s\} q_s(t) = [\Phi]\{q(t)\} \quad (3)$$

In Eq.(3) $q_s(t)$, $\{\phi_s\}$, $[\Phi]$, $\{q(t)\}$ represent the modal (or normal) coordinates, mode shape vector of the s^{th} mass-normalized mode, the mode shape matrix and the array of modal coordinates, respectively. Substituting Eq.(3) into Eq.(2), the dynamic equation of motion can be re-written.

$$[M][\Phi]\{\ddot{q}(t)\} + [C][\Phi]\{\dot{q}(t)\} + [K][\Phi]\{q(t)\} = \{f(t)\} \quad (4)$$

Pre-multiplying Eq.(4) by the transpose of mode shape matrix $[\Phi]^T$, Eq.(2) is projected onto the modal basis. By using the modal mass, stiffness and damping matrices

described in Eq.(6) to (8), the equation of motion is re-arranged in modal coordinates as shown in Eq.(9).

$$[\Phi]^T [M] [\Phi] \{\ddot{q}(t)\} + [\Phi]^T [C] [\Phi] \{\dot{q}(t)\} + [\Phi]^T [K] [\Phi] \{q(t)\} = [\Phi]^T \{f(t)\} \quad (5)$$

$$[\Phi]^T [M] [\Phi] = \begin{bmatrix} m \\ \vdots \\ m \end{bmatrix} \quad (6)$$

$$[\Phi]^T [K] [\Phi] = \begin{bmatrix} k \\ \vdots \\ k \end{bmatrix} \quad (7)$$

$$[\Phi]^T [C] [\Phi] = \begin{bmatrix} c \\ \vdots \\ c \end{bmatrix} \quad (8)$$

$$\begin{matrix} \begin{bmatrix} m \\ \vdots \\ m \end{bmatrix} \\ (N \times N) \end{matrix} \begin{matrix} \{ \ddot{q}(t) \} \\ (N \times 1) \end{matrix} + \begin{matrix} \begin{bmatrix} c \\ \vdots \\ c \end{bmatrix} \\ (N \times N) \end{matrix} \begin{matrix} \{ \dot{q}(t) \} \\ (N \times 1) \end{matrix} + \begin{matrix} \begin{bmatrix} k \\ \vdots \\ k \end{bmatrix} \\ (N \times N) \end{matrix} \begin{matrix} \{ q(t) \} \\ (N \times 1) \end{matrix} = \begin{matrix} \begin{bmatrix} \Phi \\ \vdots \\ \Phi \end{bmatrix}^T \\ (N \times N) \end{matrix} \begin{matrix} \{ f(t) \} \\ (N \times 1) \end{matrix} \quad (9)$$

It should be noted that in this work the modes are assumed to be orthogonal also with respect to the damping matrix. In general this is not true and is a good approximate only if the damping is small and frequencies are well separate. The assumption of modal damping will be made here to simplify the presentation of the method. In order to ensure that modes are also orthogonal with respect to the damping matrix, the damping matrix is assumed to have the form used in Eq.(1) which can also be written in the matrix notation by using a diagonal matrix E prescribing damping values to be assigned for each mode:

$$[E] = \begin{bmatrix} 2\xi_1\omega_1 & & \\ & \ddots & \\ & & 2\xi_s\omega_s \end{bmatrix} \quad (10)$$

where ξ_s and ω_s stand for the critical damping ratio and angular frequency of the s^{th} mode. Then the C matrix is formed using the relation given in Eq.(11)

$$[C] = [M] [\Phi] [E] [\Phi]^T [M] \quad (11)$$

The new form displayed in Eq.(9) enables the vibration behavior of a MDOF system to be analyzed as the superposition of independent SDOF (Single Degree of Freedom) systems. Therefore, Eq.(12) can be written for each mode to represent the corresponding SDOF system.

$$m_s \ddot{q}_s(t) + c_s \dot{q}_s(t) + k_s q_s(t) = \{\phi_s\}^T \{f(t)\} \quad s = 1, \dots, N \quad (12)$$

In Eq.(12), m_s , c_s and k_s represent the modal mass, damping and stiffness of the s^{th} mode, respectively. Eq.(13) is acquired by dividing Eq.(12) by m_s .

$$\ddot{q}_s(t) + 2\xi_s \omega_s \dot{q}_s(t) + \omega_s^2 q_s(t) = \frac{1}{m_s} \{\phi_s\}^T \{f(t)\} \quad (13)$$

This equation formulates the response of a SDOF system vibrating under the action of a general force and can be solved by Duhamel's integral or convolution given in Eq.(14).

$$q_s(t) = \int_{-\infty}^t \{\phi_s\}^T \{f(\tau)\} g_s(t-\tau) d\tau \quad (14)$$

In the equation above, $g_s(t)$ is the impulse response of the s^{th} SDOF system and can be written as follows;

$$g_s(t) = \frac{1}{m_s \omega_s^d} e^{-\xi_s \omega_s t} \sin(\omega_s^d t), \text{ for } t \geq 0 \text{ and } g_s(t) = 0, \text{ for } t < 0, \quad (15)$$

where ω_s^d represents the damped natural frequency $\omega_s^d = \omega_s \sqrt{1 - \xi_s^2}$. Substituting Eq.(14) into (3) we get Eq.(16). Similarly, Eq.(17) is just a simplified version of (16) derived to calculate the response $x_{ak}(t)$ of a single output point "a", due to a single force input $f_k(t)$ applied at point k .

$$\{x(t)\} = \sum_{s=1}^N \{\phi_s\} \{\phi_s\}^T \int_{-\infty}^t \{f(\tau)\} g_s(t-\tau) d\tau \quad (16)$$

$$x_{ak}(t) = \sum_{s=1}^N \phi_{as} \phi_{ks} \int_{-\infty}^t f_k(\tau) g_s(t-\tau) d\tau \quad (17)$$

Assuming that the applied force is a sudden impulse (Dirac delta function) and using the formulation given in Eq.(15), Eq.(17) can be re-arranged as follows;

$$x_{ak}(t) = \sum_{s=1}^N \frac{\phi_{as} \phi_{ks}}{m_s \omega_s^d} e^{-\xi_s \omega_s t} \sin(\omega_s^d t) \quad (18)$$

The resulting equation (18), clearly indicates that the response at point “a” due to an impulse applied at point k , can be expressed as the summation of modal impulse responses or as the summation of N decaying sinusoids. Decaying rate of each sinusoid is characterized by ξ_s and ω_s .

Note that when the modal damping assumption cannot be used (i.e. in case of general damping) expressions similar to (17) and (18) can be written, but then with complex modes [25].

4. NExT and Correlations for Finite Length Discrete Data Series

This section aims at investigating the effect of length of the analyzed data series on estimating modal parameters, more specifically, on estimating the modes with high damping. The theoretical background of the standard NExT algorithm is not repeated in detail in this article. However, a mathematical derivation, which is similar to the one introduced in the reference publications [1-3], is presented. Using discrete time and frequency domain representations enables the effect of finite length of the data to be taken into account in the calculations.

The resulting formulation is then analyzed from a different point of view which makes it possible to detect highly damped modes even from data series with short duration. It should be noted that modes with very high damping ratios can also be identified by using standard NExT algorithm but it requires analyzing very long time histories (see section 2).

The discrete cross-correlation R_{abk} between two data series x_{ak} and x_{bk} , which are finite length discrete response signals measured at locations “a” and “b” due to a general force input f_k applied at point k , is computed as in Eq.(19);

$$R_{abk}[n] = \frac{1}{Z} \sum_{m=0}^{Z-1} x_{ak}[m] x_{bk}[m+n]_{\langle Z \rangle} \quad (19)$$

In Eq.(19), Z represents the number of data points in the analyzed data blocks. The series x_{ak} and x_{bk} both have Z data points, which are measured with a constant sampling frequency of f_s . Similarly, n stands for the delay or shift for which the correlation function is computed. The delay can be represented in terms of both the number of points n and time T , where $T = n \frac{1}{f_s}$.

As mentioned before, in this work, application of NExT to finite length time series is discussed by using both time and frequency domain representations. Frequency domain analysis of finite length data can be performed by discrete Fourier transform operation which assumes that the investigated data block is periodic and repeats itself with a period equal to its length. Therefore, the summation shown above can be carried out for any successive Z data points selected from this periodically extending data series. This approach is widely known as circular convolution and/or cross-correlation. In Eq.(19) the symbol $\langle Z \rangle$ (the subscript of x_{bk}) stands for the modulo and is an indication of the periodicity of the data (with period Z). As can be seen in Eq.(19), if the summation is performed until $m = Z - 1$, one needs $Z + n$ data points for x_{bk} . The required number of data points is provided by using a series extended by periodic summation [26, 27].

Using the modal superposition principle and the result of Eq.(17), two response signals x_{ak} and x_{bk} can be written as follows;

$$x_{ak}[m] = \sum_{s=1}^N \phi_{as} \phi_{ks} y_{sk}[m] \quad (20)$$

$$x_{bk}[m+n] = \sum_{r=1}^N \phi_{br} \phi_{kr} y_{rk}[m+n] \quad (21)$$

In Eq.(20) $y_{sk}[m]$ represents the discrete form of the response which is calculated by the convolution operation $\int_{-\infty}^{m/f_s} f_k(\tau) g_s(t-\tau) d\tau$ in Eq.(17). It can be considered as the response of the s^{th} modal amplitude under the action of the force applied to the k^{th} location of the MDOF system. By substituting Eq.(20) and (21) into (19), calculation of the correlation function $R_{abk}[n]$ can be re-formulated as follows;

$$R_{abk}[n] = \frac{1}{Z} \sum_{s=1}^N \sum_{r=1}^N \phi_{as} \phi_{ks} \phi_{br} \phi_{kr} \sum_{m=0}^{Z-1} y_{sk}[m] y_{rk}[m+n]_{(Z)} \quad (22)$$

Similarly, the discrete Fourier transform of a data series $x[n]$ is defined as;

$$X_D[l] = \mathcal{F}_D(x[n]) = \sum_{n=0}^{Z-1} x[n] e^{-2\pi i \frac{n}{Z} l} \quad l = 0, 1, 2, \dots, N-1 \quad (23)$$

where i , and \mathcal{F}_D stand for the complex number $\sqrt{-1}$ and the discrete Fourier transform operation, respectively. Using the definition given in Eq.(23), the discrete Fourier transform of the cross-correlation function $R_{abk}[n]$ can be calculated as shown in Eq.(24);

$$\mathcal{F}_D(R_{abk}[n])_l = \sum_{n=0}^{Z-1} R_{abk}[n] e^{-2\pi i \frac{n}{Z} l} \quad (24)$$

Substituting (22) into (24) one gets;

$$\mathcal{F}_D(R_{abk}[n])_l = \frac{1}{Z} \sum_{s=1}^N \sum_{r=1}^N \phi_{as} \phi_{ks} \phi_{br} \phi_{kr} \sum_{n=0}^{Z-1} \sum_{m=0}^{Z-1} y_{sk}[m] y_{rk}[m+n]_{(Z)} e^{-2\pi i \frac{n}{Z} l} \quad (25)$$

The shift property [26, 28] for the Fourier transform can be written as;

$$\mathcal{F}_D(y_{rk}[m+n])_l = \sum_{n=0}^{Z-1} y_{rk}[m+n]_{(Z)} e^{-2\pi i \frac{(n+m)}{Z} l} e^{2\pi i \frac{m}{Z} l} = Y_{rk}[l] e^{2\pi i \frac{l}{Z} m} \quad (26)$$

In the equation above $Y_{rk}[l]$ represents the discrete Fourier transform of $y_{rk}[n]$.

Therefore, Eq. (25) becomes;

$$\mathcal{F}_D(R_{abk}[n])_l = \frac{1}{Z} \sum_{s=1}^N \sum_{r=1}^N \phi_{as} \phi_{ks} \phi_{br} \phi_{kr} \sum_{m=0}^{Z-1} y_{sk}[m] Y_{rk}[l] e^{2\pi i \frac{l}{Z} m} \quad (27)$$

We note that

$$Y_{sk}^*[l] = Y_{sk}[-l] = \sum_{m=0}^{Z-1} y_{sk}[m] e^{2\pi i \frac{l}{Z} m} \quad (28)$$

The symbol $*$ is used for the complex conjugate. Eq.(27) can be re-arranged by using (28);

$$\mathcal{F}_D(R_{abk}[n])_l = \frac{1}{Z} \sum_{s=1}^N \sum_{r=1}^N \phi_{as} \phi_{ks} \phi_{br} \phi_{kr} Y_{sk}[-l] Y_{rk}[l] \quad (29)$$

In Eq.(29) $Y_{sk}[-l]$ and $Y_{rk}[l]$ can be calculated as follows;

$$Y_{sk}[-l] = H_s[-l] F_k[-l] = H_s^*[l] F_k^*[l] \quad (30)$$

$$Y_{rk}[l] = H_r[l] F_k[l] \quad (31)$$

In the equations above $H_r[l]$ and $H_s[l]$ represent the frequency response functions of the r^{th} and s^{th} modal coordinates, respectively. Frequency response functions are acquired by computing the discrete Fourier transforms of the corresponding impulse response functions $g_r(t)$ and $g_s(t)$ described in Eq.(15). Similarly, $F_k[l]$ is the discrete Fourier transform of the finite length force data. Using Eq.(30) and (31), Eq.(29) can be modified further as follows;

$$\mathcal{F}_D(R_{abk}[n])_l = \frac{1}{Z} \sum_{s=1}^N \sum_{r=1}^N \phi_{as} \phi_{ks} \phi_{br} \phi_{kr} H_s^*[l] F_k^*[l] H_r[l] F_k[l] \quad (32)$$

In Eq.(32), the multiplication $F_k^*[l] F_k[l]$ is nothing but the Fourier transform of the auto-correlation function of the force, $\mathcal{F}_D(R_{ffk}[n])_l$.

$$\mathcal{F}_D(R_{ffk}[n])_l = \frac{1}{Z} F_k^*[l] F_k[l] \quad (33)$$

If we now make the assumption that the force is random white noise, its Fourier transform has a constant magnitude with random phase and its auto-correlation can be expressed as $R_{ffk}[n] = \alpha_k \delta(n)$, namely the squared RMS α_k of the random force, times a Dirac Delta function. Therefore, the Fourier transform of the auto-correlation function, is a real constant over l , and is equal to α_k [23, 28]. Note that here we have implicitly assumed that the correlation interval $T = n \frac{1}{f_s}$ is large enough for the assumption $R_{ffk}[n \neq 0] = 0$ to hold.

The final form of Eq.(32) can be written as;

$$\mathcal{F}_D(R_{abk}[n])_l = \sum_{s=1}^N \sum_{r=1}^N \alpha_k \phi_{as} \phi_{ks} \phi_{br} \phi_{kr} H_s^*[l] H_r[l] \quad (34)$$

Similar to Eq.(28) $H_s^*[l]$ can be re-written as

$$H_s^*[l] = H_s[-l] = \sum_{m=0}^{Z-1} g_s[m] e^{2\pi i \frac{l}{Z} m} \quad (35)$$

where $g_s[m]$ stands for the impulse response function of the s^{th} mode as formulated in (15), written in discrete form with Z data points. Re-applying the shift theorem on $H_r[l]$ in (36), we find,

$$H_r[l] e^{2\pi i \frac{l}{Z} m} = \mathcal{F}_D(g_r[n+m])_l = \sum_{n=0}^{Z-1} g_r[n+m] e^{-2i\pi \frac{n}{Z} l} \quad (36)$$

where $g_r[n+m]$ is the impulse response of the r^{th} mode shifted by m points. Eq.(37) is obtained by substituting Eq.(35) and (36) into Eq.(34) and by changing the order of summation.

$$\mathcal{F}_D(R_{abk}[n])_l = \sum_{n=0}^{Z-1} \{R_{abk}[n]\} e^{-2\pi i \frac{n}{Z} l} = \sum_{n=0}^{Z-1} \left\{ \sum_{s=1}^N \sum_{r=1}^N \alpha_k \phi_{as} \phi_{ks} \phi_{br} \phi_{kr} \sum_{m=0}^{Z-1} g_s[m] g_r[n+m] \right\} e^{-2\pi i \frac{n}{Z} l} \quad (37)$$

From Eq.(37) one can conclude that cross-correlation functions, when approximated by convoluting only on a finite number of data points (or finite time length L), can be computed as follows;

$$R_{abk}[n] = \sum_{s=1}^N \sum_{r=1}^N \alpha_k \phi_{as} \phi_{ks} \phi_{br} \phi_{kr} \left\{ \sum_{m=0}^{Z-1} g_s[m] g_r[n+m] \right\} \quad (38)$$

If f_s (sampling frequency) is very high compared to the eigenfrequencies of the investigated system, the innermost summation can be replaced by an integral. Since in the integral form, $R_{abk}(T)$ (originating from $R_{abk}(n\Delta t)$) and impulse response functions g_s and g_r are represented as continuous functions of time (t), Eq.(37) should be modified such that the continuous correlation functions can also be considered. The relationship between the continuous Fourier transform $X(f)$ of a function $x(t)$ and the values of the discrete Fourier transform $X_D(l)$, of N equally spaced samples of the function $x(n)$ can be described as follows [28].

$$X\left(\frac{l}{Z\Delta t}\right) = X(l\Delta f) = \Delta t X_D(l) \quad (39)$$

Similarly, the term Δt is needed to scale the expression written for $R_{abk}[n]$ so that it can also be used to represent the continuous correlation functions for which the delay is expressed not in number of points (n) but in time such as $R_{abk}(T)$ or $R_{abk}(n\Delta t)$.

$$R_{abk}[n\Delta t] = \sum_{s=1}^N \sum_{r=1}^N \alpha_k \phi_{as} \phi_{ks} \phi_{br} \phi_{kr} \left\{ \sum_{m=0}^{Z-1} g_s[m] g_r[m+n] \Delta t \right\} \quad (40)$$

Eq.(40) can be written in integral form as in Eq.(41).

$$R_{abk}(T) \approx \sum_{s=1}^N \sum_{r=1}^N \alpha_k \phi_{as} \phi_{ks} \phi_{br} \phi_{kr} \int_0^L g_s(\lambda) g_r(\lambda + T) d\lambda \quad (41)$$

where L is the duration of the data series, namely $L = Z \Delta t$. Eq.(41) is very similar to the formulation given in the derivation of the NExT algorithm presented in the reference articles [1-3]. The original equation states that;

$$R_{abk}(T) = \sum_{s=1}^N \sum_{r=1}^N \alpha_k \phi_{as} \phi_{ks} \phi_{br} \phi_{kr} \int_0^{\infty} g_s(\lambda) g_r(\lambda + T) d\lambda \quad (42)$$

As can be seen, the only difference between the two expressions is the upper bound of the integrals. Eq.(42) is derived for continuous response series by using correlation functions which are defined as in Eq.(43);

$$R_{abk}(T) = \lim_{\Gamma \rightarrow \infty} \frac{1}{\Gamma} \int_{-\Gamma/2}^{\Gamma/2} x_{ak}(t+T) x_{bk}(t) dt \quad (43)$$

Since it implicitly requires the observation of the functions for an infinitely long period of time, Eq.(42) gives the exact value of the correlation function. Whereas, Eq.(41), which is derived from Eq.(19), gives an approximation calculated by using finite length discrete time series.

It is worth mentioning that the reasoning followed in this section, showing that the correlation computed with finite length signals, Eq.(19), can be written as Eq.(41), is based on the assumption that the signal length is finite, but yet long enough so that

1. the finite length correlation of the random force, R_{ffk} , can be considered as a Dirac function (see Eq.(34)) ;
2. the use of periodic extension in Eq.(19) is a good approximation in the computation of the finite length correlation.

In this paper, we are interested in identifying frequencies with high damping, using the fact that the finite length correlation can be written as in Eq.(41). We implicitly assume

that the finite length used is long enough for the two conditions discussed above to be reasonably satisfied.

5. A NExT procedure to estimate frequencies with high damping

The effect of the length of the analyzed data series (measurement duration) on the estimated modal parameters is not explicitly mentioned in the derivation of the standard NExT algorithm. However, in practice it is recommended to use data series which contain at least 500 cycles of the lowest frequency in the investigated data block. Since NExT is applied in identification of the modes with low damping ratios, the recommended data lengths are quite sufficient to estimate the modal parameters accurately.

Following the procedure explained in the reference articles [1-3], we can re-write the term $g_r(\lambda + T)$ in Eq.(41) by using Eq.(15). Developing, one finds

$$\begin{aligned} g_r(\lambda + T) &= \frac{1}{m_r \omega_r^d} e^{-\xi_r \omega_r (\lambda + T)} \sin(\omega_r^d (\lambda + T)) \\ &= \frac{1}{m_r \omega_r^d} e^{-\xi_r \omega_r (\lambda + T)} \left(\sin(\omega_r^d \lambda) \cos(\omega_r^d T) + \cos(\omega_r^d \lambda) \sin(\omega_r^d T) \right) \\ &= \left[e^{-\xi_r \omega_r T} \cos(\omega_r^d T) \right] \frac{e^{-\xi_r \omega_r \lambda} \sin(\omega_r^d \lambda)}{m_r \omega_r^d} + \left[e^{-\xi_r \omega_r T} \sin(\omega_r^d T) \right] \frac{e^{-\xi_r \omega_r \lambda} \cos(\omega_r^d \lambda)}{m_r \omega_r^d} \end{aligned} \quad (44)$$

The resulting equation given below in (45) is obtained by substituting Eq.(44) and (15) into (41) and by re-arranging the parts which are functions of T .

$$R_{abk}(T) = \sum_{r=1}^N \left[G_{abk}^r e^{-\xi_r \omega_r T} \cos(\omega_r^d T) \right] + \left[H_{abk}^r e^{-\xi_r \omega_r T} \sin(\omega_r^d T) \right] \quad (45)$$

The coefficients G_{abk}^r and H_{abk}^r are expressions which are independent of T and further defined in Eq.(46) and (47), respectively.

$$G_{abk}^r = \sum_{s=1}^N \frac{\alpha_k \phi_{as} \phi_{ks} \phi_{br} \phi_{kr}}{m_r \omega_r^d m_s \omega_s^d} \int_0^L e^{-(\xi_r \omega_r + \xi_s \omega_s) \lambda} \sin(\omega_s^d \lambda) \sin(\omega_r^d \lambda) d\lambda \quad (46)$$

$$H_{abk}^r = \sum_{s=1}^N \frac{\alpha_k \phi_{as} \phi_{ks} \phi_{br} \phi_{kr}}{m_r \omega_r^d m_s \omega_s^d} \int_0^L e^{-(\xi_r \omega_r + \xi_s \omega_s) \lambda} \sin(\omega_s^d \lambda) \cos(\omega_r^d \lambda) d\lambda \quad (47)$$

Equation (45) is the basis of the NExT method since it shows that the correlation of output signals is similar to the impulse response function and can thus be used to identify eigenfrequencies, damping ratios and eigenmodes.

In the current work, similar analyses are performed for finite length time histories and a new approach for detecting high damping modes is introduced. As can be shown above, when discrete time series with finite length L are analyzed, Eq.(42) is replaced by Eq.(41), the upper bound of which is not ∞ but L . Therefore, different from the derivation of the standard NExT approach, for the formulations presented below, the upper limits in Eq.(46) and Eq.(47) are changed to L .

Using the first trigonometric identity in Eq.(48), the integral in G_{abk}^r (Eq.(46)) can be rearranged as in Eq.(49) and then evaluated leading to Eq.(50).

$$\sin \theta \sin \psi = \frac{\cos(\theta - \psi) - \cos(\theta + \psi)}{2} \quad \text{and} \quad \sin \theta \cos \psi = \frac{\sin(\theta + \psi) + \sin(\theta - \psi)}{2} \quad (48)$$

$$\frac{1}{2} \left[\int_0^L e^{-(\xi_r \omega_r + \xi_s \omega_s) \lambda} \cos((\omega_s^d - \omega_r^d) \lambda) d\lambda - \int_0^L e^{-(\xi_r \omega_r + \xi_s \omega_s) \lambda} \cos((\omega_s^d + \omega_r^d) \lambda) d\lambda \right] \quad (49)$$

$$= \frac{1}{2} \left[e^{-(\xi_r \omega_r + \xi_s \omega_s) \lambda} \left(\left[\frac{-(\xi_r \omega_r + \xi_s \omega_s) \cos((\omega_s^d - \omega_r^d) \lambda) + (\omega_s^d - \omega_r^d) \sin((\omega_s^d - \omega_r^d) \lambda)}{(\omega_s^d - \omega_r^d)^2 + (\xi_r \omega_r + \xi_s \omega_s)^2} \right] \dots \right) \right]_{\lambda=0}^{\lambda=L} \quad (50)$$

Eq.(50) can be further simplified by using a parameterization and re-written as in Eq.(51).

$$\frac{1}{2} \left[e^{-(\xi_r \omega_r + \xi_s \omega_s) \lambda} \left(\frac{\sin((\omega_s^d - \omega_r^d) \lambda - \gamma_{rs})}{\sqrt{P_{rs}^2 + Q_{rs}^2}} - \frac{\sin((\omega_s^d + \omega_r^d) \lambda - \beta_{rs})}{\sqrt{R_{rs}^2 + Q_{rs}^2}} \right) \right]_{\lambda=0}^{\lambda=L} \quad (51)$$

where, $P_{rs} = (\omega_s^d - \omega_r^d)$, $R_{rs} = (\omega_s^d + \omega_r^d)$ and $Q_{rs} = (\xi_r \omega_r + \xi_s \omega_s)$.

Similarly, $\gamma_{rs} = \arctan(Q_{rs}/P_{rs})$ and $\beta_{rs} = \arctan(Q_{rs}/R_{rs})$

Using the second trigonometric identity in Eq.(48), the integral in H'_{abk} (Eq. (47)) can be re-arranged as in Eq.(52) and then evaluated leading to Eq.(53).

$$\frac{1}{2} \left[\int_0^L e^{-(\xi_r \omega_r + \xi_s \omega_s) \lambda} \sin((\omega_s^d + \omega_r^d) \lambda) d\lambda + \int_0^L e^{-(\xi_r \omega_r + \xi_s \omega_s) \lambda} \sin((\omega_s^d - \omega_r^d) \lambda) d\lambda \right] \quad (52)$$

$$= \frac{1}{2} \left[e^{-(\xi_r \omega_r + \xi_s \omega_s) \lambda} \left(\left[\frac{-(\xi_r \omega_r + \xi_s \omega_s) \sin((\omega_s^d + \omega_r^d) \lambda) - (\omega_s^d + \omega_r^d) \cos((\omega_s^d + \omega_r^d) \lambda)}{(\omega_s^d + \omega_r^d)^2 + (\xi_r \omega_r + \xi_s \omega_s)^2} \right] + \dots \right) \right. \\ \left. \left[\dots \frac{-(\xi_r \omega_r + \xi_s \omega_s) \sin((\omega_s^d - \omega_r^d) \lambda) - (\omega_s^d - \omega_r^d) \cos((\omega_s^d - \omega_r^d) \lambda)}{(\omega_s^d - \omega_r^d)^2 + (\xi_r \omega_r + \xi_s \omega_s)^2} \right] \right]_{\lambda=0}^{\lambda=L} \quad (53)$$

Using the definitions given above for P_{rs} , R_{rs} , Q_{rs} , γ_{rs} and β_{rs} Eq.(53) can be simplified to Eq.(54).

$$\frac{1}{2} \left[e^{-(\xi_r \omega_r + \xi_s \omega_s) \lambda} \left(-\frac{\cos((\omega_s^d + \omega_r^d) \lambda - \beta_{rs})}{\sqrt{R_{rs}^2 + Q_{rs}^2}} - \frac{\cos((\omega_s^d - \omega_r^d) \lambda - \gamma_{rs})}{\sqrt{P_{rs}^2 + Q_{rs}^2}} \right) \right]_{\lambda=0}^{\lambda=L} \quad (54)$$

Substituting Eq.(51) and (54) into Eq.(45) yields;

$$R_{abk,L}(T) = \sum_{s=1}^N \sum_{r=1}^N \frac{1}{2} \frac{\alpha_k \phi_{as} \phi_{ks} \phi_{br} \phi_{kr}}{m_r \omega_r^d m_s \omega_s^d} e^{-\xi_r \omega_r T} \left[e^{-(\xi_r \omega_r + \xi_s \omega_s) \lambda} (Part1 + Part2) \right]_{\lambda=0}^{\lambda=L} \quad (55)$$

The new subscript L used in $R_{abk,L}(T)$ shows that the calculation of the correlation function is performed for a certain data length L . In Eq.(55);

$$\begin{aligned}
 Part1 &= \frac{1}{\sqrt{P_{rs}^2 + Q_{rs}^2}} \left[\cos(\omega_r^d T) \sin((\omega_s^d - \omega_r^d)\lambda - \gamma_{rs}) - \sin(\omega_r^d T) \cos((\omega_s^d - \omega_r^d)\lambda - \gamma_{rs}) \right] \quad (56) \\
 &= \frac{1}{\sqrt{P_{rs}^2 + Q_{rs}^2}} \left[-\sin(\omega_r^d T - (\omega_s^d - \omega_r^d)\lambda + \gamma_{rs}) \right]
 \end{aligned}$$

Similarly,

$$\begin{aligned}
 Part2 &= \frac{1}{\sqrt{R_{rs}^2 + Q_{rs}^2}} \left[-\cos(\omega_r^d T) \sin((\omega_s^d + \omega_r^d)\lambda - \beta_{rs}) - \sin(\omega_r^d T) \cos((\omega_s^d + \omega_r^d)\lambda - \beta_{rs}) \right] \quad (57) \\
 &= \frac{1}{\sqrt{R_{rs}^2 + Q_{rs}^2}} \left[-\sin(\omega_r^d T + (\omega_s^d + \omega_r^d)\lambda - \beta_{rs}) \right]
 \end{aligned}$$

Before going into the following steps of the proposed approach, Eq.(55) can be modified further. The system may be excited by several uncorrelated forces acting on different locations simultaneously. All these contributions can be summed up over the index k . The final form of the equation can be written as follows;

$$R_{ab,L}(T) = \sum_{s=1}^N \sum_{r=1}^N \sum_{k=1}^N \frac{1}{2} \frac{\alpha_k \phi_{as} \phi_{ks} \phi_{br} \phi_{kr}}{m_r \omega_r^d m_s \omega_s^d} e^{-\xi_r \omega_r T} \left[e^{-(\xi_r \omega_r + \xi_s \omega_s)\lambda} (Part1 + Part2) \right]_{\lambda=0}^{\lambda=L} \quad (58)$$

While calculating Eq.(58), for simplicity, the parts computed for the bounds $\lambda = 0$ and $\lambda = L$ can be investigated as two separate terms $R_{ab}^1(T)$ and $R_{ab,L}^2(T)$, respectively:

$$R_{ab,L}(T) = R_{ab}^1(T) + R_{ab,L}^2(T) \quad (59)$$

The first term $R_{ab}^1(T)$, which corresponds to the bound $\lambda = 0$, can be written as in Eq.(60)

$$R_{ab}^1(T) = \sum_{s=1}^N \sum_{r=1}^N \sum_{k=1}^N \frac{1}{2} \frac{\alpha_k \phi_{as} \phi_{ks} \phi_{br} \phi_{kr}}{m_r \omega_r^d m_s \omega_s^d} e^{-\xi_r \omega_r T} \left[\frac{1}{\sqrt{P_{rs}^2 + Q_{rs}^2}} \sin(\omega_r^d T + \gamma_{rs}) + \frac{1}{\sqrt{R_{rs}^2 + Q_{rs}^2}} \sin(\omega_r^d T - \beta_{rs}) \right] \quad (60)$$

It should be noted that $R_{ab}^1(T)$ is the same as the final outcome of the standard NExT derivation [1-3]. Indeed, if the upper bounds of the integrals in Eq.(46) and Eq.(47) are computed for $\lambda = \infty$, the term $e^{-(\xi_r \omega_r + \xi_s \omega_s)\lambda}$ in Eq. (58) equals to zero and thus $R_{ab,L=\infty}^2(T) = 0$. Eq.(60) is nothing but the summation of sine functions having the same frequency but different phase angles. Therefore, it can be represented as a single sine function with a new phase angle θ_r and coefficient A_{ra} :

$$R_{ab}(T) = \sum_{r=1}^N \frac{\phi_{br} A_{ra}}{m_r \omega_r^d} e^{-\xi_r \omega_r T} \sin(\omega_r^d T + \theta_r) \quad (61)$$

In references [1-3], Eq.(61) is reported to be the most important conclusion which the NExT theory is based on: it shows that the cross correlation between the responses at locations “a” and “b” can be considered as an impulse response measured at location “a” due to an impulse force acting at location “b”. Both equations can be expressed as sum of N decaying sinusoids having frequencies of ω_r^d and damping ratios ξ_r .

Similarly, term $R_{ab,L}^2(T)$, which corresponds to $\lambda = L$, can be written as in Eq.(62).

$$R_{ab,L}^2(T) = \sum_{s=1}^N \sum_{r=1}^N \sum_{k=1}^N \frac{\alpha_k \phi_{as} \phi_{ks} \phi_{br} \phi_{kr}}{m_r \omega_r^d m_s \omega_s^d} \frac{1}{2} e^{-\xi_r \omega_r T} e^{-(\xi_r \omega_r + \xi_s \omega_s)L} \left(\begin{array}{l} \frac{-1}{\sqrt{P_{rs}^2 + Q_{rs}^2}} \sin(\omega_r^d T - (\omega_s^d - \omega_r^d)L + \gamma_{rs}) - \dots \\ \dots \frac{1}{\sqrt{R_{rs}^2 + Q_{rs}^2}} \sin(\omega_r^d T + (\omega_s^d + \omega_r^d)L - \beta_{rs}) \end{array} \right) \quad (62)$$

Eq.(62) shows the effect of considering finite length measurement duration: it expresses the difference $R_{ab,L}(T) - R_{ab}^1(T) = R_{ab,L}(T) - R_{ab,L=\infty}(T)$ between the impulse-like response obtained when an infinite time series is considered, and the cross-correlation computed in practice. It is observed that even for relatively low values of L (e.g. 100 seconds in our earlier example) it has a very small amplitude due to the term $e^{-(\xi_r \omega_r + \xi_s \omega_s)L}$. Thus it seems that neglecting the finiteness of the measured signal does not have a significant effect and cannot be directly related to high damping modes not being extracted. The reason for highly damped modes to be badly detected in the NExT method is probably

that their contribution to the overall response is small compared to the contributions of lightly damped modes. However, Eq.(62) can still be used as an alternative approach for detecting these highly damped modes.

Assuming $T = 0$, $R_{ab}^1(0)$ (obtained from Eq.(60)) can be simplified to summation of some constant coefficients only. Similarly, $R_{ab,L}^2(0)$ (shown in Eq.(62)) is reduced to:

$$R_{ab,L}^2(0) = \sum_{r=1}^N \sum_{s=1}^N \sum_{k=1}^N \frac{1}{2} \frac{\alpha_k \phi_{as} \phi_{ks} \phi_{br} \phi_{kr}}{m_r \omega_r^d m_s \omega_s^d} e^{-(\xi_r \omega_r + \xi_s \omega_s)L} \left(\begin{array}{l} \frac{1}{\sqrt{P_{rs}^2 + Q_{rs}^2}} \sin((\omega_s^d - \omega_r^d)L - \gamma_{rs}) - \dots \\ \dots \frac{1}{\sqrt{R_{rs}^2 + Q_{rs}^2}} \sin((\omega_s^d + \omega_r^d)L - \beta_{rs}) \end{array} \right) \quad (63)$$

In the proposed approach, correlation functions are calculated for *varying measurement durations* L . A new data series is generated by using just the first points ($T = 0$) of the calculated correlation functions (in other words, by using the mean square $R_{ab,L}(0)$ computed for a signal length of L). Therefore, it would be more appropriate to represent the calculated parameter as $\mathfrak{R}_{ab,0}(L)$ instead of $R_{ab,L}(0)$. By using this new definition Eq.(59) can be re-written as follows

$$\mathfrak{R}_{ab,0}(L) = R_{ab,L}(0) = cst + \mathfrak{R}_{ab,0}^2(L) \quad (64)$$

where the first term is constant with respect to L as can be seen from Eq.(60). A graphical illustration of this new approach can be seen in Figure 5.2. This representation is different from the common application of Natural Excitation Technique because in the standard procedure, correlation functions are calculated only once by using data series of fixed duration L and are assumed to represent impulse response functions. These correlation functions are then analyzed for varying T values where T represents the time parameter t in the corresponding impulse response function.

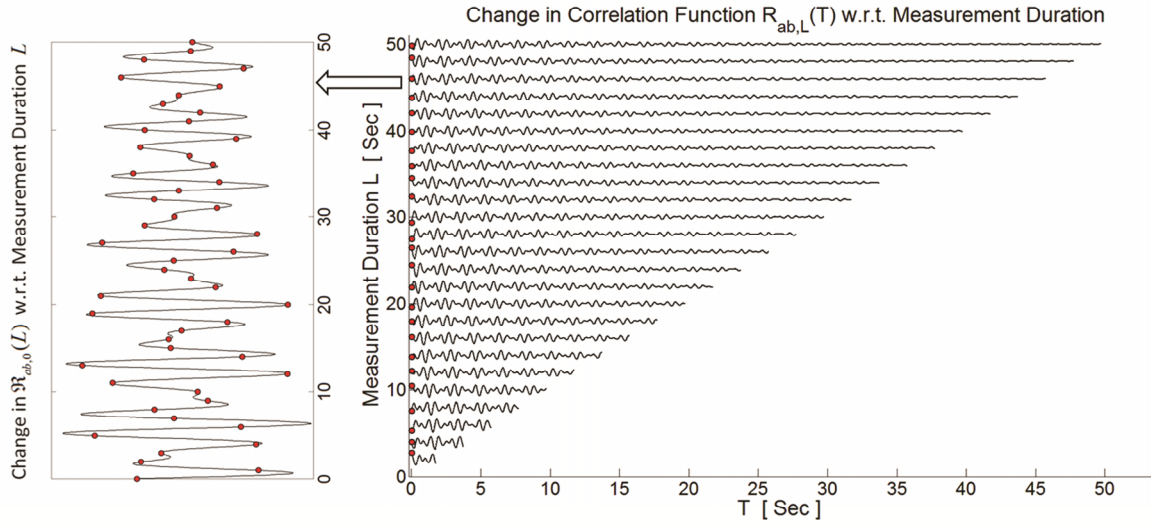


Figure 5.2. Graphical representation of the proposed analysis method

$\Re_{ab,0}(L)$ is the sum of a constant and several sinus functions of L included in $\Re_{ab,0}^2(L)$. Indeed, from Eq.(63), $\Re_{ab,0}^2(L) = R_{ab,L}^2(0)$ appears to be a combination of several sinusoids of the form $\sin((\omega_s^d - \omega_r^d)L)$ and $\sin((\omega_s^d + \omega_r^d)L)$. One important point to note is that using the trigonometric relation given below in Eq.(65), the first part which involves $\sin((\omega_s^d - \omega_r^d)L - \gamma_{rs})$ is expected to cancel out because during the double summation (over s and r), it is just added with its negative.

$$\frac{1}{\sqrt{P_{rs}^2 + Q_{rs}^2}} \sin((\omega_s^d - \omega_r^d)L - \gamma_{rs}) = -\frac{1}{\sqrt{P_{sr}^2 + Q_{sr}^2}} \sin((\omega_r^d - \omega_s^d)L - \gamma_{sr}) \quad (65)$$

However, the frequency domain analysis of $\Re_{ab,0}(L)$ data (generated by using the model in Figure 5.1) clearly reveals that the components related to $\sin((\omega_s^d - \omega_r^d)L - \gamma_{rs})$ still exist in the investigated data. A possible explanation can be that correlation functions calculated by using discrete time series are not exactly the same as the functions described in this article by continuous integrals. Even very small differences may be important since the amplitude of $\Re_{ab,0}^2(L)$, which is the part containing the sinusoids, is very small.

This new signal representation makes it possible to utilize alternative frequency indicators to monitor the eigenfrequencies of the investigated system. As shown in Table 5.2, for the 5 DOF system example, spectral density analysis of $\mathfrak{R}_{ab,0}(L)$ includes 25 additional frequencies (also called control frequencies here) which provide extra information to be used in the dynamic analysis. These new indicators enable a highly damped mode, which cannot be identified by the standard approach, to be detected by using the eigenfrequencies already extracted or known a priori. This will be explained in the next section.

Frequency	$^*\omega_1^d$	ω_2^d	ω_3^d	ω_4^d	ω_5^d
$^*\omega_1^d$	$^*\omega_1^d \pm ^*\omega_1^d$
ω_2^d	$\omega_2^d \pm ^*\omega_1^d$	$\omega_2^d \pm \omega_2^d$
ω_3^d	$\omega_3^d \pm ^*\omega_1^d$	$\omega_3^d \pm \omega_2^d$	$\omega_3^d \pm \omega_3^d$
ω_4^d	$\omega_4^d \pm ^*\omega_1^d$	$\omega_4^d \pm \omega_2^d$	$\omega_4^d \pm \omega_3^d$	$\omega_4^d \pm \omega_4^d$
ω_5^d	$\omega_5^d \pm ^*\omega_1^d$	$\omega_5^d \pm \omega_2^d$	$\omega_5^d \pm \omega_3^d$	$\omega_5^d \pm \omega_4^d$	$\omega_5^d \pm \omega_5^d$

Table 5.2. Control frequencies obtained from $\mathfrak{R}_{ab,0}(L)$ data (* shows the highly damped mode for our test case)

6. Analysis Procedure and Obtained Results

This section aims at describing the applied procedure in more detail and at evaluating the efficiency of the proposed method by presenting the eigenfrequency estimations made for the 5 DOF model shown in Figure 5.1. It should be noted that the highly damped 1st mode could not be detected by LSCE time domain identification algorithm (utilizing standard NExT approach) unless the length of the analyzed time series is increased up to 5000 cycles.

Before searching for a missing highly damped mode, 4 eigenfrequencies (ω_{2-5}^d) associated with low damping modes are assumed to have been already extracted, using for instance the standard NExT and LSCE procedure. The reliability of the method is directly related to the number of control frequencies and significantly increases depending on the system order or more specifically, the number of eigenfrequencies

identified beforehand. As shown in Table 5.2, for the investigated system, spectral densities of the corresponding $\mathfrak{R}_{ab,0}(L)$ data consist of 9 different frequency combinations ($\omega_1^d \pm \omega_{2-5}^d$ and $\omega_1^d + \omega_1^d$), which are related to the investigated mode ω_1^d .

Step 1: Generation of $\mathfrak{R}_{ab,0}(L)$ data by calculating correlation functions $R_{ab,L}(T)$ for varying measurement durations.

For the 5 DOF system example, there exist 25 different correlation functions. In standard NExT application, a correlation function (e.g. $R_{23}(T)$) is computed only once by using all the available data points of the time series $x_2[t]$ and $x_3[t]$. However, in the proposed approach, calculation of the correlation function is repeated for different measurement durations of L .

The number of data points that will be added to the analyzed data blocks of $x_2[t]$ and $x_3[t]$ can be decided by the user. Increasing the number of data points in the blocks by one, each time the analysis is repeated, corresponds to increasing the measurement duration by $\frac{1}{f_s}$ seconds and enables the generated $\mathfrak{R}_{ab,0}(L)$ data to have the same sampling frequency as the original measurements $x_2[t]$ and $x_3[t]$. This procedure is performed for each correlation function $R_{ab}(T)$ and a separate $\mathfrak{R}_{ab,0}(L)$ data is computed. Since only the first points ($T = 0$) of the calculated correlation functions $R_{ab,L}(T)$ are needed and $R_{ab}(T) = R_{ba}(-T)$, performing the necessary computations for only 15 correlation functions (out of 25) would be sufficient.

Step 2: Calculation of PSD (Power Spectral Density) of the $\mathfrak{R}_{ab,0}(L)$ data

The obtained $\mathfrak{R}_{ab,0}(L)$ series are investigated in frequency domain by calculating their power spectral densities (PSD). One important point to note is that in this work, the interpretation of spectral density results is different from the common application in structural dynamics. $\mathfrak{R}_{ab,0}(L)$ data is considered to be a combination of the above

mentioned decaying sinusoids and non-decaying broadband random noise. The source of the noise is difficult to determine. However, it can be attributed to the fact that when L is small, the two assumptions mentioned at the end of Section 4 are not yet fully satisfied or to the measurement error which is inherent in the recorded data. In this work the proposed technique is tested on both noise-free simulated time series and series whose noise to signal ratio is 5 %. Effect of measurement noise on the estimated modal parameters and the stability of the analysis technique are discussed in the following sections.

As L increases, the amplitudes of the sinusoids decrease quickly due to the term $e^{-(\xi_r \omega_r + \xi_s \omega_s)L}$, while the random noise part still has similar amplitudes. If the resulting data is analyzed in frequency domain, there appear so-called “frequency holes” caused by the rapid attenuation. In other words, the frequencies related to the decaying parts appear in the plots as valleys not peaks. Therefore, the obtained spectra should be reversed. This can be done by just inverting the spectral amplitudes obtained from PSD analyses. Since $\log\left(\frac{1}{A(w)}\right) = -\log(A(w))$, when the resulting graph is shown in logarithmic scale, the overall shape will be very similar to a usual PSD graph, the sign of the y axis being reversed. The relative amplitudes of the frequencies will be the same while peaks and valleys are reversed. In the following sections spectral amplitudes are all reversed and the term “peak” is used to represent an “inverted valley”.

Instead of analyzing the $\mathfrak{R}_{ab,0}(L)$ data as a single block, it is recommended (provided that the necessary frequency resolution is achieved) to use smaller FFT windows and to perform successive PSD analyses simply by shifting the block until all the available $\mathfrak{R}_{ab,0}(L)$ data is scanned and analyzed. These blocks may also have some overlapping parts. The parameters of the frequency domain investigation (e.g. the number of data points in the FFT blocks and length of the overlapping sections) can be determined by the user in accordance with the dynamic properties of the investigated system. During this process the calculated PSD amplitudes are recorded to generate a peak database.

Step 3: Selection of Dominant Peaks and Formation of the Peak Database

The proposed approach is based on the idea that if a candidate frequency (ω_{can}) is believed to be the missing eigenfrequency (ω_1^d in this case), in theory, it is expected that several control frequencies associated with the candidate (as shown in bold in the second column of Table 5.2) should also be observable in PSD plots of the $\mathfrak{R}_{ab,0}(L)$ data and therefore exist in the peak database. For the 5 DOF system analyzed in this work, 4 eigenfrequencies with low damping ratios (ω_{2-5}^d) are assumed to be determined previously. By using these 4 known frequencies, for each candidate (ω_{can}), 9 different control frequencies ($\omega_{can} \pm \omega_{2-5}^d$ and $\omega_{can} + \omega_{can}$) can be calculated and one can check whether they do exist in the peak database or not.

The number of control frequencies, which can be related to a candidate ω_{can} , is an important measure showing the possibility of the examined candidate being a true eigenfrequency. For the investigated system (with 4 frequencies known beforehand) this number can vary between 0 and 9, 0 meaning that none of the control frequencies calculated for the candidate have a match in the peak database and thus, most probably, that it is not the missing eigenfrequency being searched for. Similarly, 9 means that all the control frequencies calculated for the candidate also exist in the database so the probability of the examined frequency being a true eigenfrequency is very high.

In generating the database it becomes very important how to define a peak and how to distinguish a dominant peak from relatively weaker ones. During the PSD analysis stage, the frequencies, whose amplitudes are greater than a threshold value (prescribed by the user), are accepted as a peak and recorded in the database. Amplitude is a dimensionless parameter showing how different a certain frequency is from its neighboring frequencies. It can be described as the ratio of the PSD amplitude of a certain frequency to the amplitude of the smoothed PSD computed by moving average. Figure 5.3 shows how spectral amplitude is calculated. In the figure below the blue curve shows the smoothed PSD values.

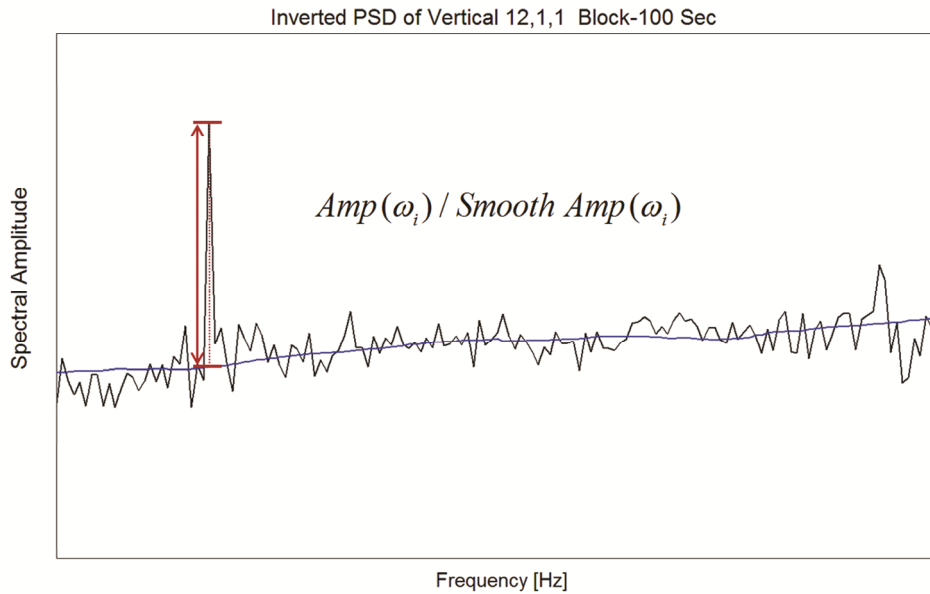


Figure 5.3. Calculation of the amplitude of a peak

The decision of which peaks will be used in evaluating the candidates can be made in two different ways. Following each PSD analysis, the amplitudes of the frequencies which are accepted as peaks are recorded and only the frequencies, whose cumulative amplitude is above a certain value, are selected.

For the 5 DOF model investigated in this work, each $\mathfrak{R}_{ab,0}(L)$ series is of 300 seconds ($L \in [0, 300]$). As mentioned before, instead of analyzing the data as a single FFT block, smaller blocks of 100 seconds, which provide a frequency resolution of 0.01 Hz, are used. Successive PSD analyses are performed by shifting the FFT blocks 10 seconds until the whole $\mathfrak{R}_{ab,0}(L)$ data is scanned. Therefore, the FFT block of 100 seconds is shifted 20 times until the 300 seconds data is scanned completely. Applying the same procedure to 15 different $\mathfrak{R}_{ab,0}(L)$ series requires 300 FFT/PSD analyses in total.

For each PSD analyses, the amplitude of a certain frequency (e.g. 0.6 Hz) is checked whether it is greater than a user defined threshold value or not. If it is greater than the threshold, the investigated frequency (0.6 Hz) is accepted as a peak and its amplitude is recorded. If not, its amplitude is not taken into account in the calculation of the cumulative amplitude. This procedure is repeated for each one of the 300 PSD

analyses. When the analyses are completed, the summation of the amplitudes of 0.6 Hz is noted as its cumulative spectral amplitude.

As an alternative approach, it is also possible to count the number of times 0.6 Hz has an amplitude greater than the threshold and is accepted as a peak during these 300 PSD analyses. Both approaches were tested in this work and cumulative spectral amplitude criterion was observed to produce better results. Therefore, it was used to obtain the graphs presented below.

Step 4: Evaluation of Candidate Frequencies

The selected peaks are then used to determine the possibility of a candidate frequency (ω_{can}) being a true eigenfrequency of the system. Within a given bandwidth (e.g. [0 10] Hz) all frequencies are scanned systematically by using a prescribed frequency increment (e.g. 0.01 Hz). During this procedure, each frequency is considered to be a possible candidate, 9 different control frequencies are calculated for it ($\omega_{can} \pm \omega_{2-5}^d$ and $\omega_{can} + \omega_{can}$) and one checks how many of them match with those in the database.

If several candidates have 9 control frequencies matching with those in the database and appear to be an eigenfrequency, the threshold and cumulative spectral amplitude values can be increased. This will result in fewer frequencies to be accepted as a peak and a smaller database to be generated. Since only very dominant frequencies satisfy these new conditions and survive, such an approach will definitely reduce the effect of noise and provide the user with a better visualization of the important frequencies that are more likely to be the true eigenfrequencies of the system.

However, if the threshold is increased further, even the control frequencies related to the eigenfrequencies may be eliminated from the database along with the noisy or minor peaks. In this case, even the true eigenfrequencies may not have 9 control frequencies matching with the database. As the threshold is increased the number of control frequencies that can be related to the candidates is reduced.

7. Application on Numerically Generated Noise-Free Response Data

The results presented in this section are obtained by applying the above mentioned analysis procedure to numeric data generated by using the 5 DOF system shown in Figure 5.1, with system characteristics given in Table 5.1. The generated data series are noise-free. The stability of the proposed method and the effect of measurement noise on the estimated eigenfrequencies are investigated in the following section. Figure 5.4 shows the eigenfrequencies estimated for a threshold of 10 and a cumulative spectral amplitude limit of 1000. These two dimensionless parameters are prescribed by the user and determine the size of the peak database. It is recommended to start the analyses with relatively small values and to increase them gradually until stable graphs are obtained. Such an approach makes it possible to monitor how the estimated frequencies change depending on the selected analysis parameters and facilitates the interpretation of the results. Starting values may differ depending on the system and can be determined after a few trials.

In Figure 5.4, red lines show the exact values of the damped eigenfrequencies of the 5 DOF system. The x-axis represents the candidate frequencies. Since 4 of the eigenfrequencies are known a priori, maximum 9 control frequencies ($\omega_{can} \pm \omega_{2-5}^d$ and $\omega_{can} + \omega_{can}$) can be calculated numerically for each candidate. The y-axis displays how many of these control frequencies also exist in the peak database which includes the results of the frequency domain analysis of 15 different $R_{ab,0}(L)$ series.

It should be noted that the highly damped first mode (ω_1^d) at 0.55 Hz could not be identified by using standard NExT approach (together with LSCE). However, the proposed technique clearly indicates that there is a candidate at 0.53 Hz which is highly probable to be the undetected eigenfrequency. The y-coordinate of this candidate shows that 4 of the control frequencies computed for it also exist in the database. This is the second highest value observed in the plot. The maximum value 7 is obtained for approximately 1.77 Hz and corresponds to the second eigenfrequency (ω_2^d) indeed. It should be noted that the value calculated for 0 Hz is 5 but it is not considered to

represent a real mode, therefore it is neglected. Similarly, another candidate at 3.56 Hz, which has also 4 control frequencies in common with the database, corresponds to the fourth eigenfrequency (ω_4^d). As shown in the graph, the third eigenfrequency (ω_3^d) has 3 control frequencies matching with the database but it is not very easy to determine its exact value from the figure.

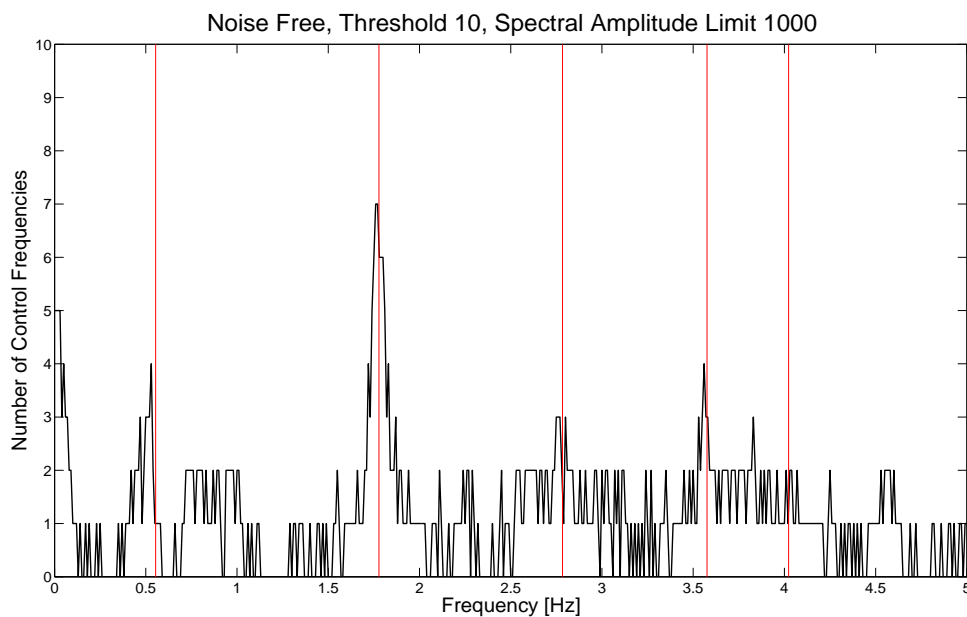


Figure 5.4. Damped natural frequencies estimated from noise-free data for threshold 10, amplitude limit 1000

In Figure 5.4 above, there also exists a candidate at 3.83 Hz which has 3 control frequencies. This frequency seems to be an eigenfrequency but in fact it is not. As shown in Figure 5.6 and Figure 5.7, this noisy frequency disappears when the calculations are repeated for different threshold values. Indeed repeating the same analyses with different limit parameters enables the user to understand which frequencies are stable and more likely to be related to the system. This procedure is very similar to plotting stability diagrams which are also obtained by repeating the same identification steps by using different analysis parameters. For the selected limit values, there is not a clear distinguishable peak around 4.02 Hz where ω_5^d is located. The candidate representing ω_5^d becomes more evident in the following figures as threshold and spectral amplitude limit are increased further.

Figure 5.5 shows the eigenfrequencies estimated for threshold of 10 and spectral amplitude limit of 6800. As higher values are assigned to these parameters, fewer frequencies are accepted as a peak resulting in a smaller database to be created for comparisons. Therefore, even if the examined candidate corresponds to one of the eigenmodes of the system, some of the control frequencies calculated for this candidate may be already eliminated from the database.

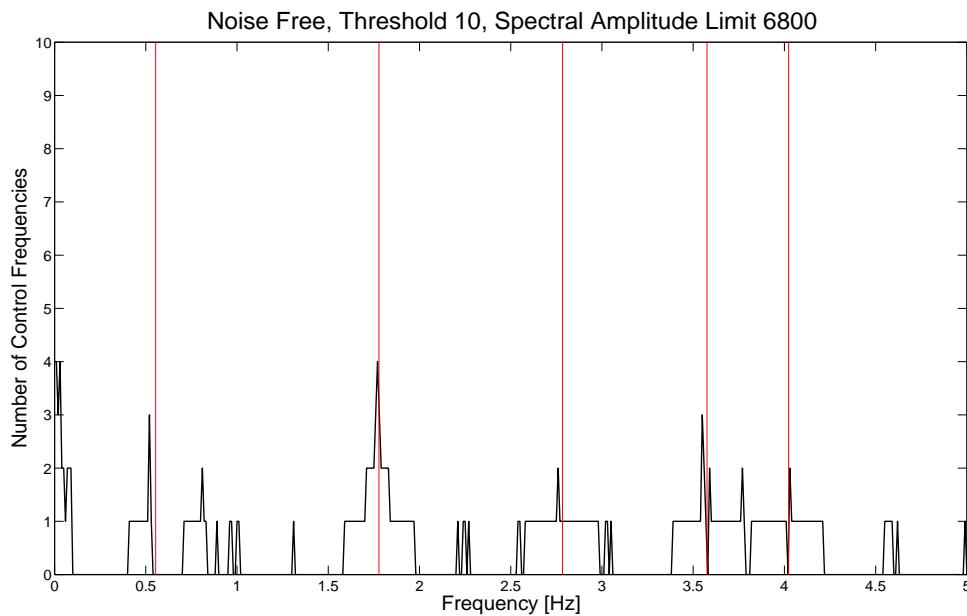


Figure 5.5. Damped natural frequencies estimated from noise-free data for threshold 10, amplitude limit 6800

As can be seen in Figure 5.5, for ω_1^d and ω_4^d , the number of control frequencies is decreased from 4 to 3. Likewise, the peak representing ω_2^d has only 4 control frequencies (instead of 7) in common with the database. The numbers calculated for ω_3^d is also reduced from 3 to 2. However, it is easier to determine the exact value of the estimation since a clear peak appears at 2.76 Hz. Similarly, a distinguishable peak can be seen around 4.02 Hz where ω_5^d is located.

Increasing the threshold and spectral amplitude limit values seems to cause some useful information to be deleted. However, compared to Figure 5.4, the resulting graph of Figure 5.5 is much simpler and easier to interpret. Although the misleading candidate

at 3.83 Hz (seen in Figure 5.4) disappears when the analyses are repeated by using different parameters, two new candidates at 0.81 Hz and 3.77 Hz appear in Figure 5.5. Whether these candidates represent the true eigenfrequencies or not can be understood by increasing the threshold and amplitude limit parameters further.

One important point to note is that as can be seen in Figure 5.5, when the analyses are repeated for different limit values, the eigenfrequency estimations are observed to deviate $\pm \Delta f$ where Δf stands for spectral resolution of the FFT analysis (0.01 Hz in this case). In Figure 5.5 the candidates suggested for ω_1^d and ω_4^d are located at 0.52 Hz and 3.55 Hz, respectively. Compared to Figure 5.4, the estimated peaks seem to shift 0.01 Hz to the left. Such a problem can be solved by using smaller frequency increments.

Figure 5.6 shows the eigenfrequencies estimated for threshold of 100 and spectral amplitude limit of 3000. As the limit values are increased the number of control frequencies that can be related to the eigenfrequencies of the system is decreased further. In Figure 5.6 for ω_1^d and ω_4^d , the number of control frequencies is decreased from 3 to 2. Unfortunately, the peak around 4.02 Hz, where ω_5^d is located, cannot be easily noticed in the figure. Depending on the selected values, the frequency estimated for ω_2^d shifts to 1.79 Hz which is 0.01 Hz (Δf) greater than the exact value of 1.78 Hz.

Figure 5.7 shows the eigenfrequencies estimated for threshold of 200 and spectral amplitude limit of 38000. Since the value assigned to the cumulative amplitude is quite high, the corresponding database includes only a few very dominant frequencies which can fulfill these requirements. As can be seen in the graph, only the control frequencies, which are calculated for the candidates representing the true eigenmodes, match with these dominant frequencies surviving in the database. Although no estimation could be made for ω_1^d , 4 eigenfrequencies $\omega_2^d - \omega_5^d$ can be easily noticed. Due to insufficient resolution and leakage, for each estimation two separate peaks appear, which are located at a distance of $\pm \Delta f$ from the identified exact value.

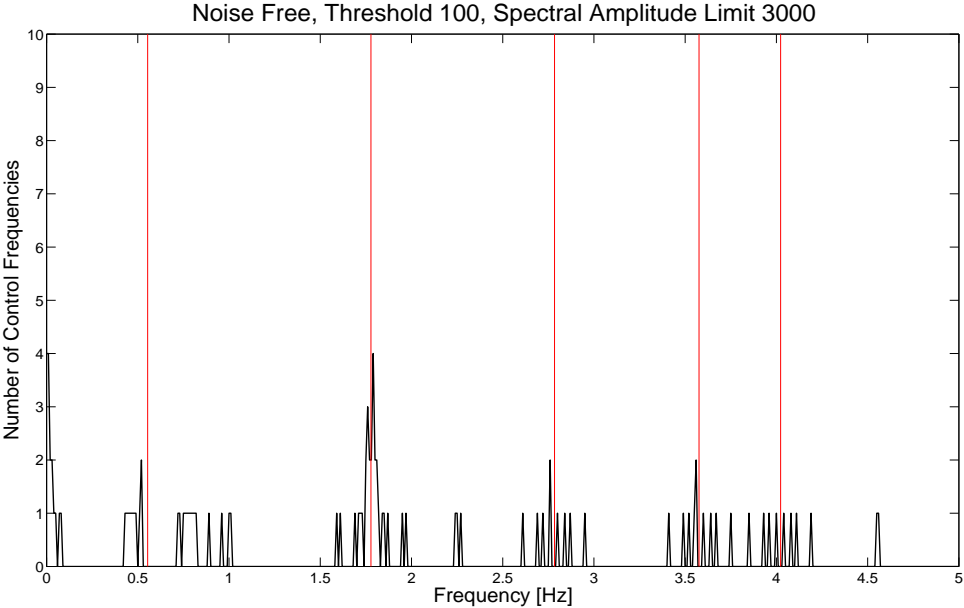


Figure 5.6. Damped natural frequencies estimated from noise-free data for threshold 100, amplitude limit 3000

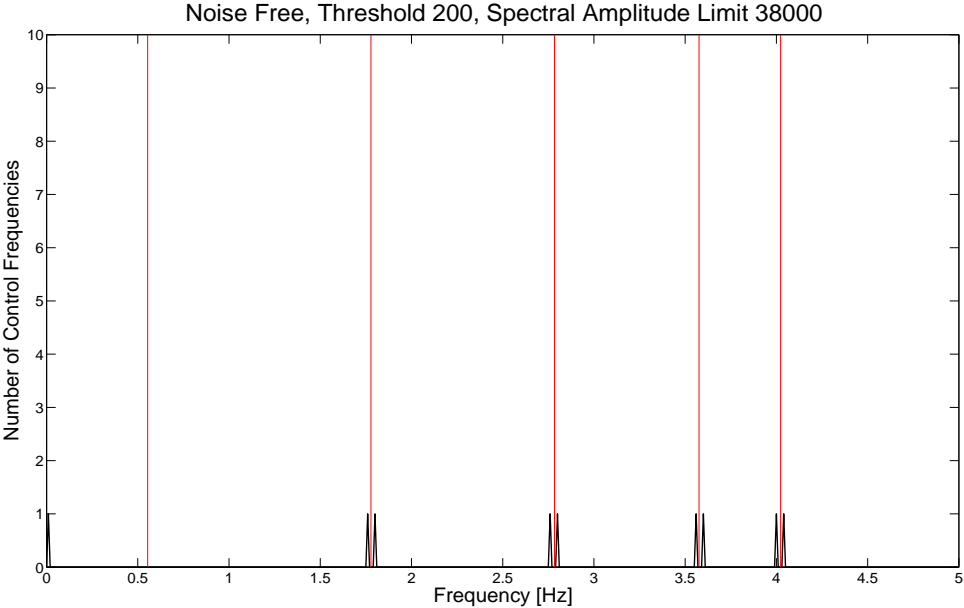


Figure 5.7. Damped natural frequencies estimated from noise-free data for threshold 200, spectral amplitude 38000

As shown in Figure 5.4 and Figure 5.5, the frequencies estimated for the 1st mode can slightly differ depending on the selected parameters. The difference between these

values (0.53 and 0.52 Hz) equals to the frequency resolution of the spectral analysis. The accuracy of the estimation made for ω_1^d is evaluated by taking both frequencies (0.53 and 0.52 Hz) into account. Using the exact value of the eigenfrequency (0.55 Hz), it can be concluded that the proposed approach is able to detect the highly damped mode with an average accuracy of 95%. Table 5.3 summarizes the damped eigenfrequency estimations made for the 5 DOF system and the corresponding accuracies. Although the eigenfrequencies ω_{2-5}^d are known a priori and used as input to calculate the control frequencies, some independent checks could be made for them as well by verifying that they appear as peaks in the stability plots of the present method.

Frequency	Exact [Hz]	Estimated [Hz]	Accuracy
* ω_1^d	0.55	0.52-0.53	95.40%
ω_2^d	1.78	1.77-1.79	99.40%
ω_3^d	2.78	2.76	99.30%
ω_4^d	3.58	3.55-3.56	99.30%
ω_5^d	4.02	4.02	100.0%

Table 5.3. Eigenfrequencies estimated for the 5 DOF system ($\hat{\cdot}$ shows the highly damped mode)

As can be seen in Table 5.1, the lowest eigenfrequency of the system is 0.55 Hz which corresponds to a fundamental period of 1.82 seconds. The investigated time histories of 300 seconds include just 165 cycles of the lowest frequency. Approximately 5000 cycles are required to extract the same frequency by using standard NExT approach. Therefore, it can be concluded that the proposed method can detect the highly damped ω_1^d by using data blocks which are approximately 30 times shorter than those required by the existing methods.

8. Effect of Measurement Noise on the Estimated Eigenfrequencies

The results presented in this section were obtained by applying the proposed method to numeric data generated by using the 5 DOF system shown in Figure 5.1. Following the

generation of the response data 5 % (noise to signal ratio) noise was added as described below:

- Normalized zero-mean random noise series with amplitudes in [-1 1] was created.
- A noise level (noise to signal ratio) was chosen. 5 % noise was considered to be sufficient for the targeted applications.
- The standard deviation of the noise-free response data was calculated.
- Scaled random noise was generated by multiplying the normalized noise by the standard deviation of the noise-free response and prescribed noise ratio (5 %), and then added to the noise-free data series.

The resulting noisy data was then processed as described through steps 1-4 above. Through the analyses it was observed that adding 5 % noise to analyzed data series has two different effects on the estimations:

- It increases the visibility of the true eigenfrequencies. As mentioned before the peaks shown in the PSD analyses are in fact not actual peaks but valleys caused by the so called frequency holes. Adding random noise provides extra energy which is uniformly distributed throughout the analyzed frequency bandwidth. Since the energy content of the regions between the holes is increased the holes become more manifest.
- It causes some noisy frequencies to appear as potential candidates. Therefore, the resulting graph is relatively more difficult to interpret compared to the graphs of noise-free data. Whether these candidates are related to the true eigenfrequencies or not can be understood by repeating the analyses for different limit values.

Below, Figure 5.8, Figure 5.9 and Figure 5.10 show the eigenfrequencies estimated for various threshold and spectral amplitude limit values. As can be seen from the figures, all 5 eigenfrequencies ($\omega_1^d - \omega_5^d$) can be observed very easily. Even ω_5^d , which cannot be detected from the figures drawn above for noise-free data, has a clear distinguishable peak. Despite some small frequency shifts ($\pm \Delta f$), the eigenfrequency estimations have almost the same pattern in all 3 figures. In Figures 5.8-5.10 ω_2^d is the most dominant candidate in the graphs and followed by ω_4^d . The other 3 eigenfrequencies $\omega_{1,3,5}^d$ have

always less number of control frequencies than ω_2^d and ω_4^d . However, they are still more dominant than the noisy peaks and can be easily distinguished among other candidates.

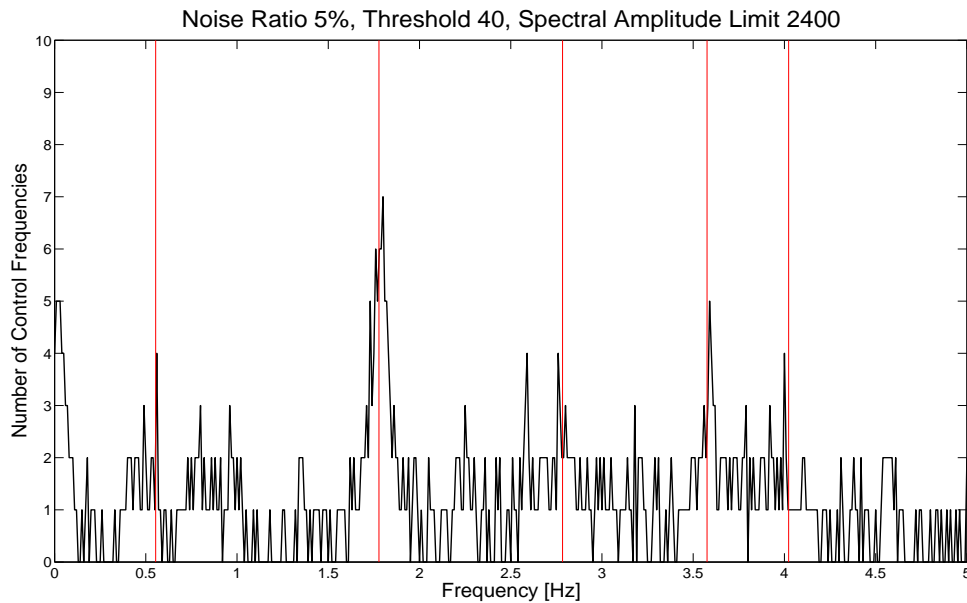


Figure 5.8. Damped natural frequencies estimated from noisy data for threshold 40, spectral amplitude 2400

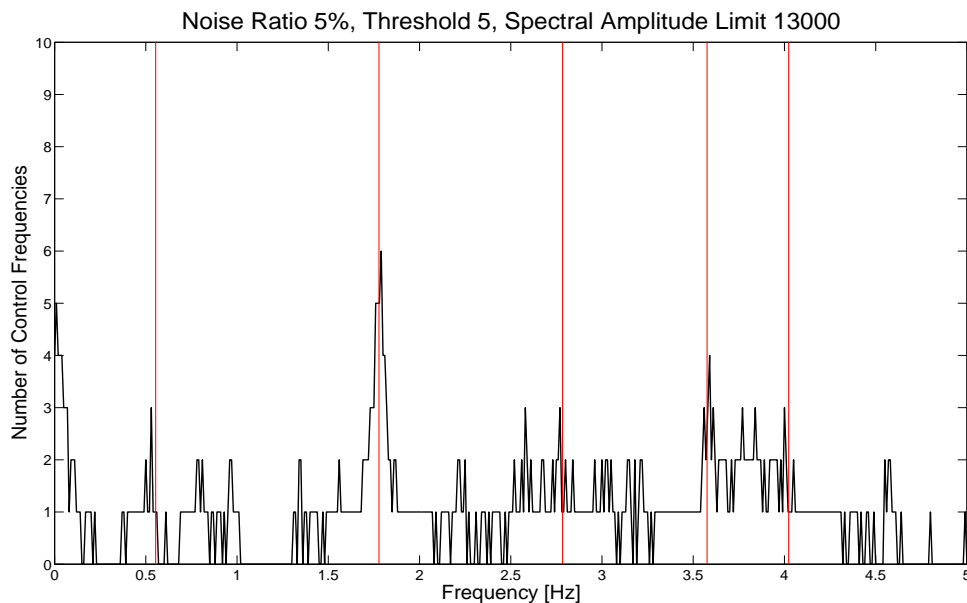


Figure 5.9. Damped natural frequencies estimated from noisy data for threshold 5, spectral amplitude 13000

The number of misleading candidates that seem to be potential eigenfrequencies is definitely higher compared to the previous figures of noise-free data but these noisy peaks do have less control frequencies than the true eigenfrequencies and most of them disappear when the analyses are repeated for different limit values. However, some of them can still be critical and require more detailed investigations. In Figure 5.8 and Figure 5.9 the candidate at 2.59 Hz has the same number of control frequencies as the eigenfrequencies but as the limit values are increased further, in Figure 5.10, one can deduce that it is not related to the system. On the other hand, the peak at 0.8 Hz survives in all three graphs and may require further analyses to determine whether it is indeed related to the system or not.

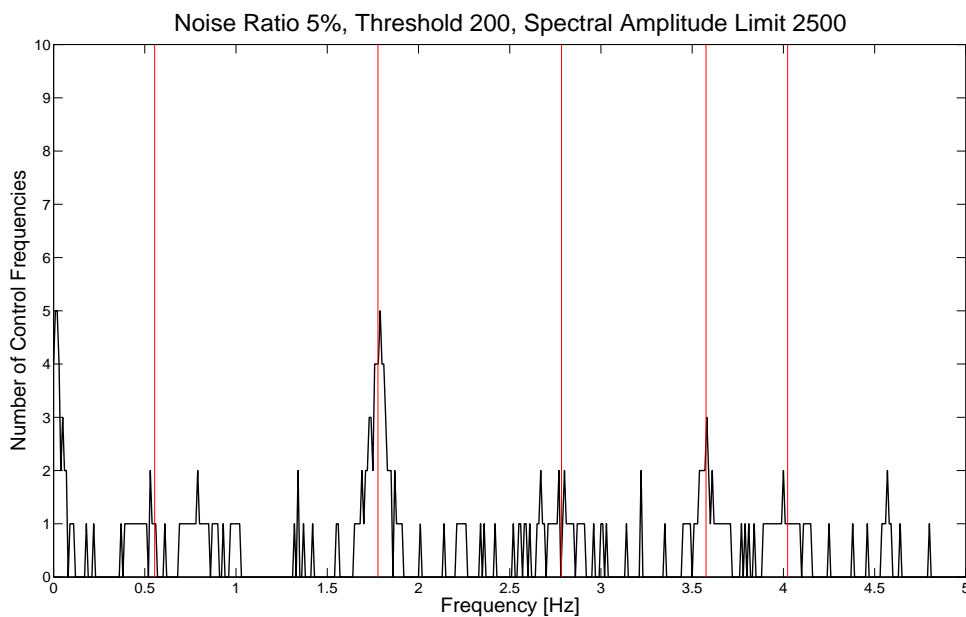


Figure 5.10. Damped natural frequencies estimated from noisy data for threshold 200, spectral amplitude 2500

Based on the results of the analyses performed it can be concluded that by using the proposed approach stable eigenfrequency estimations can be made and highly damped first mode ω_1^d can be detected from noisy data whose noise to signal ratio is approximately 5 %.

9. Conclusions

Extracting high damping modes is a challenging task for almost all types of system identification algorithms. For NExT based analysis methods, it is observed that estimation of these modes requires very long data series to be analyzed. Low damping modes can still be identified by using relatively short measurement durations having 200-300 cycles. However, this number increases significantly (4000-5000 cycles) when the investigated mode is highly damped. For a MW scale wind turbine 5000 cycles correspond to uninterrupted data blocks of approximately 4-5 hours. However, finding such long measurement periods during which wind speed, rotor speed and pitch angle stay constant is a very challenging task. Therefore, a new method is needed to be able to detect these modes using relatively shorter data blocks.

Results of the analyses clearly indicate that the proposed approach enables the eigenfrequencies related to the highly damped modes to be determined by using very short time histories. The data block analyzed in this work (including the overlapping parts) is just 300 seconds and includes only 165 cycles of the lowest frequency. This duration is 30 times shorter than those required by the standard NExT algorithm.

The frequencies estimated for the 1st mode, ω_1^d (0.52 and 0.53 Hz) are observed to differ slightly depending on the selected threshold and cumulative amplitude limit parameters. This difference equals to Δf , the frequency resolution of the spectral analysis. The values presented in this work are obtained by using FFT/PSD blocks of 100 seconds which provide a frequency resolution of 0.01 Hz. Using the estimated (0.52 and 0.53 Hz) and exact (0.55 Hz) values of ω_1^d , it can be concluded that the proposed approach is able to detect the eigenfrequencies of highly damped modes with an average accuracy of 95%. This accuracy can be further improved by selecting smaller frequency increments. The reliability of the estimations is directly related to the number of control frequencies that can be generated for each candidate or more specifically, the number of eigenfrequencies known a priori.

Threshold and cumulative spectral amplitude limit are dimensionless parameters determined by the user. It is recommended to start the analyses with relatively small values and to increase them gradually until stable graphs are obtained. Such an approach makes it possible to monitor how the estimated frequencies change depending on the selected analysis parameters and facilitates the interpretation of the results. Starting values may differ depending on the investigated system and can easily be determined after a few trials.

As the noise ratio of the response data gets higher the visibility of the eigenfrequencies increases. However, some noisy frequencies appear as potential eigenfrequency candidates and the resulting graph becomes more difficult to interpret compared to the graphs of noise-free data. Results of the analyses verify that the proposed approach enables stable eigenfrequency estimations to be made and highly damped eigenfrequencies to be detected from noisy data whose noise to signal ratio is approximately 5 %. The noise level tested is believed to be sufficient for the targeted applications.

Since highly damped eigenfrequencies can be identified from data series which are approximately 30 times shorter than those required by the standard algorithms, the proposed method is expected to be very useful for instance for structural health monitoring of slowly time varying systems such as wind turbines.

References

- [1] G.H. James, T.G. Carne, J.P. Lauffer, Modal testing using natural excitation, in: Proceedings of the 10th International Modal Analysis Conference, San Diego, California, 1992.
- [2] G.H. James, T.G. Carne, J.P. Lauffer, The Natural Excitation Technique (NExT) for modal parameter extraction from operating structures, *Journal of Analytical and Experimental Modal Analysis* 10 (4) (1995) 260-277.
- [3] G.H. James, T.G. Carne, P. Veers, Damping measurements using operational data, *ASME Journal of Solar Energy Engineering* 118 (1996) 190-193.
- [4] T.G. Carne, J.P. Lauffer, A.J. Gomez, Modal testing of a very flexible 110m wind turbine structure, in: Proceedings of the 6th International Modal Analysis Conference, Kissimmee, Florida, USA, 1988.
- [5] D.T. Griffith, R.L. Mayes, P.S. Hunter, Excitation methods for a 60 kW vertical axis wind turbine, in: Proceedings of the 28th International Modal Analysis Conference, Jacksonville, Florida, USA, 2010.

- [6] R. Osgood, G. Bir, H. Mutha, B. Peeters, M. Luczak, G. Sablon, Full-scale modal wind turbine tests: comparing shaker excitation with wind excitation, in: Proceedings of the 28th International Modal Analysis Conference, Jacksonville, Florida, USA, 2010.
- [7] T.G. Carne, G.H. James, The inception of OMA in the development of modal testing technology for wind turbines, *Mechanical Systems and Signal Processing* 24 (2010) 1213-1226.
- [8] M. Ozbek, D.J. Rixen, T.W. Verbruggen, Remote monitoring of wind turbine dynamics by laser interferometry: Phase1, in: Proceedings of the 27th International Modal Analysis Conference, Orlando, Florida, 2009.
- [9] F. Meng, M. Ozbek, D.J. Rixen, M.J.L. Tooren, Comparison of system identification techniques for predicting dynamic properties of large scale wind turbines by using the simulated time response, in: Proceedings of the 28th International Modal Analysis Conference, Jacksonville, Florida, 2010.
- [10] M. Ozbek, D.J. Rixen, O. Erne, G. Sanow, Feasibility of monitoring large wind turbines using photogrammetry, *Journal of Energy* 35 (12) (2010) 4802-4811.
- [11] M. Ozbek, D.J. Rixen, Operational modal analysis of a 2.5 MW wind turbine using optical measurement techniques and strain gauges, *Journal of Wind Energy* (2012) (Article in Press).
- [12] M. Ozbek, F. Meng, D.J. Rixen, M.J.L. van Tooren, Identification of the dynamics of large wind turbines by using photogrammetry, in: Proceedings of the 28th, International Modal Analysis Conference, Jacksonville, Florida, 2010.
- [13] M. Ozbek, D.J. Rixen, Optical measurements and operational modal analysis on a large wind turbine: Lessons learned, in: Proceedings of the 29th International Modal Analysis Conference, Jacksonville, Florida, 2011.
- [14] C. Gentile, A. Saisi, Ambient vibration testing and condition assessment of the Paderno iron arch bridge (1889), *Construction and Building Materials*, 25 (2011), 3709-3720.
- [15] D. Tcherniak, S. Chauhan, M.H. Hansen, Applicability limits of operational modal analysis to operational wind turbines, in: Proceedings of the 28th International Modal Analysis Conference, Jacksonville, Florida, 2010.
- [16] D. Tcherniak, S. Chauhan, M. Rossetti, I. Font, J. Basurko, O. Salgado, Output-only modal analysis on operating wind turbines, application to simulated data, in: Proceedings of the European Wind Energy Conference, Warsaw, Poland, 2010.
- [17] S. Chauhan, D. Tcherniak, M.H. Hansen, Dynamic characterization of operational wind turbines using operational modal analysis, in: Proceedings of the China Wind Power 2010, Beijing, China, 2010.
- [18] G. James, M. Kaouk, T. Cao, Progress in Operational Analysis of Launch Vehicles in Nonstationary Flight, in: Proceedings of the 31th International Modal Analysis Conference, Garden Grove, California, 2013.
- [19] P. Mohanty, D.J. Rixen, Operational modal analysis in the presence of harmonic excitation, *Journal of Sound and Vibration* 270 (2004) 93-109.
- [20] P. Mohanty, D.J. Rixen, Modified SSTD method to account for harmonic excitations during operational modal analysis, *Mechanism and Machine Theory* 39 (12) (2004) 1247-1255.

- [21] M.S. Allen, M.W. Sracic, S. Chauhan, M.H. Hansen, Output-only modal analysis of linear time-periodic systems with application to wind turbine simulation data, *Mechanical Systems and Signal Processing* 25 (2011) 1174-1191.
- [22] D.L. Brown, R.J. Allemang, R. Zimmerman, M. Mergeay, Parameter estimation techniques for modal analysis, *SAE Technical Paper Series*, (790221) (88) (1979) 828-846
- [23] N.M.M. Maia, J.M.M. Silva, J. He, N.A.J. Lieven, R.M. Lin, G.W. Skingle, W.M. To, A.P.V. Urgueria, *Theoretical and Experimental Modal Analysis*, Research Studies Press Ltd., Somerset, England, 1997.
- [24] L. Hermans, H.D. van Auweraer, *Modal Testing and Analysis of Structures Under Operational Conditions: Industrial Applications*, *Mechanical Systems and Signal Processing*, 13 (2) (1999) 193-216.
- [25] M. Geradin, D.J. Rixen, *Mechanical Vibrations: Theory and Application to Structural Dynamics*, Wiley & Sons, Chichester, England, 1997
- [26] A.V. Oppenheim, R.W. Schaffer, *Discrete-Time Signal Processing*, Prentice Hall, Englewood Cliffs, New Jersey, 1989. 0-13-216292-X.
- [27] J.G. Proakis, D.G. Manolakis, *Digital Signal Processing, Principles, Algorithms, and Applications*, Macmillan, New York, 1992. 0-02-396815-X.
- [28] G.R. Cooper, C.D. McGillem, *Probabilistic Methods of Signal and Systems Analysis*, Oxford University Press, New Delhi, 2011, ISBN-13: 978-0-19-569189-4

CHAPTER 6

Conclusions and Future Research Topics

This thesis aims at making a contribution to one of the most challenging fields of experimental and operational modal analyses, namely testing and analyzing the in-operation vibration characteristics of large wind turbines. The major conclusions and contributions of the thesis are expressed in more detail below in accordance with the research objectives defined in the Introduction section.

- ***Investigating the feasibility of monitoring wind turbine dynamics by using non-contact optical measurement systems (photogrammetry and laser interferometry) and evaluating the acquired accuracy.***

The optical measurement methods, laser interferometry and photogrammetry, which are proposed as alternative turbine monitoring systems, were shown to provide very valuable information about the dynamic response of the structure. The accuracies reached by these non-contact measurement techniques are very promising. Provided that high quality laser signals are obtained, LDV (laser Doppler vibrometer) can measure the vibration of several turbine components (blade, nacelle and tower) with very high accuracy (at micrometer scale). A recently developed SLR (Super Long Range) lens system enables an increased measurement range up to 300 meters. The intensity of the laser signals is related to the reflectivity of the surface which the laser is targeted to. In this research project, the required surface reflectivity was ensured by placing retro-reflective stickers on the turbine structure. It is also promising that, higher capacity laser systems (such as Polytec RSV 150 - Remote Sensing Vibrometer), which can reach the necessary signal levels even with the laser beams reflecting from ordinary blade or tower material, have now reached the market.

Although laser vibrometer could only measure the motion of a single point at a time, a high spatial resolution could be obtained by taking measurements from the markers distributed throughout the blade successively. 12 different turbine modes could be successfully extracted from the measurements performed on parked turbine. Strain

measurements taken by 8 strain gauges placed on the blades and tower were used as reference to evaluate the efficiency of the laser measurements. Results of the analyses showed that all the modes extracted from the strain data taken by 8 sensors could also be detected from the laser measurements. Even very small frequency and damping variations due to the change in instantaneous blade pitch angle, wind speed and direction could be identified by the laser vibrometer placed at a distance of 200 meters from the turbine.

Since it was very difficult to keep the laser on the same point while the turbine was rotating, LDV tests were only performed at parked condition. A laser vibrometer which can track the motion of the turbine and keep the laser on the same measurement spot during rotation is believed to be very useful for determining the in-operation vibration characteristics of wind turbines. Therefore, development of such a measurement system is highly recommended as a future research topic.

Similarly, it was also shown that photogrammetry is capable of acquiring accurate 3D deformation measurements on the rotor. Within the scope of this work, the dynamic response of the rotor was captured at 33 different locations simultaneously by using 4 CCD (charge coupled device) cameras while the turbine was rotating. Although photogrammetry is efficiently used at smaller scales by a wide variety of disciplines, it was applied for the very first time to a multi-MW scale wind turbine during this research project.

Results of the analyses show that deformations of the turbine can be measured with an average accuracy of ± 25 mm from a measurement distance of 220 m. Considering the fact that for a rotating wind turbine deformations measured in flapwise direction can be as high as ± 1000 mm, this accuracy can be evaluated to be high. It was observed that the measurement error is due to calibration errors caused by the rotation of the blades and therefore are frequency dependent. The overall error is composed of several components whose frequencies are integer multiples of the rotation frequency P . The $1P$ component of the measurement error can be easily corrected by spatial filtering. However, the $2P$ component has a spatial distribution which is very similar to the observed deformed shape of the blade. This component

constitutes the major part of the total error. The amplitudes of the other error components 3P and 4P are much smaller. For vibration frequencies greater than 5P, the obtained accuracy is much higher and in the range of ± 5 mm.

Photogrammetric measurements enabled several important frequencies governing the response of the turbine (such as 1P-5P harmonics) and some of the lower eigenfrequencies of the blades to be identified. First edgewise and first flapwise modes could easily be detected from the recorded data.

One important point to note is that the photogrammetric measurement systems (including both the camera and flashlights), image processing software and calibration methods utilized in this research were not specifically designed and optimized to be used in monitoring large wind turbines. Therefore, conducting similar photogrammetric measurements by using more specialized hardware and image processing software can increase the accuracy further and is recommended as a future research topic. More accurate measurements are expected to be taken by using new imaging hardware, which has better resolution and sensitivity.

- ***Analyzing the vibration data recorded on a multi-MW scale wind turbine by using some state of the art identification tools and investigating the system parameters (e.g. eigenfrequencies, damping ratios) that can be extracted from the analyzed time histories:***

In this work, the vibration data acquired by using 3 different measurement systems namely, conventional strain gauges, photogrammetry and laser interferometry, were analyzed by using an OMA algorithm based on NEXt (Natural Excitation Technique) and LSCE (Least Square Complex Exponential) methods. The results of the analyses provided very valuable information on the vibration characteristics of the structure. Within the scope of the research, twelve different turbine modes were successfully calculated from the measurements taken on the parked turbine by using strain gauges and LDV (laser Doppler vibrometer).

Similarly, seven different turbine modes could be identified from the in-operation measurements by using strain gauges and photogrammetry. Only four of these in-operation vibration modes have been previously reported to be identified in

literature. During the analyses reported in this thesis, three additional modes could be extracted from the measured vibration response for the very first time.

The extracted modal parameters were qualitatively compared with the results presented in a study from literature, which includes both aeroelastic simulations and in-field measurements performed on a similar size and capacity wind turbine. Obtained results are in good coherence with those presented in reference studies.

- ***Determination of the challenges in testing and monitoring the in-operation vibration characteristics of wind turbines and investigating possible reasons of uncertainty in the estimated modal parameters by using simulation data.***

In order to determine possible reasons of the uncertainty in the estimated modal parameters, and the applicability limits of the utilized system identification algorithms, several modal analyses were also conducted on the time histories generated by using an analytical mass – spring – damper model and an aeroelastic simulation tool (MBDyn-AeroDyn). Such an approach made it possible to produce response data for systems whose dynamic characteristics (eigenfrequencies and damping ratios) are known a priori.

The modal parameters were estimated by applying identification algorithms on these generated data series and then compared with the known values. These analyses were performed by using two state of the art modal analysis methods, NEXt (Natural Excitation Technique) and SSI (Stochastic Subspace Identification) which are based on different mathematical theories. The comparison of the results obtained by using different techniques made it possible to examine specifically the performance of the applied methods and to determine their limitations in processing vibration response of large wind turbines.

The MBDyn-AeroDyn aeroelastic simulations and SSI analyses presented in this thesis were performed by Fanzhong Meng from Delft University of Technology, Faculty of Aerospace Engineering, Wind Energy Department.

The first method, SSI (Stochastic Subspace Identification) has been confirmed to extract the highly damped modes accurately. However, since the method has a

relatively more complicated algorithm, it is not straightforward to modify it to overcome some specific problems related to the wind excitation.

Compared to SSI, NExT based methods have a more flexible structure allowing the necessary modifications to be made according to the specific features of the application. Indeed, early versions of OMA tools were particularly developed to solve the problems encountered during dynamic testing of wind turbines. However, during these analyses, it was observed that NExT has some limitations in identifying the modal parameters related to the modes with high damping ratios. The method requires very long time histories to be processed in order to extract the parameters of highly damped modes. Low damping modes can still be identified from short data series. However, very long time histories are needed to accurately extract the high damping modes.

Therefore, the applicability of the standard NExT algorithm to wind turbines, for which some of the important modes (first flapwise rotor modes) have very high aeroelastic damping, is limited. During the analyses, it was observed that for a MW scale wind turbine the necessary measurement duration can be as high as 4-5 hours. However, in practice finding such long measurement periods, during which wind speed, rotor speed and pitch angle stay constant, is a very challenging task.

- ***Modifying and optimizing the utilized analysis techniques to overcome some of the problems resulting from the complicated nature of the turbine structure and wind loading:***

In order to overcome the above mentioned problems related to measurement duration, in this thesis a new approach, which is based on NExT in theory, has been introduced. The proposed method enables eigenfrequencies of the high damping modes to be estimated by using data series which are approximately 30 times shorter than those required for standard NExT algorithm. Results of the analyses show that eigenfrequencies of highly damped modes can be estimated with an average accuracy of 95%.

The stability of the proposed method and the possible effects of measurement noise on the estimated modal parameters were investigated by adding 5% noise (noise to signal ratio) to the analyzed data blocks. During the analyses, it was observed that addition of noise has both positive and negative effects on the estimations. As the noise ratio of the response data gets higher, the visibility of the eigenfrequencies of the system increases. However, some misleading noisy frequencies appear as potential eigenfrequencies and the resulting graphs become more difficult to interpret compared to the graphs of noise-free data. Results of the analyses verify that the proposed approach enables stable eigenfrequency estimations to be made and highly damped eigenfrequencies to be detected from noisy data whose noise to signal ratio is approximately 5%. The noise level tested is believed to be sufficient for the applications at hand.

Identification of the corresponding damping ratios is not included in this work. Although initial results show that damping can also be extracted by using the same approach, more detailed investigations are required to establish the mathematical relations showing the applicability of the method for damping estimations. As a future research topic, it is recommended to extend the proposed algorithm so that damping can also be identified from the investigated data series.

Similarly, applying the method to real measurement data is expected to enable us to understand possible drawbacks and the points to be improved and therefore considered as a future research direction.

Acknowledgements

I feel myself very lucky that during my PhD, I have had the opportunity to be a member of a very distinguished research group, the Engineering Dynamics section of the Faculty of 3ME (Mechanical, Maritime and Materials) which is one of the best teams in its field. I am very thankful to all my friends, colleagues, teaching and administration staff for creating such an amazing atmosphere for research. This thesis would not be the same or even possible without their help and support. It is now the opportunity to acknowledge these people for contributing to my work, as well as for the pleasant time I have had during my stay in the Netherlands.

First of all, I would like to express my deep and sincere gratitude to my promotor Professor Daniel J. Rixen for accepting me as a PhD candidate in his group and for giving me the opportunity to do research. It was a great chance for me to have a supervisor like you. Your continuous support, encouragement and invaluable guidance made me finalize this work. You contributed in every single step and never hesitated to spend your time in reviewing papers, deriving equations or even taking measurements on wind turbines in a muddy potato field. I know that you spent quite a lot of time cleaning your car afterwards; it is a pity that most wind turbines are located in fields. I will always remember your extraordinary intelligence, enthusiasm, dedication, self discipline and endless energy.

I am also very grateful to Professor Paul van Woerkom for his continuous support and help during my stay in the Netherlands. You have been very kind and encouraging from the first day we have met. You are definitely a gentleman from good old times not from the modern pragmatist world. I highly appreciate your passion for teaching and deep engineering perspective. I am also thankful to you for translating the proposals and the summary in Dutch.

I would like to thank Professor A. de Boer, Professor A. Brandt, Professor G.J.W. van Bussel, Professor Christof Devriendt, Professor R.P.B.J. Dollevoet and Professor L.J. Sluys for accepting to be members of my committee and for reviewing my thesis.

I would like to express my sincere appreciation to Professor Gijs van Kuik, for his help and support in writing proposals for We@Sea program and for his invaluable guidance at the beginning of my research.

I would also like to acknowledge Fanzhong Meng, from the Faculty of Aerospace Engineering, Wind Energy Department, for performing the aeroelastic simulations and SSI (Stochastic Subspace Identification) analyses mentioned in Chapter 4.

I am also indebted to Oliver Erne, Gunter Sanow, Pieter Schuer and Wim Cuypers from GOM mbH (Optical Measuring Techniques) for their extensive help and collaboration during the in-field measurements.

I would like to thank the members of the Engineering Dynamics Section, Arend Schwab, Edwin de Vries, Dennis de Klerk and Paolo Tiso. I am also very thankful to Jodi Kooijman for sharing his experience about the lab equipment and sensors; Sven Voormeeren for his help during the in-field tests, and Stephan Hannot, Paul van der Valk and Saumya Kadawathagedara for their support and friendship.

A very special thank goes to Alexander Steenhoek, Alex you were always the first person I would go to when I needed a favor because I knew that you would immediately come to help and do everything you can no matter how busy you were.

I am very thankful to my roommate Umut for his endless patience and help. We shared the same office for two years. We worked together, sometimes fifteen hours a day. I feel myself very lucky to have a friend like you during the difficult times of doing a PhD.

Ali, the life in our office definitely gained momentum after you joined us. I am very happy to know such an energetic person.

I am also very grateful to the secretaries of our department, Corinne, Birgit and Marli. I really admire your abilities in problem solving and making arrangements. You are the angels that keep everything in its place and make the system run efficiently.

It was a great chance for us that when we arrived in the Netherlands, we already had a very close friend living in Delft. Elif, with your help we did not have any difficulty in

getting used to our new life. We found ourselves in a cozy atmosphere surrounded by a lot of new friends. We are very thankful to you, Senlav and Nihal Teyze for everything you did for us and for becoming our family in Delft.

Begüm and Şenol, we sincerely appreciate your efforts to bring Turkish friends living in Delft together. We will always remember the barbecue parties, Eurovision and football nights you organized. Thank you very much for your kind hospitality.

Lupita, Dennis, Sonja and Pascal thank you for your sincere friendship. We will never forget our nice trips, the great weddings and all the joyful time we spent together.

Dear Emine and Oğuzhan, we are grateful for all your support, friendship and your efforts to help us get used to living in the Netherlands.

Our dear friends Anıl, Tolga, Hilal, Emrah, Pervin, Anıl, Çağrı, Aylin, Nejla, Gülay, Atilla... We were like a big team through all these years and our team got bigger and bigger with the babies joining us. Thank you very much for all your friendship.

And very special thanks to my family... I am deeply indebted to my parents Sonay and Metin Özbek; my parents in-law Emine and Kaya Açar, my brother Mehmet and sisters in-law Ayşe Ufuk Açar and Ayşen Özbek for their continuous support and encouragement.

My little sweetheart Selen, thank you very much for being such a wonderful daughter and for giving me the motivation and energy I needed while writing this thesis.

Last but not least, I would like to thank my wife Ayda, for her endless patience, understanding and love through all these years. Without your help and support it would definitely not be possible to walk in this challenging path....

Muammer Özbek

Curriculum Vitae

Mr. Muammer Özbek was born on May 16, 1976 in Kayseri, Turkey. He completed his undergraduate study in 1999, in the field of civil engineering at Bogazici University, Istanbul, Turkey. He received his M.Sc degree from the same university in December 2002 as a structural engineer. From January 2003 to April 2006 he worked as researcher at Bogazici University, Kandilli Observatory and Earthquake Research Institute, Earthquake Engineering Department.

In September 2006, he started his PhD at Delft University of Technology, Faculty of Mechanical, Maritime and Materials Engineering, Engineering Dynamics section under the supervision of Prof. Daniel J. Rixen.